Master Thesis in Geographical Information Science nr 168

Investigating the influence of the tidal regime on harbour porpoise *Phocoena phocoena* distribution in Mount's Bay, Cornwall

Duncan Jones

2023
Department of
Physical Geography and Ecosystem Science
Centre for Geographical Information Systems
Lund University
Sölvegatan 12
S-223 62 Lund
Sweden

Investigating the influence of the tidal regime on harbour porpoise *Phocoena phocoena* distribution in Mount's Bay, Cornwall

Author: Duncan Jones (2023)

Master degree thesis, 30/ credits in Master in Geographical Information Science Department of Physical Geography and Ecosystem Science, Lund University

Supervisor Valentijn Venus
UT-ITC Twente University

Acknowledgments

I would like to express my gratitude to Valentijn Venus who supervised my project. His patience and careful guidance have helped me to make it a much clearer and a greatly improved piece of work. I would also like to thank Marijke De Boer who first inspired me to collect data from the boat and supported me in developing robust data collection protocols. Her advise started me on the road to developing my knowledge of GIS and statistics in order to better understand Mount's Bay and it's sea creatures.

Thanks also to Peter Miller at the Plymouth Marine Laboratory. He allowed me access to the satellite the data I used and provided it in a processed form, which was extremely helpful.

My kind and patient proof readers, Anya Finch, Kate Finch, Ellie Keppie and Hannah Wilson also deserve thanks. Without their help this thesis would not be as easy to read nor as grammatically accurate.

Investigating the influence of the tidal regime on harbour porpoise *Phocoena phocoena* distribution in Mount's Bay, Cornwall

Abstract

Unintentional by-catch in fishing gear is a significant cause of mortality of harbour porpoises in UK waters. Understanding the spatial distribution of harbour porpoises at fine scales and how this changes over time is essential when trying to understand where these lethal interactions might occur.

Mount's Bay in Cornwall, UK is an important area for harbour porpoises. However knowledge of how they use the Bay is limited. Effort and sightings data were collected over eight years between 2011 and 2018 from a wildlife watching vessel. The data shows a high sightings rate for the Bay and confirms the relative high density of porpoises when compared to areas of the UK traditionally considered as strongholds.

Harbour porpoises are present in high numbers year round. However, a seasonal pattern in their occurrence was identified, with numbers peaking in September. Areas where porpoises consistently occur are considered to be important foraging habitat due to their high foraging nature.

To better understand the distribution of porpoises in the bay and how it changes with the tide cycle, Maximum Entropy Modelling (MaxEnt) with files correcting for survey biases was used. By analysing various environmental variables, the models identified the most important factors that influence the likelihood of porpoises being present. These include the longitudinal position within the bay, the depth of the water, the type of substrate on the seafloor, the distance from the nearest significant seafloor slope, and the distance from the nearest tide front.

In addition, a General Additive Model for Location Scale and Shape (GAMLSS) was also used to model the likelihood of porpoise occurrence in relation to thermal front features remotely sensed by satellites.

Identifying Important Areas for Harbour Porpoises

The variables longitude, depth, distance from the nearest significant seabed slope, and distance from the nearest tide front can be combined to describe the location of turbulent oceanographic processes. The models identify specific spatially focused areas that are important for porpoises and demonstrate that the position of these areas changes throughout the tide cycle. The results indicate that these changes are associated with tidal processes. Tidal processes have been found to concentrate

plankton and nekton, which would enhance the foraging success of harbour porpoises and likely explain this relationship.

Key Words: Geography, Geographical Information Systems, GIS, Habitat Modelling, Harbour Porpoise, MaxEnt, Tidal Processes, Conservation

Advisor: Valentijn Venus
Master degree project 30 credits in Geographical Information Sciences, 2023
Department of Physical Geography and Ecosystem Science, Lund University
Thesis nr 168

Contents

List of abbreviations

ABM: Agent Based Modelling
AIC: Akaike Information Criteria
ASCII: American Standard Code for Information Interchange
AUC: Area Under the Curve
AVHRR: Advanced Very High Resolution Radiometer
BRT: Boosted Regression Tree
CCO: Channel Coast Observatory
CHL: Chlorophyll
DEL: Delaporte
E: East
ENE: East North East
ESE: East South East
ERM: Ecological Response Model
Fdense: Front Density
Fdist: Front Distance
Fperc: Front Persistence
GAM: General Additive Model
GAMLSS: Generalized Additive Models for Location, Scale and Shape
GD: Global Deviance
GDAL: Geospatial Data Abstraction Library
GLM: General Linear Model
GLMM: General Linear Mixed Effects Model
GIS: Geographical Information System
GP: Bayesian Modelling with Gaussian Process
GPS: Global Positioning System
JNCC: Joint Nature Conservation Committee
LOESS: locally estimated scatter plot smoothing
MASS: Modern Applied Statistics with S
MaxEnt: Maximum Entropy Modelling
MODIS: Moderate Resolution Imaging Spectroradiometer
MinxEnt: Minimum Cross Entropy
MLM: Machine Learning Model
NB-GAM: General Additive Model with a Negative Binomial Distribution
NBI: Negative Binomial
N: North
NE: North East
NNW: North North West
NW: North West
NRQR: Normalized Randomized Quantile Residuals
OMS: Observation per Metre Searching

PIG: Poisson Inverse Gaussian
PO: Poisson
POp: Platform of Opportunity
PPP: Predicted Probability of Presence
QGIS: Quantum Geographical Information System
QQ: Quantile-Quantile Plot
QR: A decomposition used to solve the linear least squares problem
RPPP: Relative Predicted Probability of Presence
S: South
SAC: Special Area of Conservation
SAGA: System for Automated Data Geoscientific Analysis
SBC: Schwarz Bayesian Information Criteria
SCANs: large-scale ship and aerial survey to study the distribution and abundance of cetaceans in European Atlantic waters.
SDM: Species Distribution Model
SE: South East
SST: Sea Surface Temperature
SSE: South South East
SSW: South South West
STEPGaic: Stepwise Model Selection using a Generalized Akaike Information Criterion
SW: South West
SW II: Shearwater II a sailing catamaran
TIN: Triangulated Irregular Network
TW-GAM: General Additive Model with a Tweedie Distribution
UK: United Kingdom
UKBAP: UK Biodiversity Action Plan
VCOV: Variance-Covariance
W: West
WNW: West North West
WSW: West South West
ZIP Zero Inflated Poisson
ZIP-GAM: General Additive Model with a Zero Inflated Poisson Distribution

List of Tables

List of Figures

1 Introduction

The harbour porpoise is a species afforded a high level of protection in UK and European waters. Despite this, much of the knowledge of the ecology of the species is still somewhat inferred and patchy. This is due to the secretive nature of the species, its small size and the difficulty and expense of conducting studies on the ocean (de Boer 2013; Virgili et al. 2018). In order to better protect the species it is necessary to identify key habitat areas both spatially and temporally. Due to the limited understanding of the species' behavioral ecology, areas with higher occurrence rates are identified as important foraging habitat (Johnston et al. 2005; van Beest et al. 2017). All studies support the theory that porpoises must feed almost continuously on high energy food in order to maintain good body condition. Presumably this means they must consistently seek areas which provide adequate feeding opportunities. It is likely that their seasonal meso scale movements and their regular macro scale movements reflect this need to consistently stay around productive foraging areas (Johnston et al. 2005; Gilles et al. 2016; Nielsen et al. 2018). Therefore it can be assumed that areas with high densities of harbour porpoises represent key foraging habitat and that regular macro scale movements indicate that the location of these areas is dynamic.

An anthropogenic threat to porpoises comes from bycatch, which is when a non target species becomes entangled in fishing gear. Bycatch was the cause of death for 36% of, stranded small cetaceans, assessed by postmortem, in Cornwall, in 2021 (Hawtrey Collier et al. 2021). Bycatch is currently recognised as being poorly monitored and under recorded (Dolman et al. 2022). Harbour porpoises are particularly vulnerable to bycatch in gill nets (Dolman et al. 2022). The International Council for the Exploration of the Sea (ICES) areas 29E4 and 28E4 cover Mount's Bay, Cornwall and 29E4 has the highest gill net fishing effort in the UK (Calderan and Leaper 2019). In an area with high gill net fishing effort it is essential to understand how the fishing effort overlaps spatially and temporally with important harbour porpoise habitat in order to understand the bycatch risk.

At present, species distribution models for harbour porpoises in the UK are restricted either spatially such as Jones et al. (2014) and Waggitt et al. (2018) or temporally, or in some cases, both, hindering their ability to identify areas of high risk overlap. While spatial limitations are commonly addressed and acknowledged, temporal constraints are often overlooked (Jones et al. 2014; Waggitt et al. 2018). However, it should also be noted that spatial limitations may lead to distribution maps that are too coarse to be effective for the purpose of identifying high, bycatch risk areas. For example 25 km² resolution (Heinänen and Skov 2015). Recently Special Areas of Conservation (SAC) for harbour porpoises were designated around the UK (Heinänen and Skov 2015). The spatial designations largely relied upon the surface density

models, for harbour porpoises, produced from the SCANs III survey, which is a large-scale ship and aerial survey to study the distribution and abundance of cetaceans in European Atlantic waters. The SCANs surveys take place at the end of June and start of July and thus they are temporally limited and inappropriate for habitat modelling for a species such as the harbour porpoise, which shows seasonal meso scale movements (Hammond et al. 2021). Platform of opportunity data has the potential to provide better temporal coverage for use in distribution modelling. If a robust modelling approach suited to the species distribution data is adopted (de Boer 2013).

Many studies produce a single distribution prediction. This prediction represents a mean or median predicted distribution of a species. The result is likely to be a generalisation, and therefore the predicted highest density areas may differ from predictions generated from temporally segregated data, especially when modelling at a fine scale. Fishing effort can be both spatially and temporally discrete, just as porpoise distribution is. Therefore, there is a need to understand the temporal as well as the spatial when modelling porpoise distribution in order to accurately identify bycatch risk areas. There are some studies that consider time within the modelling process but they are typically extremely spatially focused < 10 km² (Waggitt et al. 2018; Jones et al. 2014). Johnston et al. (2005) demonstrated harbour porpoise distribution changed in relation to tidal features over a wider area > 100 km² (Johnston et al. 2005). Modelling distribution at fine resolutions over areas > 100 km² would be a valuable first step in identifying bycatch risk areas.

It is likely that porpoises use oceanographic features and the processes around them to maximise their foraging success in Mount's Bay, Cornwall. The currents and processes around these features may have the effect of aggregating fish by disrupting their swimming or focusing fish by concentrating their food. Many oceanographic processes focus particulates in the water column. The particulates are made up of nutrients, phytoplankton and zooplankton. The food availability at these sites attracts and aggregates fish (Thorpe 2005; Embling et al. 2012; Jones et al. 2014; Cox et al. 2018; Gilles et al. 2016; Waggitt et al. 2018).

The objective of this study is to utilise data collected by a wildlife watching vessel, which serves as a platform of opportunity (POp), to develop a spatial model of the distribution of harbour porpoises in Mount's Bay, Cornwall at each hour of the tidal cycle. A further aim is to investigate whether this distribution is influenced by tidally driven processes.

Research questions:

1) Does harbour porpoise distribution change across the tide cycle in Mount's Bay, Cornwall?

2) Are the changes in harbour porpoise distribution in Mount’s Bay linked to tidally driven features?

Hypothesis: The location of harbour porpoise sites of persistent presence change across the tide cycle and coincide with topographic features on the sea floor, tidal flow rate and direction

2. Background

2.1 Biology and Ecology of the harbour porpoise

The harbour porpoise *Phocoena phocoena* (Figure 1) is a member of the phocoenidae family, which is a sub group of the odontocetes. The odontocetes include the toothed whales, dolphins and porpoises.

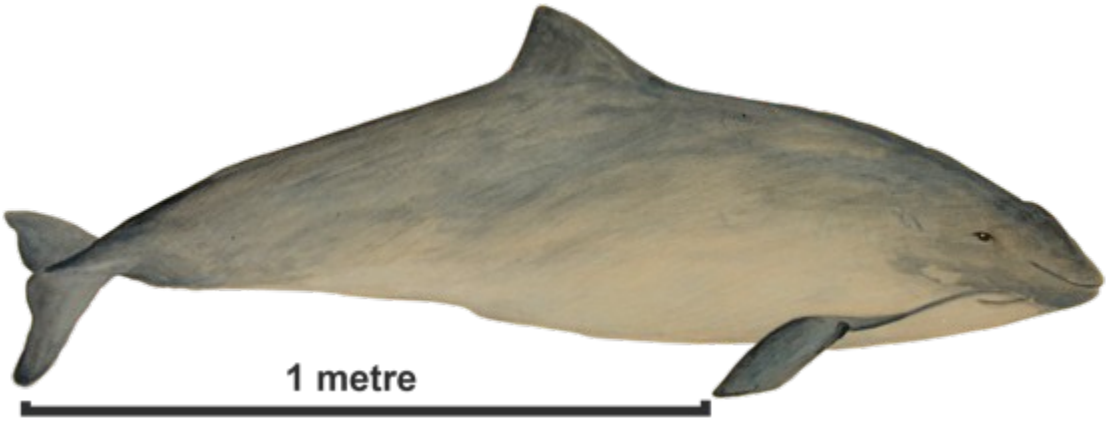

Figure 1: A harbour porpoise (Knee, 2018)

The harbour porpoise largely occurs in the coastal waters of the Northern Hemisphere and they are usually found in smaller groups when compared to other odontocetes. This is thought to be a predator avoidance measure (Keener et al. 2018). They can be targeted as prey by orcas, *Orcinus orca,* and are subject to harassment by other large marine mammals such as common bottlenose dolphins, *Tursiops truncatus,* often with lethal outcomes (Simon et al. 2010) and grey seals, *Halichoerus grypus*. In response to these threats porpoises adopt the approach of stealthy small groups and high frequency echolocation, which is undetectable by the threat species (Verfuß et al. 2009; Sørensen et al. 2018). The undetectability of these echolocations lead many to theorise that porpoises were silent at times other than when foraging (Kyhn et al. 2013). However in a recent study porpoises were recorded constantly emitting click streams in order to communicate with others and co-ordinate interactions (Sørensen et al. 2018).

Population studies have recorded mean group sizes as being anywhere between one and five animals with maximum observed group sizes of greater than 100 (Berggren and Arrhenius 1995; Bjorge and Oien 1995; de Boer et al. 2018). Typically females are between 1.53 - 1.63 m and 55 - 65 kg, while males are typically 1.41 – 1.49 m and 46 – 51 kg (Lockyer 2003b). The relative small size of porpoises means that they are constantly burning energy through heat loss. In order to combat this they must maintain their blubber in good condition and constantly forage successfully (Wisniewska et al. 2016).

2.2 Foraging Ecology

Leopold (2015) found that targeted prey species vary depending on location. However gadoids, clupeids, and sand eels both *Ammodytes tobianus* and *Ammodytes marinus* are commonly found to be important (Yasui and Gaskin 1986; Pierce, Santos and Cerviño 2007; Wisniewska et al. 2016; Rojano-Donãte et al. 2018). Young porpoises consume large numbers of gobies, which are less nutritious than other species targeted, possibly because they are easy to catch (Leopold, 2015).

A 2016 study used high-resolution movement and prey echo recording tags attached with suction cups in order to better understand porpoise foraging (Wisniewska et al. 2016). This study drew slightly different conclusions than previous autopsy based studies as to how and what species porpoises targeted as their key prey. Wisniewska et al. (2016) found that harbour porpoises had an extremely high foraging rate targeting up to 550 small fish an hour with a capture rate greater than 90%. The fish targeted in this study were typically smaller, being between 3 cm and 10 cm compared to 5cm and 25cm (estimated from ottolith size) in previous studies (Leopold, 2015; Wisniewska et al. 2016). It is important to note that all other studies extrapolate fish sizes from the ottoliths found in the stomachs of stranded animals and this process is far from exact (Pierce et al 2007). Previous to this study it has been impossible to understand the frequency of feeding and presumably this might vary depending on size and nutrition value of the species being targeted (Leopold 2015).

Hoekendijk et al. (2018) suggested that the Wisniewska et al. (2018) study had potential limitations because the porpoises had been caught and held in static fishing gear for up to 24 hours prior to being tagged and released. The data collected by the tags is from the following 15 to 24 hours of the porpoises' life. It must be considered that these porpoises would have been stressed and starved for the previous 24 hours and that this must have influenced their behaviour. It is likely that their normal foraging rate is not as intensive as that shown in the Wisniewska et al. study (Hoekendijk et al. 2018).

2.3 Mating

Although harbour porpoise mating attempts are recorded throughout the year they are considered to peak in the summer (Desportes et al. 2003; Keener et al. 2018). Male porpoise testicles increase in mass at this time in order to maximise their opportunity to pass on their genes (Desportes et al. 2003). This has been shown in both a captive environment and through the autopsies of stranded porpoises in Denmark (Desportes et al., 2003). In the wild porpoise mating attempts are often associated with breaching and in the majority of observed cases the male porpoise approaches from the left.

Approaches are initiated from below with enough speed to leap in to the air following their mating pass (Keener et al. 2018). The mating pass appears to follow an ambush approach.

For example within Mount's Bay, Cornwall, these mating passes are observed in August and September. This is a time of year when porpoise numbers are observed to peak in the Bay. It is unknown whether these peaks in numbers are linked to maximising mating opportunities or if the porpoises are present in large numbers due to food availability and that this coincides with their peak mating period.

2.4 Range Patterns

Harbour porpoises have been observed to show much individual variation in the distances they might range and over how much time. Knowledge of migratory behaviour is limited to a small number of studies during which harbour porpoises were satellite tagged (Lockyer 2003a). In all cases individual behaviours varied greatly. However studies suggest a porpoise may typically range over tens of kilometres a day. It was observed that the core foraging area for six harbour porpoises tagged in the Bay of Fundy ranged between 122 km² and 415 km² for the months of August and September, with monthly ranges being between 2850 km and 22 103 km for individuals (Johnston et al. 2005). It is thought that movements are most likely to be linked to prey availability because an animal the size of a harbour porpoise cannot carry significant fat stores to support prolonged periods of fasting (Johnston et al. 2005). Typically harbour porpoise habitat is considered to be the coastal shelf seas where the depth is less than 200 m. However they have been recorded in much deeper water. This is believed to be a seasonal behaviour (International Whaling Commission, 1995; Nielsen et al. 2018). On one occasion a porpoise was seen in deeper water off the Norwegian coast and it was presumed to be migrating from the shelf seas of Norway to the Faroe Islands(Bjorge and Oien 1995).

It was found that the West Greenland population migrates between shelf waters of less than 200 m in depth and deeper waters off the shelf edge. It has been theorised that this behaviour is adopted to avoid sea ice that forms in the more northern shelf waters of West Greenland (Nielsen et al. 2018). The groups of porpoises tagged in the Nielson study were carrying tags in May, June, July and August of 2012, 2013 and 2014. During this time they covered a combined area of
4 144 749 km². This demonstrates the wide ranging nature of harbour porpoises and the propensity for seasonal migration in order exploit optimum foraging habitats.

2.5 Conservation Status and Threats to the Harbour Porpoise in the UK and Cornwall

The harbour porpoise is recognised as an Annex II species by the European Habitats Directive (Commission of European Communities, 2007). This status required the UK government to maintain the species and its habitats in a favourable condition. The UK Biodiversity Action Plan (UKBAP) lists the harbour porpoise as a priority species. It is thought that 40% of the world population can be found in UK waters (Evans and Prior 2012), and recent sightings data suggests that the south west Cornish coast is of particular importance to this species (Jones et al. 2014; de Boer et al. 2018). The data gathered from recorded porpoise sightings and the high adult calf ratio of 28.67% in July and 29.53% in August (de Boer et al. 2018) indicate Mount's Bay, Cornwall is a particularly important habitat for this species, when it is compared with other areas (Baines and Earl 1999; Evans and Baines 2009; Embling et al. 2010; Evans and Prior 2012; Oakley et al. 2016). The South Cornwall coast, including Mount's Bay, has not been considered for a Special Area of Conservation (SAC) despite demonstrating the three key requirements the Joint Nature Conservation Committee (JNCC) use for designation: 1) continued regular presence , 2) good population density (in relation to neighbouring areas), 3) a high ratio of young to adults during certain periods of the year and other biological elements are characteristic of these areas, such as very developed social and sexual life (JNCC 2017).

February 2019 was the deadline for the designation of five candidate SACs, identified in a 2017 Joint Nature and Conservation Committee (JNCC) report, for harbour porpoises in UK waters (JNCC 2017). The new conservation areas are all large in size (1000s of km^2). The large size of these areas is due to the highly mobile nature of the harbour porpoise and follows Eric Hoyt's 2005 recommendations regarding protected areas for cetaceans (Hoyt 2005). In order to meet the conservation obligation of these SACs it is necessary to identify activities that have a potentially negative impact on harbour porpoises and their habitat. Harbour porpoises face a number of threats from anthropogenic activity (King et al. 2015) in particular noise pollution, disturbance from vessel traffic, by-catch in static fishing gear and chemical pollution (Dyndo et al. 2015; Murphy et al. 2015; Dolman et al. 2016; Wisniewska et al. 2018) with by-catch being recognised as a continuing serious threat within European waters (Rogan et al. 2021). Due to their high foraging nature harbour porpoises are particularly vulnerable to anthropogenic disturbance (Wisniewska et al. 2016; Hoekendijk et al. 2018). The large coverage of the proposed reserves mean that detrimental activities are unlikely to be controlled across a whole reserve. With this in mind it is important to consider spatially and temporally focused approaches to management within the reserves. However implementing a management approach such as this would be difficult because current knowledge of how porpoises use areas at fine scales is limited.

2.6 Surveying Small Cetaceans

Studying cetaceans is both costly and logistically difficult. The nature of their environment precludes regular surveys and often presents conditions unsuitable for collecting robust data. These limitations mean that current knowledge of population abundance and the spatial and temporal variations in this abundance are both limited (de Boer, 2013). This lack of data has lead to an increase in the use of POp data in an effort to fill this knowledge gap (Embling et al. 2010; Evans and Prior 2012; de Boer et al. 2018; Correia et al. 2019; Robbins et al. 2019).

Line transect studies are often used to estimate abundance. A vessel follows a pre planned survey route and researchers record the number of animals sighted along the route. The information is then extrapolated to estimate the population size across the whole area of sea (Buckland et al. 2004). This is a widely used approach and is used in the Small Cetaceans od the Atlantic and North Sea survey (SCANS) to assess cetacean abundance in the North East Atlantic, North and Baltic seas (SCANS-III, 2017).

Acoustic monitoring is used to record the number of animals at a location. A device is deployed at sea that can record the sounds emitted by odontecetes (Zimmer 2011). The number of detections made can be used as a proxy for the number of cetaceans present within the detection range of the deployed device (Zimmer 2011). Acoustic monitoring devices can also be towed behind vessels conducting line transect surveys (Barlow and Taylor 2005). Acoustic listening devices have been successfully used in a number of small cetacean studies (Cox et al. 2017; Clay et al. 2018; Nuuttila et al. 2018).

Spatial studies often involve line transect surveys and acoustic surveys. They aim to apply these techniques over a wider area and/or wider time frame to better understand the distribution of odontecetes spatially and or temporally across an area (Thompson et al. 2015). Spatial studies are often used to inform habitat modelling (Fujioka et al. 2014).

POp data is increasingly used in spatial studies (Kiszka et al. 2007; de Boer 2013). In these instances, data from a variety of platforms such as: wildlife watching vessels, oil platforms, ferries, cruise ships, cargo ships and hydrocarbon survey vessels is used to conduct spatial, fixed point and mark recapture studies (Evans and Hammond 2004; Evans 2008; de Boer 2013; de Boer et al. 2018; Correia et al. 2019). The data collection methodology will often follow a non standard approach and can be applied inconsistently. The appropriateness and usefulness of data collected in this way must be carefully considered before analysis (Evans and Hammond 2004; Hauser et al. 2006; de Boer 2013). The main shortcoming of POp data is spatial bias. The platform

being used is performing a role and the data collection is secondary to this role (de Boer, 2013). When using a standard approach to collect spatial data, the survey route will be carefully designed to make sure each part of the survey area has equal chance of being visited (Buckland et al. 2004). Survey coverage will be planned following either a random, random stratified or systematic sampling approach (Viddi et al. 2010).

On POps, data is collected by an observer while the platform conducts normal duties and, in this case, accepted survey protocols (random and systematic) are not followed (de Boer 2013). The POp will invariably visit some parts of the proposed survey area on more occasions than others (Viddi et al. 2010). If spatial analysis or species distribution modelling is to be conducted using data collected from POps, the bias must be accounted for and mitigated against (Zhang and Zhu 2018). This is possible if POps have collected positional data regularly during a survey (Viddi et al. 2010; Alves et al. 2018). The positional data can be used to identify survey coverage which identifies the spatial bias. It can then be accounted for in the analysis of the data. One approach is to subset the dataset into areas with comparative coverage (de Boer et al., 2018). Another is to temporally subset the data to generate a final dataset with even spatial coverage. In some cases it is appropriate to generate a weighting for the spatial bias which can be included as a variable in statistical modelling (Viddi et al. 2010; Johnston et al. 2020).

2.7 Habitat Modelling for Harbour Porpoises and Small Cetaceans

Habitat modelling, which is a form of species distribution modelling, is a relatively new approach that allows us to understand how animals use their environment and this knowledge can be used to inform conservation decisions (Embling et al. 2010). Habitat modelling for cetaceans presents some unique challenges. They inhabit a hostile environment for humans and often the conditions make survey and detection of animals challenging (de Boer 2013; Oakley et al. 2016). The animals being studied only spend a fraction of their lives at the surface making them hard to detect and only giving researchers a glimpse of their lives.

For example surface observations are often linked to behaviours. These are usually categorised as travel, foraging, resting, socialising and leaping (Bas et al. 2017; Oakley et al. 2017; Roberts et al. 2019). Without knowledge of what is happening below the surface it is difficult to fully understand if these interpretations of surface behaviour are truly representative of behaviour. If datasets used to identify habitats linked to behaviour are from surface observations alone, then the limitations of correctly identifying behaviours from surface observations must be taken into account. Areas with the highest densities of animals are identified as important habitats and statements of why these habitats are important are usually restricted to

suggesting they are important foraging areas (Johnston et al. 2005; Embling et al. 2010, 2012; De Boer et al. 2014; Jones et al. 2014; Heinänen and Skov 2015).

Conducting studies on the water is logistically challenging and expensive (Williams et al. 2017). This limits the number of studies carried out and the time scale over which they are conducted. Due to cost and lack of resources studies are usually either temporally or spatially limited (de Boer 2013; de Boer et al. 2018). Temporally limited surveys are often large scale and are designed to assess the abundance of species over large areas at the time of the survey. They are not designed to be used for distribution modelling (Heinänen and Skov 2015; de Boer et al. 2018). The SCANs surveys are a prime example. The object of the SCANs is to calculate abundance estimates for various cetacean species in the North East Atlantic, North Sea and Baltic Sea. They are carried out once a decade and over a month long period during June and July (SCANs-III, 2017). They can provide a good idea of species distribution at the time of the surveys but do not account for animal movements over time (de Boer 2013; de Boer et al. 2018).

Spatially limited studies often run across longer time period: in some cases they span a complete year and sometimes multiple years. De Boer et al. use data spanning 2011 to 2017 covering March to November in each year for Mount's Bay in Cornwall (de Boer 2018). Gilles et al. used data from aerial surveys spanning 2005 to 2013 covering March to November for the central and southern North Sea (Gilles et al. 2016). These studies can provide a clear picture of animal distribution within the study area and map changes with time. This is useful for identifying habitat selection and the drivers influencing it. If key habitats can be identified within the study area then this information could, with caution, be used to identify potential important habitat outside of the study area. If areas with similar characteristics were selected. Skov et al. (2015) identified important areas for harbour porpoises in data deficient areas using this approach (Heinänen and Skov 2015).

2.8 Statistical Approaches to Habitat Modelling

Different statistical approaches to habitat modelling are often debated and a myriad of approaches taken. The modelling approach selected is usually influenced by the data to be modelled. Common approaches are: general linear models (GLM), general additive models (GAM), maximum entropy models (MaxEnt), decision trees often in the form of boosted regression trees (BRT), Bayesian modelling using Gaussian Process (GP) and agent based modelling (ABM). All have been implemented successfully but there are often performance differences and the models consistently predict different habitat distributions when applied to the same dataset (Marmion et al. 2009; Golding and Purse 2016).

Virgili et al. (2018) conducted a study investigating habitat modelling for rare species and compared different modelling techniques for describing the distribution of rarely sighted small cetaceans. In this study the performance of four different models was tested and the minimum number of sightings required to generate a reliable distribution map identified for each model. The models compared were: MaxEnt, GAM with a Tweedie distribution (TW-GAM), GAM with a negative binomial distribution (NB-GAM) and GAM with a zero inflated poisson distribution (ZIP-GAM). It was found that models using presence and absence data consistently outperformed those using presence only data. In this case MaxEnt is the only model using presence only data. The suggestion is that MaxEnt should only be used when presence only data is the only data available. There is an approach to MaxEnt modelling which uses a bias file to represent survey effort. This approach to MaxEnt performs differently to the standard approach and typically increases it's accuracy. The TW-GAM performed the best of the three GAMs. This is because the Tweedie distribution comes from a family of exponential distributions and can handle clusters of data such as zero clusters. This is useful for modelling effort based cetacean data because there are often lots of zero records (Virgili et al. 2018). An alternative approach is to use agent based models.

Agent based models are a type of habitat model that focus on the actions and behaviors of individual animals or organisms, rather than the broader ecosystem as a whole. These models can be used to understand how species interact with their environment and make decisions about where to live and how to survive. They can also be used to predict the potential impacts of human actions on species populations and to inform conservation and management efforts (Railsback and Grimm 2012).

In their report trying to identify high density areas for harbour porpoises in UK waters Heinänen and Skov (2015) discussed GAM models and zero inflated data (data with lots of zeros). It was found that a hurdle GAM performed best for their data (Heinänen and Skov 2015). A hurdle GAM first tests all the predictors (factors which might influence harbour porpoise presence in an area) against presence and absence. The model establishes which predictors are required for the animals to be present. Once the hurdle of presence is overcome, all the predictors are tested to determine which are more important in influencing the variance in presence (McMahon et al. 2017). Heinänen and Scov (2015) found this method performed better than TW-GAM discussed by Virgilli et al.'s (2018) study.

GAMs are a derivative of linear models and are additive in nature. The additive nature means they do not account for interactions between variables and how these interactions can impact predictions. This can lead to over prediction or false positives (Golding and Purse, 2016). However they are useful for datasets with outliers that must be included. GAMs are non parametric, which means their predictions are

around a median average as opposed to mean average. The median average is less skewed by outliers. When compared with GLMs, which are a parametric test, GAMs are less likely to generate false positives around outliers.

Clay et al. (2016) used a two step general linear mixed effects model (GLMM) taking a hurdle approach. The first step is a presence absence assessment. Following that, presence only data were used to determine the predictor variable's influence on the time Burmeister's porpoises spent around nets (Clay et al. 2018). GLMM are often used in habitat modelling because they are capable of handling data which are not normally distributed, which is often the case for presence absence species data. They are also a parametric test and are considered to be more statistically robust. However outliers can cause them to perform poorly due to the generation of false positives. In a number of studies comparing models those based around GLM were the least predictive although they are often the most parsimonious (Reiss et al. 2011; Golding and Purse 2016).

Decision trees perform well and handle high numbers of predictor variables. The production of nested decision trees allows them to do this. However it is possible for the model to produce a limitless number of trees which can split variables to such a degree that the result is as noisy as the data itself. Ideally when modelling the goal is to pick out trends in the data. The ultimate goal is to predict all the trends without over fitting the model. Decision trees need to be applied carefully in order to avoid over fitting (Breckling et al. 2011). They are non parametric and therefore capable of handling outliers without generating false positives. They also detect relationships between predictor variables which improves the explanatory level.

Golding and Purse (2016) compared model performances and found that decision trees in the form of BRTs performed well when compared with GLM, GAM, MaxEnt and GP. The predictive ability of BRT was similar to GP and the two were found to be the most predictive of the models tested. However when a surface plot was generated with an artificial data set the BRT surface was not smooth. It did detect the non linear interaction between the variables but the non smooth surface demonstrates the nature of the model to over fit. Trends in nature would typically generate a smooth surface (Golding and Purse 2016).

ABM account for the individual behaviours of the agents (animals) in the model and are therefore capable of identifying more complex situations around predator prey relationships than other modelling approaches. This can make them more accurate at predicting animal behaviours and ecological niches. However their description of the relationships between particular environmental variables and an animals behaviour can be complex and difficult to interpret (Railsback and Grimm 2012).

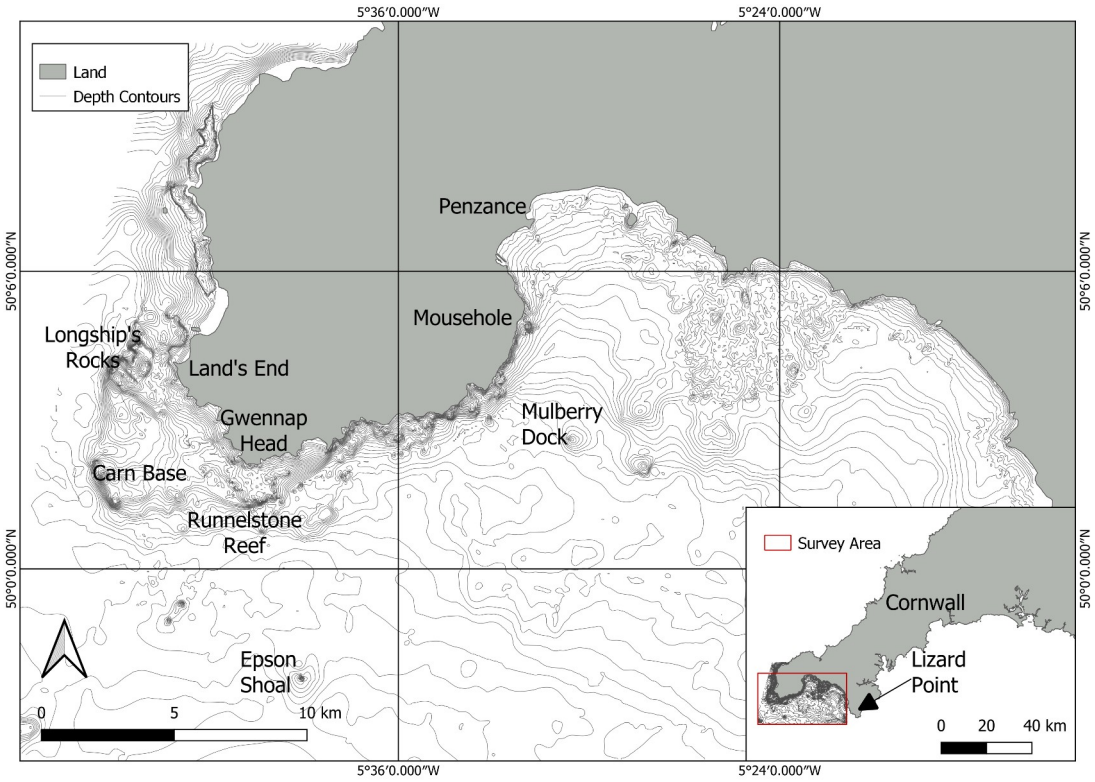

Figure 2: Mount's Bay, Cornwall, UK the study area.

2.9 Description of the Study Area

The study was undertaken between 49˚55'N - 50˚08'N, and 5˚22'W – 5˚45'W, an area in Mount's Bay off southern Cornwall, UK (Figure 2). Mount's Bay is the largest bay in Cornwall, UK and stretches from Lizard point (the most southerly point in mainland UK) westwards to Gwennap head (mainland UK's most south westerly point). The study area is wind exposed and tidally dominated. These conditions preclude regular boat surveys at certain times of the year and create a challenging environment for data collection. The area is a coastal habitat which follows the southerly coastline stretching out towards the Runnelstone Reef off Land's End.

Broad- scale tidal data from Admiralty Charts show that water is driven around this headland reef by the tidal current as it enters and exits the western Channel during a semi-diurnal tidal regime. Tidal range varies from between 1.5 m (neap tide) and 5.5 m (spring tide). Water depth in the study area ranges between 0 m and 72.5 m with a mean depth of 37.7 m (Figure 2). The pink areas highlighted in figure 2 show the steeper slopes. These sloped areas cause disruption in the tidal flow causing turbulent conditions in the water column and generating a dynamic tidal environment (Thorpe, 2005). There is a narrow inner shelf (shallow area of water) of ~0.5 km width

between Mousehole in the east and the Runnelstone Reef in the west. Along the southern edge of this shelf, the water drops abruptly from 20 m to 40 m before sloping more gently down to the maximum depth. The bay area from the latitude of Mousehole and northwards is relatively shallow and gently shelving with minimal tidal turbulence. In this part of the Bay the sea floor shelves from 30 m up to the high water mark.

There are a number of notable underwater reefs and wrecks which protrude significantly enough to impact the tidal flow. The Mulberry Dock is a ship wreck, which rises 20 m from the seabed. There is a further pinnacle to the south west of the Mulberry dock, which rises 10 m from the sea bed. The Epson Shoal is an underwater reef. The pinnacle of the reef is 38 m deep and the depth rapidly drops to 64 m around the reef structure. Eric's Patch is a reef with a double summit. The northern peak is 43 m deep and the southern peak 48 m deep. The reef drops away to a depth of 64 m. At the shallowest point, the Runnelstone Reef is 3.5 m deep and, to the south, the depth drops away to 60 m. Carn Base is an area of shallows similar to the Runnelstone Reef with a minimum depth of 10 m. Longships Rocks protrude above the high water level forming the high point of a reef complex which drops away to 50 m to the south and west. There are four sediment types found in the study area in Mount's Bay (see Figure 3).

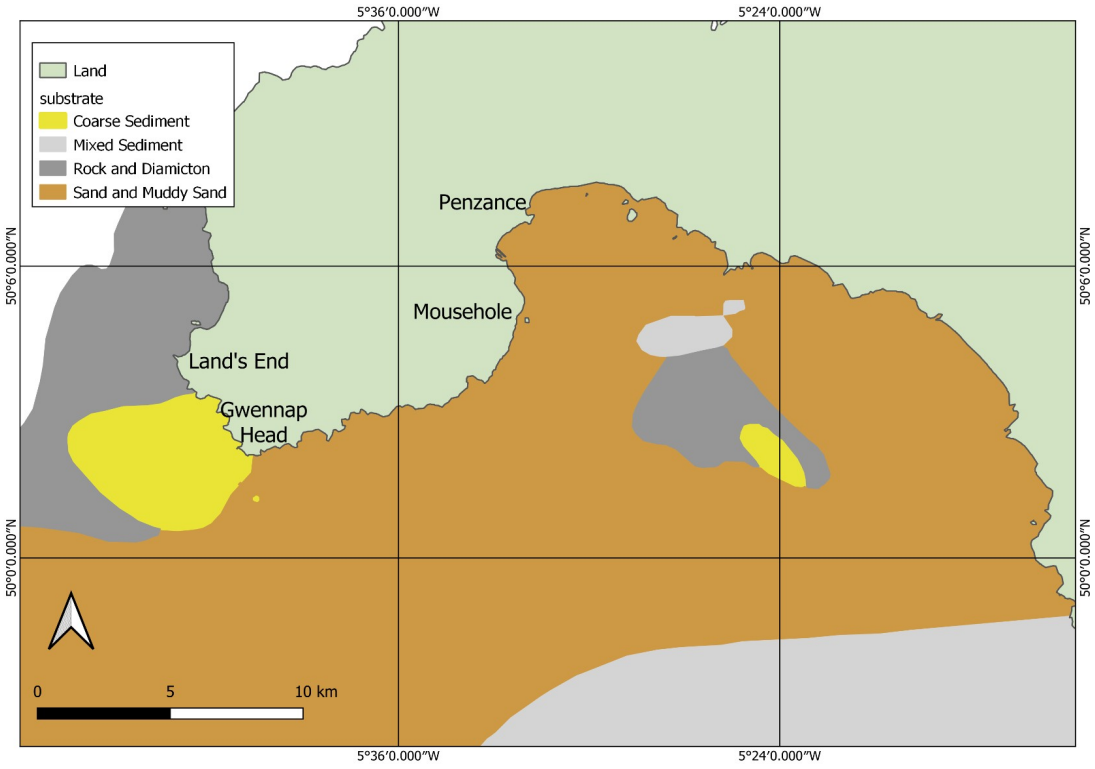

Figure 3: The sediment types of Mount's Bay, Cornwall

The dominant sediment type is sand and muddy sand (coarse (4-1 mm), medium (1-0.25 mm) and fine (0.25-0.063 mm) sand with up to 25% silt and clay) followed by rock and diamicton, coarse sediment and finally mixed sediment (from muds with gravel and sand components to mixed sediments with pebbles (64-4mm), gravels, sands and mud.

Stable cobbles (258-64mm) and boulders (>258mm) might be present) (European Environment Agency, 2019). Sediment type has been found to influence harbour porpoise distribution and it is thought this is due to its effect on the distribution of their prey species (Heinänen and Skov 2015).

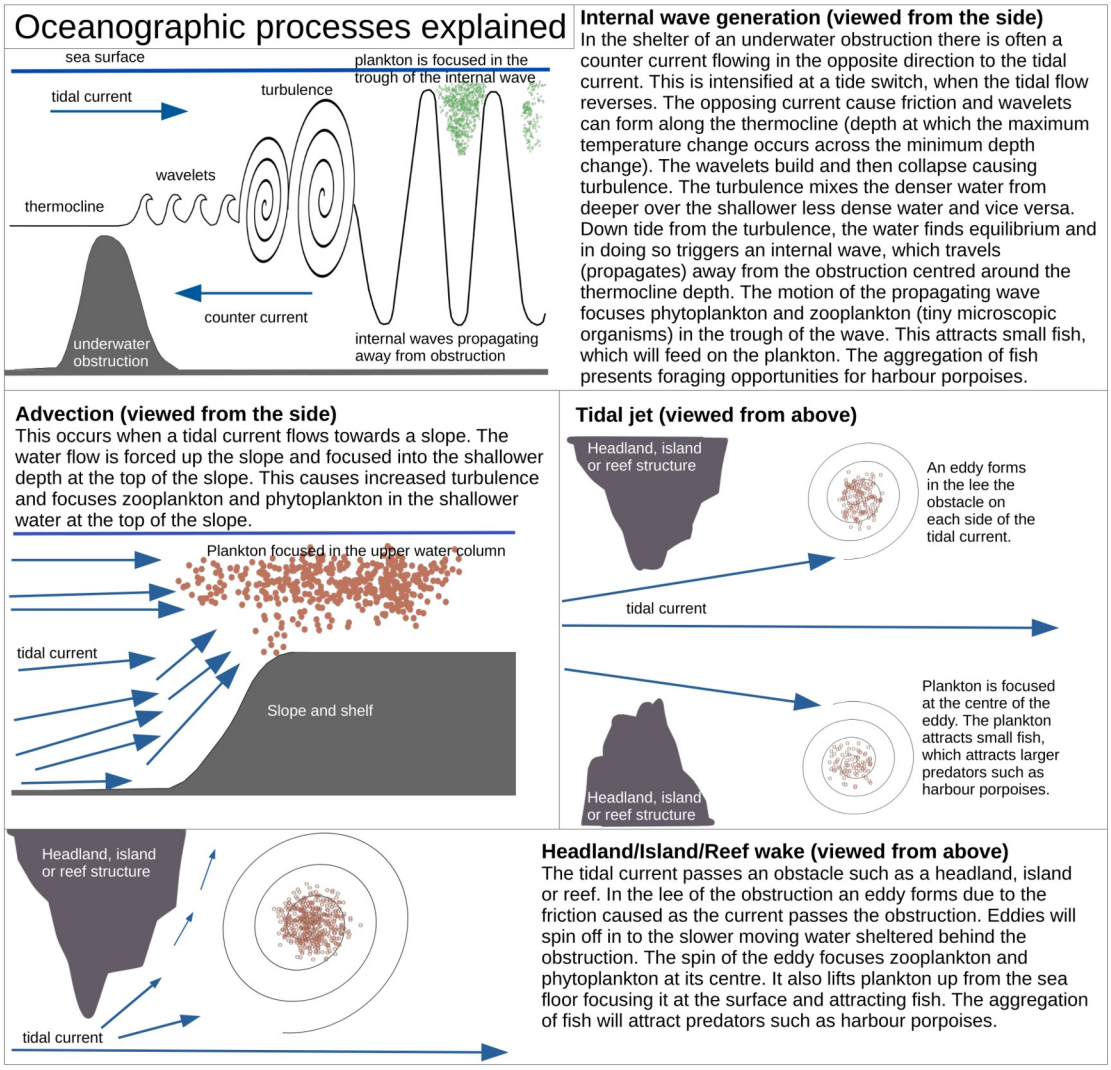

Figure 4: A description of oceanographic processes triggered by the tide interacting with bathymetric features.

2.10 Tidal Processes in Mount's Bay

The uneven bathymetry and tidal regime in Mount's Bay have the potential to generate a number of widely documented tidal processes some of which have been recorded in Mount's Bay. Jones et al. (2014) recorded internal waves propagating south east from the Runnelstone Reef and identified the process coinciding with the presence of harbour porpoises foraging in the area (Jones et al. 2014). Advection is documented to occur when a tidal flow passes across a slope in to a shallower area (Thorpe 2005). Headland and reef wake occur where a tidal flow passes a coastal protrusion or a sharp direction change in the alignment of the coast (Thorpe 2005; Johnston et al. 2005). Tidal jets form when a tidal current passes between two obstructions (Thopre 2005; Cox et al. 2018). Figure 4 explains the different tidal processes and the conditions under which they might form in more detail.

3 Methodologies

3.1 Data collection

Data on harbour porpoise sightings were collected in accordance with the Joint Cetacean Data Programme (JCDP) format during boat surveys (Table 1), which were conducted using a wildlife tour boat as a POp. (de Boer 2013; JNCC 2022).

Sighting	**Record type**
Species identified with level of certainty or the lowest level of taxonomic certainty	Text
Distance and bearing of the sighting	Metres and degrees
Group size and category of the count (best estimate, maximum or minimum)	Number
Behaviour (based on a list of categories)	Text
Effort	
Ship position	Decimal degrees
Direction of travel	degrees
Speed of travel	Metres per second
Sea state and environmental conditions	Text and number beaufort scale, metres

Table 1: Description of information collected regarding the boats track (effort) and observation records (sighting). The data collection was in compliance with JCDP protocols (JNCC, 2022)

The data were collected from the sailing catamaran Shearwater II (SW II), which is used to run wildlife watching boat tours by Marine Discovery Penzance. SW II is primarily a sailing vessel, however it occasionally uses 2 outboard engines. The impact of the noise from the engines on detection was not recorded. Boat surveys were carried out in Mount's Bay, Cornwall between mid-March/early April to late October/ mid November from 2011 to 2018. During these passenger trips, systematic surveys were conducted by two experienced observers (the skipper and a dedicated crew member). The boat followed randomly chosen straight line transects (effort) the end of each transect was usually determined by a sighting of marine megafauna (whale, dolphin, basking shark, turtle, ocean sunfish, seal and seabird of interest). Harbour porpoise sighting cues where either the observation of an animal surfacing or the observation of foraging seabirds, which led to foraging porpoises.

Whilst on random transects environmental data and data related to the platform track were collected: ship position, direction of travel, speed of travel, swell height, visibility and Beaufort sea state. During 2011-2018 the environmental data were

updated for each trip and with every sighting. From 2014 onward, environmental data were updated when conditions changed. The boat position was recorded every minute. A Garmin GPS (GPSMAP76CSx) and a Panasonic Toughpad FZ-B2 were used for data collection. At each sighting location the vessel would leave the transect to commence data collection. Data collected included estimated sighting position, heading of animal(s), group size (minimum maximum), group composition and behaviour. Survey effort would restart once the boat began travelling along the next randomly selected transect. Groups of animals were classed as being independent if they were spatially and/or temporally separated in order to prevent resampling (Stockin et al. 2009). Minimum group size was assessed visually and recorded. A group of porpoises was defined as any number of individuals observed moving in the same general direction, in apparent close association or engaged in the same activity (Shane 1990). It was not possible to assess if the same individuals/ groups were recorded more than once on subsequent surveys during the same day and some animals/groups may have been re-sampled.

On average 226 trips were carried out each year between 8th April 2011 and 2nd November 2018. Research trips were carried out when weather and sea conditions allowed. A large proportion of the trips carried out were 3 hours in duration, although in the peak season there were regular 4 hour trips and 1 ½ hour trips. The geography of Mount's Bay provides more shelter from the prevailing westerly and south westerly weather in some areas than others. These sheltered areas were surveyed more often, particularly in early spring and autumn. Feasible routes were selected to achieve relatively equal survey coverage of the inshore waters up to 5 km from the south coast. Waters between 5-10 km from the coast were surveyed less regularly.

3.2 High Resolution Bathymetry Map and Tidal Model

3.2.1 Generating a High Resolution Bathymetry Map

A detailed bathymetric model is essential for identifying accurate depth data at the locations of effort and sightings data points. This is necessary in order to understand how depth and topographic features influence harbour porpoise distribution. Often depth, slope and aspect are found to be important drivers for porpoise distribution (Heinänen and Skov 2015). An accurate bathymetric model allows accurate slope, aspect and roughness data to be generated. Several data sources were used in order to generate a robust bathymetry map. The Channel Coast Observatory (CCO) provides open source depth data for the study area out to roughly 30 m of depth and at a resolution of 1 m. Due to the high resolution nature of this data it was possible to generate a raster grid representing bathymetry at a resolution of 5 m with no interpolation. For areas not covered by this data Admiralty Maritime Charts from the UK hydrographic office were digitised and interpolated to generate a bathymetry

model. The hydrographic office charts are created using various professional hydrographic sources at varied resolutions. The data is interpolated to a 1 m depth resolution (United Kingdom Hydrographic Office 2023). Depth contours were digitised at intervals of 2 m. These were then transformed from polylines into points at 5 m intervals using the System for Automated Data Geoscientific Analysis (SAGA) tool Convert Lines to Points. The generated point data was interpolated using the triangular irregular network (TIN) interpolation in QGIS 3.10.8 (QGIS) ('Quantum GIS' 2021). TIN interpolation has been found to be accurate when compared with other techniques for generating bathymetric models (Ardron 2002; Andes and Cox 2017). TIN interpolations can generate a localised ridge effect in places leading to inaccuracies in the modelled bathymetry. A Gaussian smoother was applied using the SAGA smoothing tool to remove these artefacts from the generated raster grid (Ardron 2002). The two raster grids were combined to generate a continuous grid at a resolution of 5 m.

3.2.2 Tidal Data

Tidal data were generated using the AnyTide App produced by the National Oceanography Centre (AnyTide 2020). It provides modelled tidal flow data at a 1.8 km² resolution for the complete tide cycle each day. For each hour of the tide cycle on a typical spring and a typical neap tide, the tidal flow data was plotted in QGIS as a grid of points at 1.8 km² resolution. A 1.8 km² resolution raster was created for each hour of the tidal cycle using the tidal flow direction data. The tidal speed data was interpolated using inverse distance weighting with a weighting value of four from the grid of 1.8 km² spaced points. The weighting value of four was chosen to generate a more even change of values between points. The default value of two created localised peaks around data points and generated unlikely values in between data points. The interpolation produced a continuous surface for the tidal speed data for each hour of the tidal cycle. Two sets of tidal flow data were generated, one for spring tides and one for neap tides.

Tidal flow data can also be used to identify areas where tidal fronts might develop. Hydraulic tidal fronts are recognised as being productive areas which attract larger predators such as harbour porpoises (Johnston et al. 2005; Gilles et al. 2016; Lambert et al. 2017; Cox et al. 2018; Fernandez et al. 2018). Their productivity is enhanced seasonally as they typically form the boundary between mixed and stratified water and in this situation can be the location of persistent raised productivity (Cox et al. 2018; Suberg et al. 2019a). Tidal flow interacting with sea floor topography is what generates hydraulic tidal fronts. Changes in depth caused by underwater slopes and shallow areas generate turbulence in the water column. The level of turbulence generated is a product of tidal flow speed and depth. A stronger tidal flow generates the same turbulence in deeper water as a weaker tidal flow in shallower water.

Hydraulic tidal fronts develop at the boundaries between turbulent areas and areas where laminar flow is prevalent. Therefore the location of a tidal front is a balance between the water depth and the speed of the tidal flow. The typical position of summertime fronts can be approximated using the formula:

$$h/\langle|U|\rangle^3 = 500$$

where h is the depth in metres and U is average tidal flow speed in metres per second.

In this equation a larger product indicates increased mixing and turbulence and a lower product indicates less mixing and turbulence. 500 is an empirically determined value at which the boundary between mixed turbulent water and unmixed non turbulent water would exist (Thorpe 2007).

In reality the true location is also influenced by wind stress and stratification. However the equation provides a reasonable approximation which has been tested globally (Thorpe 2007). Typically in water of 60 m depth the effects of a current flowing at 1 ms^{-1} will occur between 60 and 90 minutes after that of water 5 m deep (Thorpe 2005). In water of 40 m depth the effects of turbulence at the seafloor were observed to take four hours to reach the the surface when stratification was limiting the turbulence. The surface products generated at hydraulic fronts can persist after the conditions generating the front have subsided. The length of time the products persist for depends on current speed and wind stress (Nimmo Smith et al. 1999). The locations of hydraulic tidal fronts where calculated using the above equation and the raster calculator in QGIS. The raster layers representing tidal flow speed were used along with the depth layer to calculate the mean front positions for each hour of the tide cycle.

3.3 Data Preparation

Initially accumulation curves of detection (see appendix 1) were generated for the categories sea state, boat speed, swell height and range to sighting. The accumulation curves identify the point at which sighting consistency drops. This is described as the inflection point (de Boer 2013; de Boer et al. 2018). The inflection point for each of the categories defined above was identified and used to filter the dataset. Only records collected under conditions that allowed for consistent detection of animals were retained. The sightings and effort data recorded in sea states of greater than 3 were filtered and removed from the data. The inflection point in the accumulation curve for harbour porpoises in sea state 4 is 33 m closer to the vessel than sea state 3 (de Boer et al. 2018). Effort and sightings recorded is sea states > 3 where removed this removed 94 949 out of 307 887 effort records. Likewise track data points showing a

boat speed less than 2 knots were removed because at these times the boat was not on effort (searching) this removed 25370 records. Another 1559 records were removed because the boat speed was greater than 10 knots. At speeds greater than 10 knots the sighting detections became inconsistent. A further 1190 records were removed because they were made when the visibility was poor. 281 of the removed records contained sightings and this reduced sighting occurrences to 1315. The sightings and track data were input into a GIS (Geographical Information System) in the open source software QGIS. A unique identification number was created by combining time and date. This was used to join relevant sightings data points to effort data points creating a single dataset. The effort data were gridded and summed at 500 m resolution in order to identify spatial bias in survey coverage. The 500 m resolution was chosen based on the inflection point of the range to sighting curve (appendix 1). Animals were consistently detected up to a distance of 300 m either side of the vessel. The effort data were used to create grid files for each hour of the tide cycle so that effort could be included in all models. This allowed the impact of bias survey coverage to be accounted for in the modelling process (De Rock et al. 2019).

The previously constructed bathymetry map was used to generate slope and aspect rasters. A value for depth, slope and aspect were extracted for every effort record. Slopes greater than 5% were selected as being significant and the aspect of these slopes calculated. The distance from each data point to these slopes was calculated using the Nearest Neighbour Join plugin version 3.1.3 (‘Quantum GIS’ 2021). This value along with the steepness and aspect of the slope were added to the dataset. The roughness at each data point location was calculated using the Geospatial Data Abstraction Library (GDal) roughness tool in QGIS (‘Quantum GIS’ 2021). This tool calculates the variation in elevation (in this case depth) by comparing a pixels value with the value of the pixels surrounding it. The roughness value at each data point was added to the data set. The data for tidal flow speed and direction were also added to each data point. In order to do this Hydrographic Office tidal data were used to identify the tidal range and hour of the tide cycle for each data point. This information was used to extract the correct tidal flow direction and speed data from the rasters created using the AnyTide app data for each data point in the dataset. The interaction between sea floor topography and tidal flow and its impact on tidal process is widely discussed in the literature. Changes in depth, uneven topography, breaks in the coastline, island structures and underwater pinnacles can all create a variety of processes, which enhance the foraging success of piscivores (Nimmo Smith et al 1999; Gómez-Gutiérrez and Robinson 2006; Embling et al. 2012, 2013; Jones et al. 2014; Benjamins et al. 2015; Cox et al. 2018). The focus of piscivores in an area has the potential to create foraging opportunities for harbour porpoises.

3.4 Satellite Data

Satellite data for sea surface temperature (SST), chlorophyll (CHL) and front metrics were generated from satellite images. The SST and CHL front metrics data were generated from images captured by the Advanced Very High Resolution Radiometer AVHRR sensor. The AVHRR images are at a resolution of 1 km² and generated from daily composites in order to remove the effects of cloud cover. An individual SST value was extracted for each effort data point. If a value was missing due to cloud cover or other technical issues -999 was used to signify no data. The match up between data point and image value allowed for up to + or - 3 days either side of each data point timestamp in order to minimise the amount of missing data. Thermal fronts were identified by Peter Miller (Plymouth Marine Laboritories) using the single-image edge detection (SIED) algorithm (Cayula and Cornillon 1992). The fronts were detected on images for 3 days either side of the time of each data point. The fronts detected were combined to create a more complete picture by removing the impact of cloud cover. Thermal fronts are areas where two sea surface temperature zones meet. In this case they are where the warmer stratified water from the Bay of Biscay meets cold tidally mixed shelf water off the coast of the UK (Suberg 2015; Suberg et al. 2019). These frontal areas are often associated with increased primary productivity (Schick 2002; Cox et al. 2017, 2018; Suberg et al. 2019). Values for front persistence (Fpers) and front density (Fdense) were calculated based in the temperature gradient across the front and the length of time it was present for. These values were added to each data point along with a value for the distance the point was from the nearest front (Fdist) and whether the point was on the cold (mixed) or warm (stratified side) of the front (Fside). The values calculated from the fronts are detailed in table 2 and described by Suberg et al. (2019) in their study (Suberg et al. 2019).

On some occasions the fronts identified using satellite SST data are likely to coincide with the tidal mixing fronts discussed in section 3.2.2. The thermal fronts are found at locations where stratified water borders turbulent water mixed from the seabed to the surface. The mixing is caused by tidal flow and wind (Thorpe 2005; Suberg et al. 2019). The stratified oceanic will influence the buoyancy flux, which was the factor not accounted for in the earlier equations used to derive approximate tidal front locations. Buoyancy flux, tidal flow and depth are the three main factors influencing the location of tidal fronts (Thorpe 2007). Stratification also influences the length of time taken for bottom turbulence to trigger billows at the surface (Nimmo Smith et al. 1999) so the level of stratification will temporally influence the tidal front processes.

The frontal data derived from satellite images is generated using composites created over several days. This temporal scale does not allow for variations in frontal locations related to the semi diurnal tide cycle to be identified. However evidence for frontal activity derived from satellite imagery might be linked to the overall

productivity of the area and influence the number of animals present in the study area (Lambert et al. 2017). Thermal boundaries and their gradients may also influence the intensity of tidal fronts.

Chlorophyll data was generated from the MODIS sensor, which provides a value for surface chlorophyll in mg m^{-3}. The MODIS images are at a resolution of 1 km^2 and made up of daily composites to avoid cloud cover where possible. The data match up between each data point and image value allows for + or – 3 days either side of the data point timestamp to reduce the number of missing values. This limits the usefulness of the satellite data for fine scale analysis because exact frontal positions move across the tide cycle and with changing weather conditions. These variations can effect chlorophyll density. The chloropyll data was provided by Peter Miller of Plymouth Marine Laboratories. The composites where created using the method described in the Suberg et al 2019 study (Suberg et al. 2019).

Name	Common name	Description	Typical value
Fvalid	Valid pixels	Total valid frontal pixels in sequence of images	Any positive integer
Fpixels	Clear pixels	Total clear frontal pixels in sequence of images	Any positive integer
Fmean	Temperature gradient	Temperature Gradient / Fvalid	0-2.54
Fcomp	Front composition	Fpers x Fprox (Fprox = additional boost when other fronts have close proximity)	0-0.254
Fprob	Front probability	Fvalid / Fclear	0-1
Fpers	Frontal persistance	Fprob x Fmean	0-0.254
Fdense	Frontal density	Fcomp + spatial smoother	0-0.254
Fdist	Front distance	Distance from nearest front	Any positive integer
Fside	Front side	Side of nearest front -1 cold side, 1 warm side, 0 on front	-1, 0, 1

Table 2: A list of the front metrics used in this study with common definitions (Suberg et al. 2019).

3.5 Collinearity of Independent Variables

All the independent variables were checked for collinearity (Appendix 2). If the relationship between two variables is collinear one will change relationally when the other changes. Collinearity in independent variables used in species distribution models (SDM) and Ecological Response modelling (ERM) can generate unreliable results (Halvorsen 2013). Before proceeding with modelling, collinearity was investigated using correlation coefficients. If it was found that any pairs of features were positively or negatively correlated, one of the two features was removed before the modelling process was started. Pearson's Correlation Coefficient was used for this process: a value of 1 would show perfect positive correlation between two features, and -1 shows perfect negative correlation. The value 0 shows no correlation between two features (Brownlee 2020). The values 0.7 and -0.7 were used as a threshold to determine if two features were overly correlated. If two features were found to have a correlation stronger than 0.7 then one of them was removed from the modelling process. Bosch et al. (2018) identified independent variables with a correlation coefficient stronger than 0.7 to be correlated (Bosch et al., 2018). Zurr et al. (2009) state that a correlation coefficient of 0.6 is acceptable, and MacLoed (2013) identifies

a correlation coefficient 0.8 as an acceptable boundary to including both independent variables in a model (Zurr et al. 2009; MacLoed 2013). 0.7 was chosen in this case because it is the mean of these three examples.

3.6 Species Distribution and Ecological Response Modelling

3.6.1 MaxEnt Model

Maximum Entropy modelling (MaxEnt) is a popular machine learning approach used to generate SDM and ERM in ecology (Halvorsen, 2013; Merow et al. 2013; Merow and Silander 2014; Morales, Fernández and Baca-González 2017). It compares well to other models in predictive ability often outperforming other presence only species distribution models (Merckx et al. 2011). MaxEnt calculates a relative predicted probability of presence (RPPP) for one or more species across a user defined geographical space by minimising the Kullback-Leibler divergence also known as relative entropy. The model minimises the relative entropy between the distribution of presence records against the predicted distribution of presence. The predicted distribution of presence is calculated using the independent variables, identified as predicting the preferred habitat for a species. In grid cells with a recorded presence of a species the values of independent variables are assessed by the model and used to predict presence in other areas of the geographic space (Elith et al. 2006; Halvorsen 2013).

Although MaxEnt is typically used as a presence only model it can also be implemented as a presence absence model (Thibaud et al. 2014). Implementing it as a presence absence model typically improves its accuracy and changes the RPPP output to a predicted probability of presence (PPP) (Halvorsen 2013). The presence absence approach is known as a discriminative approach to MaxEnt compared to the generative presence only approach. In the discriminative approach the absence data, in this case generated from the effort data (Table 1), is included with the background variables used to predict the RPPP of the species (Halvorsen 2013; Thibaud et al. 2014). Guillera-Arroita et al. (2014) argue that the discriminative approach is not a true presence absence model and the results should still be considered RPPP rather than PPP. To generate PPP results the outputs need to be scaled by dividing the number of detections against the total number of surveyed sights and using this to scale the RPPP result (Guillera-Arroita, Lahoz-Monfort and Elith, 2014). In this study the effort was used to account for surveying bias however RPPP was not scaled to PPP. Biased survey effort is considered a nuisance effect in species distribution modelling and this approach allows the model to account for it when predicting RPPP (Giné and Faria 2018).

Survey effort bias was assessed spatially and across each of the independent variables used to generate the background files (Table 5). The values of the independent variables were extracted at a 60 m² resolution across the whole survey area and they were ranked by the frequency with which they occurred. The same was then done at the location of each effort record. The frequency lists were then partitioned in to 20 bins and Spearman's rank correlation coefficient was calculated. Assessing effort against available background points is necessary to identify bias coverage in the modelling process particularly when modelling marine species, which live in dynamic environments (Fernandez et al. 2018). A score of 1 would indicate that survey coverage was perfectly even across the study area for an independent variable. A score of less than 0.5 would indicate that survey coverage is biased. To account for potential bias in survey coverage 13 bias files were generated, one for all of the survey effort and one for each hour of the tidal cycle. To generate these files survey effort was converted to polyline format and a grid with a resolution of 500 m² created in QGIS. The number of times an effort line crossed a grid was counted for each grid cell. A survey line crossing a grid cell was considered to represent a visit to that grid cell. The cumulative frequency curves (Appendix 1) assessed that porpoises were consistently detected up to 300 metres either side of the survey vessel. A 500 m² grid fits within these detection distances. The grids generated were used to create an ASCII file representing survey effort for each of the 13 models. The model uses the generated bias file to weight the modelling process. A grid cell with higher effort is considered weighted to be more influential in the model than one with low effort. Cells with no effort were given a median weighting to allow them and even chance of selection.

MaxEnt is often implemented using the default parameters (auto features, prevalence value of 0.5 and the regularisation multiplier set to 1), however this does not always produce the best results and often leads to a model with either bias or too much variance (Halvorsen 2013). Tuning machine learning models (MLM) is considered to be a balance between bias and variance (Geman et al. 1992). Bias is caused by the model being too simple and making erroneous assumptions. If a model has high bias it is likely to be under fitting and failing to pick out the trends in the data. High variance typically occurs when the model is complex and responding to and detecting small variations in the data. In this case the model is said to be over fitting. The model would have high accuracy scores when applied to the training data. However it is unlikely to be accurate at predicting in new scenarios (Geman et al. 1992). Ideally the model should accurately identify the trends in the data without being too sensitive and over fitting to the data used to train it. Over fitting is a more common problem with medium to large ecological datasets and particularly when a model is complex and includes a high number of independent variables (Merckx et al. 2011).

The regularisation parameter is a weighting used in MaxEnt to control how closely the model fits the presence data. The default setting is 1. If it is set to a value lower than 1 then the model fits the presence data more closely. The lower the value the closer the fit, which can lead to over fitting. If the value is set higher than 1 then the model will generalise beyond the presence data. The higher the value the more general the model. Higher values identify larger areas as key habitat whereas smaller values typically identify more restricted ranges (Phillips 2017). MaxEnt transforms the independent variables to create feature classes that are then used to inform the model. It has a number of different options to generate the features used in the model: linear (L), quadratic (Q), product (P), threshold (T), and hinge (H) (Phillips 2017). The default settings allow the model to include all of the feature classes and this will generate more features than independent variables. This is not always desirable because it can create an overly complex model which tends towards over fitting (Elith et al. 2011). During model selection it is important to identify the feature classes that produce the most predictive model without over fitting (Morales et al. 2017).

Variable name	**Measurement unit**	**Variable description**
Latitude	Decimal degrees	The position north from the equator
Longitude	Decimal degrees	The position west from the prime meridian
Depth	Metres	The depth at chart datum in metres calculated from bathymmetry map described in 3.2.1
Slope	Percent	Seafloor slope steepness extracted from the bathymmetry map described
Aspect	Categorical	Seafloor slope aspect extracted from the bathymmetry map described in 3.2.1 categrised as: N-ENE, ENE-ESE, ESE-S, S-WSW, WSW-WNW, WNW-N
Roughness	Metres	The difference in depth across each 5 metre grid cell on the bathymmetry
Distance to the nearest predicted tide front	Metres	Distance to the nearest tide front calculated as described in section 3.2.2
Distance the nearest significant slopes	Metres	Distance to the nearest seafloor slope > 5°
Substrate	Categorical	The type of seafloor substrate: coarse sand, mixed sediment, rock and diamicton or sand and muddy sand
Tide flow speed	Metres per second	The speed of the tidal current
Tide flow direction	Degrees	The direction of the tidal current

Table 3: The independent variables used in the MaxEnt modelling.

A number of different models were fitted to the data in order to identify RPPP and the independent variables most effective at accurately identifying RPPP. The influence of both the spatial and temporal variables described in table 3 were investigated. The variables were used to create background files. The background files were generated as ASCII files at a resolution of 60 m² because this was identified as being the minimum spatial accuracy of sightings. The first model included all of the presence data. 12 further models were then fitted, one for each hour of the tide cycle. This allowed for the effects of the temporal variables (tide front location, tide flow speed and tide flow direction) on the RPPP of harbour porpoises to be assessed. The temporal background layers were updated for each of these models. For each hour the predicted location of the tidal front for the hour of the tidal cycle being investigated and locations of tidal fronts for each of the previous three hours of tide cycle were included. This was done to account for the time lag between tidal turbulence occurring at the sea floor and rising to the surface discussed in section 3.2.2.

Each model was run using the bootstrap approach 25% of the data was randomly selected for a model run to be used as test data and 100 model runs were carried out (Mikkelsen et al. 2016). Model accuracy was assessed using the area under the receiver-operator curve (AUC) score along with the standard deviation of the AUC across 100 model runs. AUC compares the likelihood of a presence location RPPP score ranking above a background location RPPP score (Halvorsen 2013; Merow et al. 2013). It is an assessment of how accurately the model is predicting presences and is an appropriate way to evaluate MaxEnt models, particularly when the prediction area does not extend beyond the survey effort (Boyce et al. 2002). The standard deviation of AUC across the 100 model runs was also used to assess the consistency across the models. A further evaluation of model performance was carried out by comparing species observations per metre of searching effort (OMS) against the response curves output by the model for each of the environmental variables (Merow et al. 2013). The number of observations at each value of an environmental variable were calculated along with the searching effort. These values where then separated in to 20 bins and the sum of the observations divided by the sum of the effort. A histogram plot was generated and overlayed on the response curve plots. This approach allows the trend in OMS to be compared with the trend in the response curve. If a model fits the data well it would be expected that the OMS histogram and the response curve would follow a similar trend.

3.6.2 General Additive Model for Locations, Scale and Shape

The General Additive Models for Locations, Scale and Shape package (GAMLSS) (Stasinopoulos et al. 2008) was used in R 3.4.2 (R Core Team, 2017) to fit the effort/sightings data to various models, using distributions suitable for count data in order to find the most appropriate model for the data set (Stasinopoulos et al. 2008).

Initially the independent variables included were all of the satellite data categories along with year and month. The response variable was harbour porpoise count at each unit of effort. Two different models were created, one including front persistence and the other front gradient density. This was due to their collinearity described in section 3.5 shown in appendix 3 and table 7. Scatter plots and histograms (Appendix 3) were used to identify extreme outliers, assess effort bias and assess the distribution of the independent variables. A number of different distributions designed for count data were tested: Poisson (PO), negative binomial Type 1 (NBI), Poisson-inverse Gaussian (PIG), Delaporte (DEL) and zero inflated Poisson (ZIP). The Global deviance (GD), Akaike information criteria (AIC) and Schwarz Bayesian information Criterion (SBC) were used to select the best performing model. The model with the lowest GD and highest AIC and SBC was selected as the best.

Model fit was checked by assessing and plotting the normalized randomized quantile residuals (NRQR). The NRQR were plotted against the fitted values of the model, against an index, as a kernel density estimate of NPQR and in the form of a quantile quantile (QQ) plot. If residuals are performing well then the mean will be nearly zero, their variance nearly one, the coefficient of skewness will be near zero, and the coefficient of kurtosis close to three (Stasinopoulos et al. 2008).

Once the model was selected feature selection was carried out. Feature selection is when the influence of each of the independent variables is tested, in this case: SST, CHL, Fdist, Fper, Fdense along with year and month. The function dropterm() from the MASS package was used to carry out feature selection in the model (Venables and Ripley 2002). Dropterm() iterates each time leaving out one of the variables and assesses the impact on the performance of the model. Dropterm() identifies the significance of each variable using a p-value calculated using Chi squared to test goodness of fit. A second test stepGAIC() from the MASS package was also used for feature selection. The stepGAIC() function assesses feature contribution as well and how complicated the model is with the selected features included. In statistical modelling it is always preferred to identify the simplest model with the most explanatory power. In this application of stepGAIC() a backward elimination was performed in order to eliminate independent variables with non significant predictive power. Partial dependence plots were generated for significant variables in order to visualise the relationship between the independent variable and the response variable.

4 Results

4.1 Initial Data Investigation

4.1.1 Survey Effort and Sightings

A total of 48 782 km of survey effort was included in the study after data preparation was completed. 8030 individual harbour porpoises were recorded during 1604 encounters. The average group size was five animals. Over the eight year study period the number of porpoises sighted per 100km increased peaking at 39.1 animals per 100 km in 2018 (Figure 5). When compared with other areas of the United Kingdom (UK) the number of animals sighted per 100 km in Mount's Bay suggests it has a high density of harbour porpoises. The West of Scotland is a candidate site for a special area of conservation for harbour porpoises (Heinänen and Skov 2015). A 2013 study of harbour porpoise habitat preference in the West of Scotland recorded between 4 and 13 porpoises per 100 km of survey effort across the years 2003 - 2010 (Booth et al. 2013). Between 2002-2004 Goodwin and Speedie recorded a sighting rate of 26.3 per 100 km effort for the West of Scotland and 2.5 per 100 km for West Wales another area identified as a candidate SAC for harbour porpoises (Goodwin and Speedie 2008; Heinänen and Skov 2015).

Year	Distance km	Sightings	Sightings per 100km
2011	6178	338	5.5
2012	6645	596	9.0
2013	6985	1019	14.6
2014	7471	767	10.3
2015	6466	966	14.9
2016	7235	1606	22.2
2017	3510	1060	30.2
2018	4292	1678	39.1

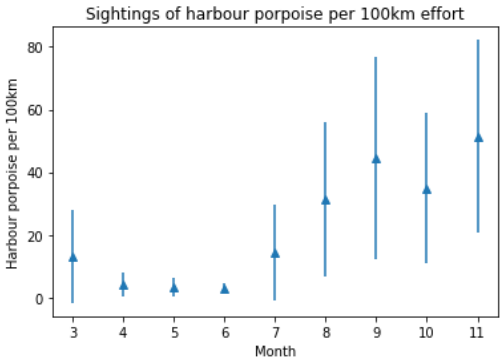

Figure 5: The table on the left shows the distance surveyed in sea state ≤ 3 and number of harbour porpoise sightings 2011-2018 in Mount's Bay, Cornwall The plot on the right shows harbour porpoises sighted per 100 kilometres travelled each month in Mount's Bay, Cornwall. Data collected between 2011 – 2018. Error bars show standard deviation across years.

The sightings rate in Mount's Bay compares favourably to sites identified as being nationally and internationally important for harbour porpoises (Booth et al. 2013; Heinänen and Skov 2015). It is important to note that the surveys in different areas were conducted with different methodologies and therefore direct comparisons should be made with caution. There is a seasonality to sightings in Mount's Bay. This indicates that the survey area is a smaller part of a wider habitat used by harbour porpoises and that the animals recorded are part of this wider population. It has been

observed that tagged porpoises range across a core foraging habitat of between 122 km² and 415 km² whilst ranging over wider areas annually (Johnston et al 2005). The survey effort covered an area of 399 km² so it is likely that they frequent a wider habitat than the study area covers. The seasonality of sightings in Mount's Bay is shown in Figure 5. An index of abundance grid (Figure 6) was created to initially assess the distribution of high density areas across Mount's Bay. The map shows that the occurrence of porpoises is not evenly distributed across the bay. Harbour porpoises are high foraging animals (Wisniewska et al. 2016) and therefore their distribution is influenced by environmental factors that enhance their foraging success (Booth et al. 2013; Jones et al., 2014; Cox et al. 2017).

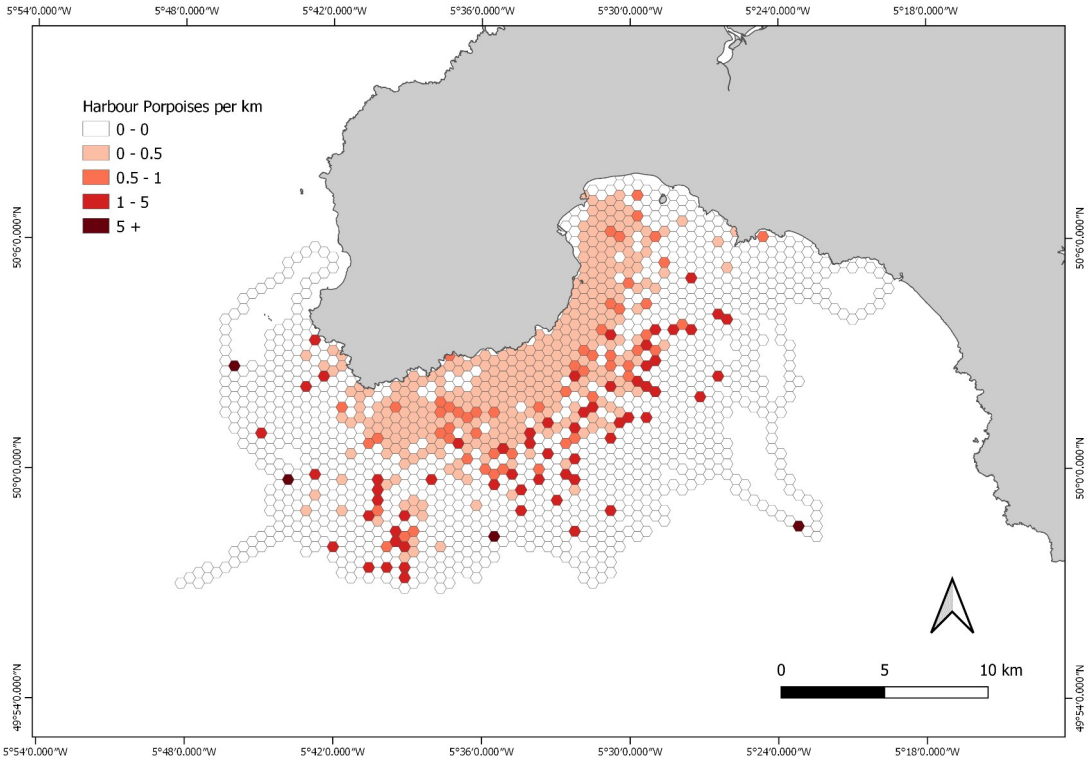

Figure 6: Harbour porpoises sighted per kilometre travelled in Mount's Bay, Cornwall gridded at 500 metre resolution.

4.1.2 Collinearity of Independent Variables

Pearson's correlation co-efficient was used to assess the collinearity of the independent variables (see appendix 2 for detailed results). It was found that the variables depth and latitude (y) had a correlation coefficient of 0.874, which is above the 0.7 threshold for retaining both variables. It was decided that depth was a more useful independent variable to include so latitude was removed from all models. It was also found that front persistence and front gradient density had correlation coefficients greater than 0.7. In order to avoid this impacting the GAMLSS models

two separate models were run. One including front persistence and the second including front gradient density.

A further collinearity test was carried out using Pearson's correlation coefficient on all of the background layers generated for MaxEnt (see appendix 2 for detailed results). A number of the tide front layers show collinearity with each other and with the complete tide front layer. However they will all be used individually within different models so the collinearity was not important in this case.

4.1.3. MaxEnt Model

4.1.3.1 Overview

A model run was completed using all of the data. This used 1210 presence locations and the background layers: aspect, aspect of the nearest slope, average chlorophyll, distance to the nearest tide front, latitude, depth, distance to the nearest slope and substrate. The background layers for aspect of nearest slope, average chlorophyll, roughness, tide speed, tide direction and slope were removed from the model because they did not provide any extra explanatory value and including them increased the complexity of the model. Table 3 provides definitions for each of the features used in the models.

A bias file representing effort across the survey area was included in the model. The model was run 100 times using bootstrap and a 25% random test sample was selected during each model run. Further models were run for each hour of the tide cycle: in each case the background layer distance to the nearest tide front was replaced by the tide front layer representing the relevant stage of the tide cycle and the bias file was also adjusted to represent survey effort for the relevant hour of the tide cycle. The number of presence points for each model are shown in table 4.

Tide Hour	Number of presence locations
HW	71
HW + 1	80
HW + 2	91
HW + 3	118
HW + 4	98
HW + 5	79
LW	172
HW – 5	116
HW – 4	106
HW – 3	96
HW – 2	107
HW – 1	76

Table 4: Number of presence records at each hour of the tide cycle.

For all models the regularisation parameter was set to one, which is the default. Different values were tested for the regularisation parameter. Reducing the regularisation parameter caused the partial dependence plots to appear more over fitted with no improvement in the AUC score and in some cases a reduced AUC score. Increasing the regularisation parameter caused a drop in AUC scores in all models. Values between 0.5 and 1.5 were tested in increments of 0.1 (Elith et al. 2011; Phillips 2017).

4.1.3.2 Effort bias

Effort bias was evaluated by comparing the values of the independent variables across the whole study area with their values at each point of recorded effort. These were ranked and partitioned in to 20 bins for comparison. The results are shown in table 5 and, whilst some of the independent variables were evenly surveyed, many were not. The default setting in MaxEnt assumes even survey coverage therefore in this case the use of bias files was necessary in order to account for the bias in survey effort (Elith et al. 2011; Halvorsen, 2013; Guillera-Arroita et al. 2014; De Rock et al. 2019).

Independent Variable	Available/Effort
Depth	0.206
Longitude	0.349
TiFrDist	1
NrSlDist	0.995
AVGChl	0.692
Aspect	0.054
AspectNrSl	0.759
Substrate	0.4

Table 5: This shows the Spearman's rank correlation coefficient between the frequency of values of independent variables at survey effort locations and the frequency of the values of independent variables across the whole study area. A value of one shows perfect correlation and would indicate even survey coverage with lower values indicating increasing survey bias.

4.2 MaxEnt Model Results

The results are presented as a series of graphs with response curves overlaid with histogram plots and distribution maps. The scale for the response curves is the relative predicted probability of presence (RPPP) and a value of 0.5 represents an even chance of presence any value over this indicates an increased likelihood of presence (Phillips and Dudík 2008) and any value below represents a likelihood of presence below 50%. In habitat modelling log odds or probability values are usually scaled from zero to one but in MaxEnt this works differently due to how the model functions and the scale can

extend beyond one (Phillips and Dudík 2008). The histogram plot represents OMS binned in to 20 categories for each variable. The OMS histogram represents the trend in OMS across the variable range and is added to identify whether the trend in OMS matches the response curve predicted by the model.

4.2.1 The Model Using all Data

4.2.1.1 Overview

The mean AUC score after 100 runs was 0.826 with a standard deviation of 0.016, which is considered a good score and suggests the model is predicting the relative presence of porpoises well. The low standard deviation value shows there is consistency in accuracy across the 100 models. Longitude is calculated to be the most important variable contributing 62.5% to the prediction, substrate is second at 16.2%, depth third at 9.6%, distance to the nearest slope is fourth at 6.8%, distance to the nearest tide front is fifth at 3.2% and aspect contributes 1.7%.

4.2.1.2 Longitude

The response curve for longitude (Figure 8 bottom left) shows two strong peaks of RPPP at -5.67 and -5.49 decimal degrees. In between these two peaks the response curve dips slightly but still predicts a high RPPP. The OMS histogram reflects the response curve with peaks in observations at -5.68 and -5.49 decimal degrees. The dip between the two peaks in the OMS histogram is more extreme than the dip in the response curve. The rise and fall at either end of the response curve reflects the rise and fall of the OMS histogram. The response curve appears to be a strongly smoothed model of the OMS histogram data. The RPPP is above 0.5 between -5.79 and -5.38 decimal degrees and this is supported by the longitude range covered by the OMS histogram data.

4.2.1.3 Substrate

The model predicts high RPPP values of 1.1 for sand and muddy sand and 1.6 for coarse sand . A negative RPPP of -0.4 is predicted over rock and diamicton and zero RPPP is predicted for mixed sediment. The location of observations plotted in figure 7 explain the response plot well. The majority of the survey area is sand and muddy sand or coarse sand covering the next most extensive area. Most of the observations are over either sand and muddy sand or coarse sand, which explains why the model has a raised RPPP for these categories. This also fits with findings in the literature which suggest that coarse sand and mud and sand are preferred habitat for harbour porpoises (Embling et al. 2010; Booth et al. 2013; Heinänen and Skov 2015; JNCC 2017; Williamson et al. 2017). There are a small amount of observations over rock

and diamicton and this small number explains the negative RPPP values. There are no observations over the mixed sediment, which explains the zero value.

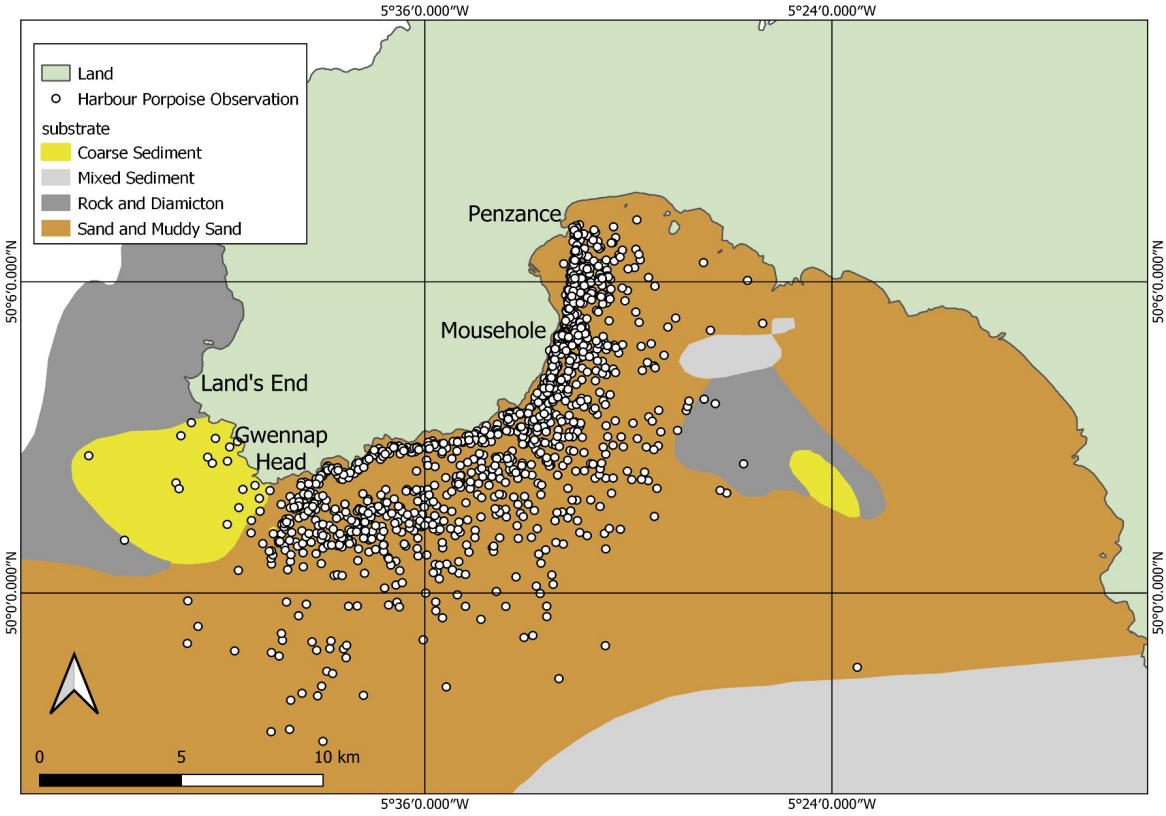

Figure 7: Harbour porpoise occurrences in relation to substrate type in Mount's Bay, Cornwall

4.2.1.4 Depth

The response curve for depth (Figure 8 top left) shows a steep increase in RPPP from -70 m to an RPPP peak of 1.7 at -58 m depth. The RPPP value stays high with a steady decrease to a value of 1.5 at -15 m depth. The RPPP declines sharply to 1 at -5 m and then to 0 at 0 m. The OMS histograms reflect the raised RPPP between -58 m and -15 m. Although the OMS histogram shows a peak between -50 and -42 m depth. The depths between -50 and – 40 m have a high amount of effort so these values are likely to be accurate. After this peak in the OMS histogram there is a decline in values that follows the trend of the response curve.

4.2.1.5 Distance from the Nearest Significant Slope

The plot for distance from the nearest slope is shown in the bottom right of Figure 8. The RPPP rises quickly to an initial peak of 0.74 at a distance of 200 m from the nearest slope. It then drops to 0.7 before climbing to 0.88 at a distance of 2000 m from the slope. It follows a concave downward curve to a value of 0.8 at 4000 m from

the front before starting a sharper decline to a value of 0.7 at 4600 m. It then steadily declines to a value of -0.8 at 11500 m. The OMS histogram follows the trend of the response curve well with peaks in OMS values at 2000 m and 4000 m. There is a dip in OMS values between these two distances, which is not reflected in the response curve. At distances further than 4000 m the OMS values drop in line with the declining values of RPPP shown by the response curve.

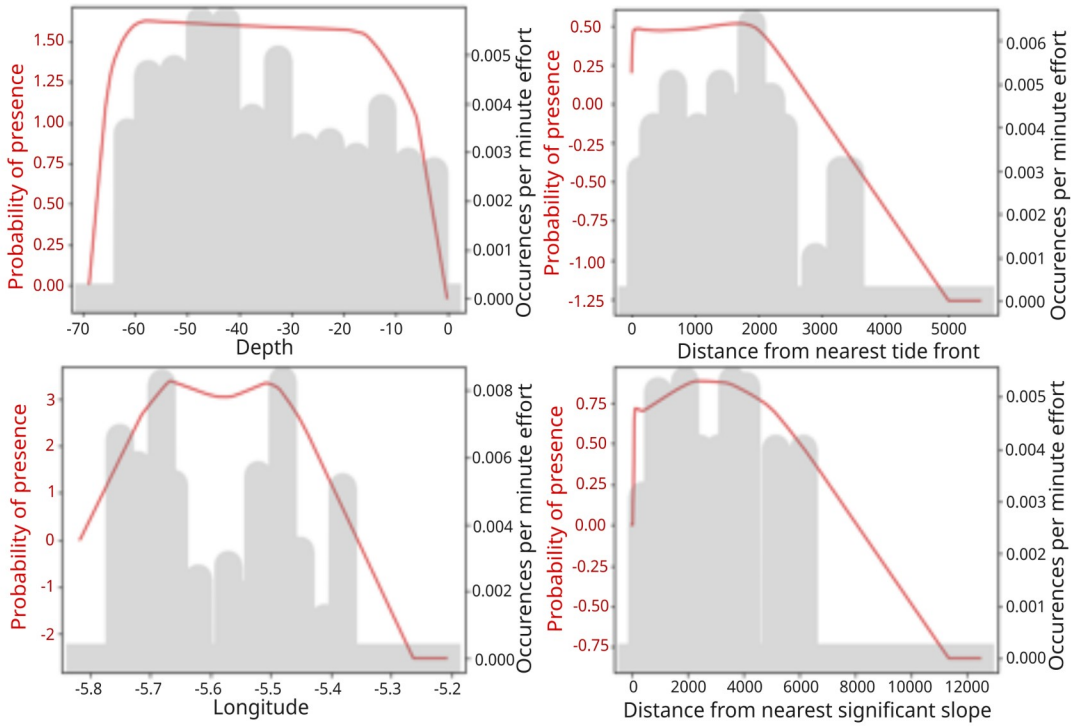

Figure 8: Response curves for variables used to predict harbour porpoise presence in Mount's Bay, Cornwall overlaid with histograms representing occurrences related to effort. The value related to the variable is on the x axis, the y axis on the left hand side represents probability of presence and the y axis on the right represents the occurrences per minute searching and relates to the histogram plot.

4.2.1.6 Distance from the Nearest Tide Front

The response curve for distance from the nearest tide front is shown in the top right of Figure 8. The RPPP is 0.25 at 0 m from the front before rising to an initial peak of 0.49 at a distance of 100 m from the nearest front. It then follows a slight concave curve to the highest RPPP peak of 0.51, 1900 m from the nearest front. Between 2000 m and 3000 m it declines steadily to an RPPP of 0. The steady decline continues between 3000 m to -1.25 at 5000 m. The OMS histogram values follow the trend of the response curve. The histogram values build more steadily between 0 m and 500 m before dipping slightly and then building again to a peak at 1900 – 2000 m. This reflects the slight concave shown in the response curve for this area and the highest peak in the response curve. After this point there is a decline in OMS histogram

values, which follows the trend shown by the response curve. The exception is the OMS value at 3000 m, which is lower than the surrounding values. This is a value that has low effort and as such the values have uncertainty attached to them. The model continues a steady decline at this point smoothing this potential anomaly.

4.2.1.7 Aspect

The model predicts an increased relative likelihood of detecting harbour porpoises over slopes facing ENE – ESE, WSW – WNW and WNW – N. The RPPP value is highest for WNW – N slopes at 0.2. Relative predicted occurrence is least likely on slopes facing S – WSW and slopes ESE – S.

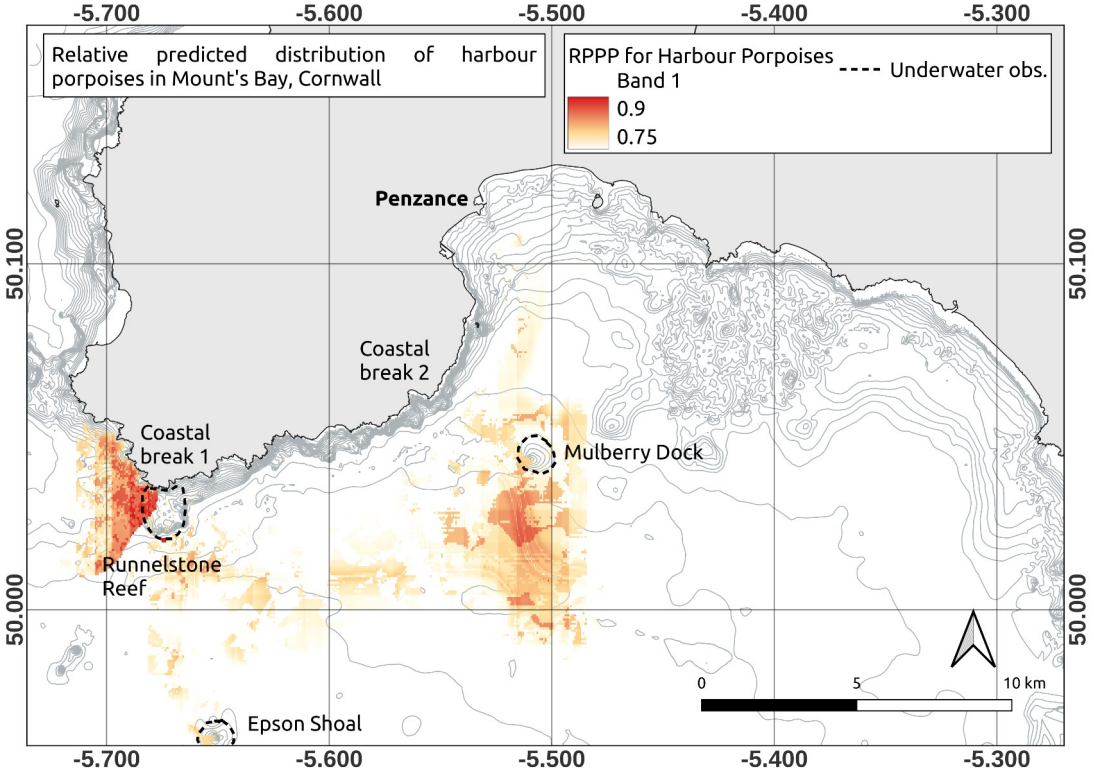

Figure 9: Relative predicted probability of presence for harbour porpoises Mount's Bay, Cornwall. Only areas with RPPP greater than 0.75 are coloured. The dashed boundaries identify key reef and wreck areas. Depth contours are also shown in order to demonstrate the complexity of bathymetry across the area.

4.2.1.8 Distribution of Relative Predicted Probability of Presence

The model predicts the areas with highest RPPP are located to the west of and over the Runnelstone Reef. There are also areas with high RPPP around the Mulberry Dock and to the south of it. There are further areas with increased RPPP between the Runnel Stone Reef and the Epson Shoal and around the Epson Shoal. There are also areas with RPPP > 0.75 between the Runnelstone Reef and the Mulberry Dock as well

as to the north of the Mulberry dock (Figure 9). The Runnelstone Reef, the Mulberry Dock and the Epson Shoal are all reef structures that will generate turbulence under certain tidal conditions. This turbulence is likely to generate oceanographic processes that may have influence kilometres from the structure. Likewise coastal break 1 and coastal break 2 and the rough bathymetry around them will generate similar turbulent effects.

4.2.2 The Models for each Hour of the Tide Cycle

The response curves and histogram plots for the models at each hour of the tide cycle are presented in appendix 5. Table 6 lists the AUC and deviation scores of the models. The models all have high AUC scores of above 0.93 with small deviations across their 100 runs. This demonstrates the model predictions are an accurate representation of the data. The influence of the environmental variables in the modelling process are also listed in table 6. In all cases longitude is the most influential variable. Depth is typically the second most influential variable and substrate the third. The models for high water and four hours after high water and two hours before high water are the exceptions. The distance to the nearest significant slope, distance to the nearest front and aspect are typically the three least influential variables. In many cases distance to the nearest significant slope is more influential than the other two (high water +2, high water +3, high water +4, high water +5, low water, high water -4, high water -3, high water -2, high water -1). At high water -1 distance to the nearest significant slope is the third most influential.

Hour of the tide cycle	AUC	Deviation	Environmental variables % contribution					
			Longitude	Depth	Substrate	Dist. nr. sig. Slope	Dist. nr. front	Aspect
High water	0.94	0.01	36.7	16.5	18.5	8.5	11.5	8.1
High water +1 hour	0.95	0.009	42.6	21.2	16.6	7.2	5.2	7.3
High water +2 hours	0.95	0.007	34.2	26.7	19.6	10.9	4	4.7
High water +3 hours	0.94	0.009	40.7	24.8	21.4	7	3.8	2.3
High water +4 hours	0.94	0.011	34.6	22.5	25.1	8.6	3	6.3
High water +5 hours	0.96	0.007	34	32	17.9	7	6.7	2.3
Low water	0.96	0.006	36.8	20.7	20.6	11.6	8.3	2
High water -5 hours	0.95	0.009	46.7	24.1	14.1	5.2	6	3.8
High water -4 hours	0.95	0.007	48.7	17.2	16.6	11.1	2.3	3.9
High water -3 hours	0.95	0.01	45.9	18.5	13.7	9.1	4.2	8.7
High water -2 hours	0.95	0.009	39.6	16.2	23.2	9.1	6.3	5.7
High water -1 hour	0.94	0.012	51.5	14	8.4	13.1	5.3	8

Table 6: The results from the discriminative MaxEnt models for each hour of the tide cycle. The performance of each model is shown by the AUC score and deviation. The percentage contribution of each variable in each of the models is also shown.

4.3 Distribution of Relative Predicted Probability of Presence for each Hour of the Tide Cycle

During the tide cycle, the areas with the highest RPPP change and appear to be linked to the speed and direction of tidal streams. Figures 10 – 21 show the RPPP prediction at each hour of the tide cycle. The figures also include depth contours highlighting significant seafloor slopes, hydraulic tide fronts and tidal arrows representing the direction and speed of the tidal current.

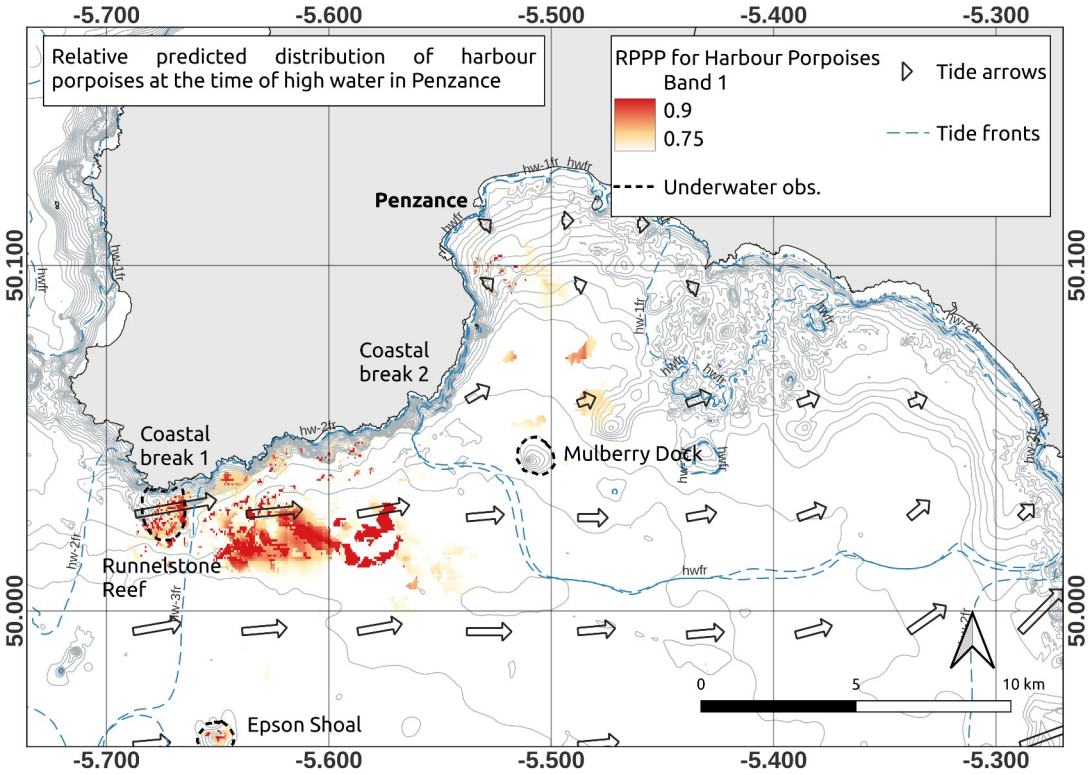

Figure 10: Relative predicted probability of presence at the time of high water in Penzance, Mount's Bay, Cornwall. Only areas with RPPP greater than 0.75 are coloured. The arrows depict the direction and strength of the tidal flow. The dashed boundaries identify key reef and wreck areas. Depth contours are also shown in order to demonstrate the complexity of bathymetry across the area. The blue dashed lines represent the tide fronts used in the modelling.

At the time of high water in Penzance, the areas with highest RPPP are around the Runnelstone Reef, to the west of the Runnelstone Reef and around the Epson Shoal. There are also a number of smaller areas closer to the coast to the west of the Runnelstone Reef and some similar areas between Penzance and the Mulberry Dock (Figure 10). The tidal stream is travelling from west to east and is strongest as it crosses the Runnelstone Reef. The tidal flow is weaker in the areas to the north of the Mulberry Dock due to the shelter caused by the direction change of the coast at coastal break 2. The elevated RPPP over the Runnelstone Reef is likely due to

advection and/or turbulence, which creates enhanced foraging opportunities. The large area to the east of the reef is situated where we would expect to find vorticity due to the reef wake effect and the tidal jets generated by the uneven topography of the reef. Similarly, the areas with raised RPPP around the Epson Shoal could be related to advection, turbulence, or the formation of internal waves (shown in Figure 4).

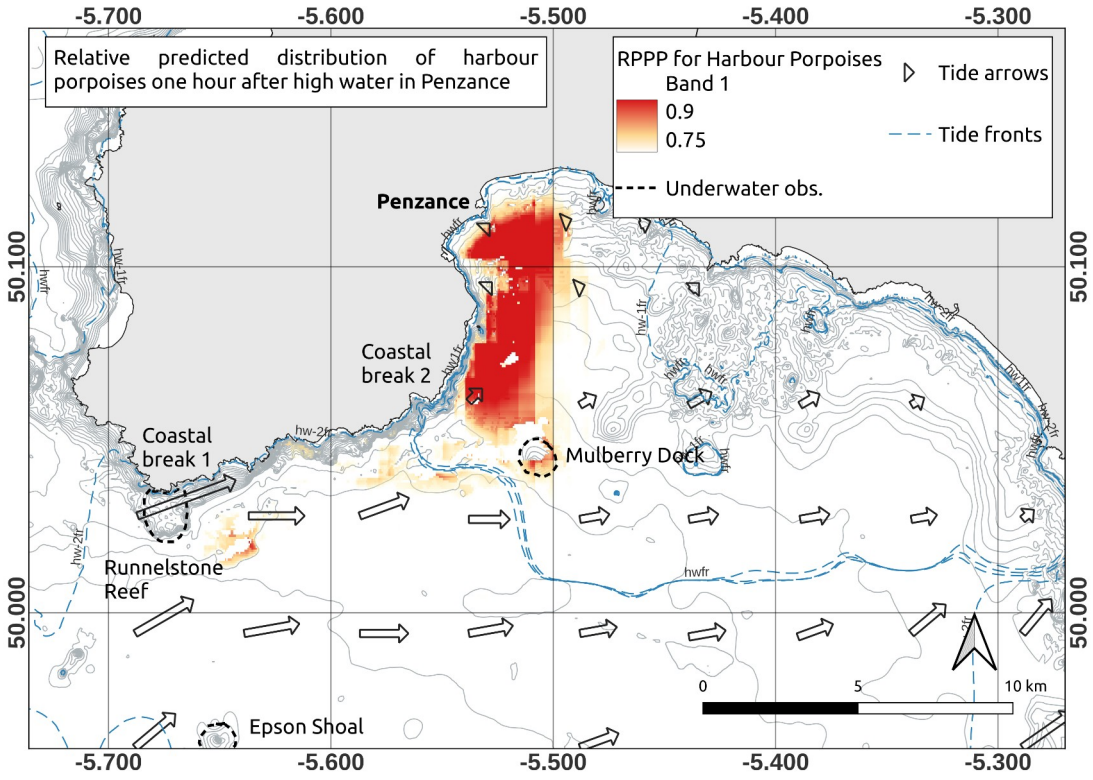

Figure 11: Relative predicted probability of presence a one hour after the time of high water in Penzance, Mount's Bay, Cornwall. Only areas with RPPP greater than 0.75 are coloured. The arrows depict the direction and strength of the tidal flow. The dashed boundaries identify key reef and wreck areas. Depth contours are also shown in order to demonstrate the complexity of bathymetry across the area. The blue dashed lines represent the tide fronts used in the modelling.

One hour after high water in Penzance, the area with the highest RPPP has moved to the east and is to the north of the Mulberry Dock and north of coastal break 2, which is in the weaker tide on the north side of the stronger tidal stream (Figure 11). At this stage of the tide cycle, the part of the bay where the RPPP is concentrated is sheltered from the strongest tidal stream by the change in direction of the coast at coastal break 2, where the coast changes from south facing to east facing. The coast changes from south facing to east facing at this point. The strength of the easterly flowing tidal stream at this stage of the tide cycle has the potential to generate vorticity (as depicted in Figure 4). The eddies produced are likely to flow up into the area of raised RPPP. The area of raised RPPP to the south of the Mulberry dock is located

where turbulent wake would form as the tide passes the wreck. There is a smaller area of elevated RPPP located to the east of the Runnelstone Reef. This area is situated where we would expect to observe reef wake conditions (as shown in Figure 4).

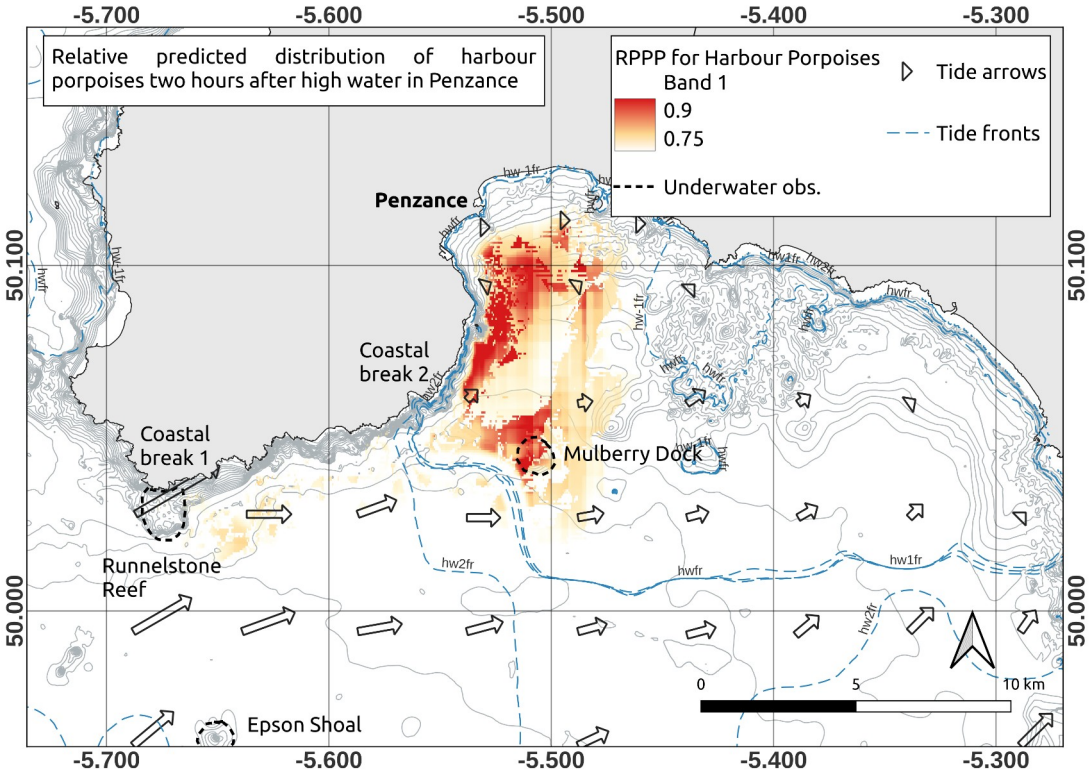

Figure 12: Relative predicted probability of presence two hours after the time of high water in Penzance, Mount's Bay, Cornwall. Only areas with RPPP greater than 0.75 are coloured. The arrows depict the direction and strength of the tidal flow. The dashed boundaries identify key reef and wreck areas. Depth contours are also shown in order to demonstrate the complexity of bathymetry across the area. The blue dashed lines represent the tide fronts used in the modelling.

Two hours after high water in Penzance, the areas with the highest RPPP are still in a similar place to the previous hour of the tide cycle along the east facing coast north of the stronger flowing tide (Figure 12). In this area there are now two focal points. The first is in a similar area to the previous hour of the tide cycle and the second is focused around the Mulberry Dock feature. Although the tidal stream is still flowing in an easterly direction at this stage of the tide cycle the strength of the flow has weakened slightly. The stronger flow of the previous hour of the tide cycle has the potential to generate vorticity (Figure 4) as it passes the coastal break. The slower tidal flow has the potential to change the tidal processes generated at the tidal break. The intensity and direction of the vortices is dependent on the speed of flow. Alternatively the reduced tidal flow could generate internal waves off the shelf by the tidal break, which would propagate in the direction of the Mulberry Dock instead of the previous

hours vorticity. The Mulberry Dock is potentially focusing particulates through advection (Figure 4). The tidal stream is stronger south and west of the Mulberry Dock. The stronger flow in the south will hold any particulates focused to the north (Thorpe 2005).

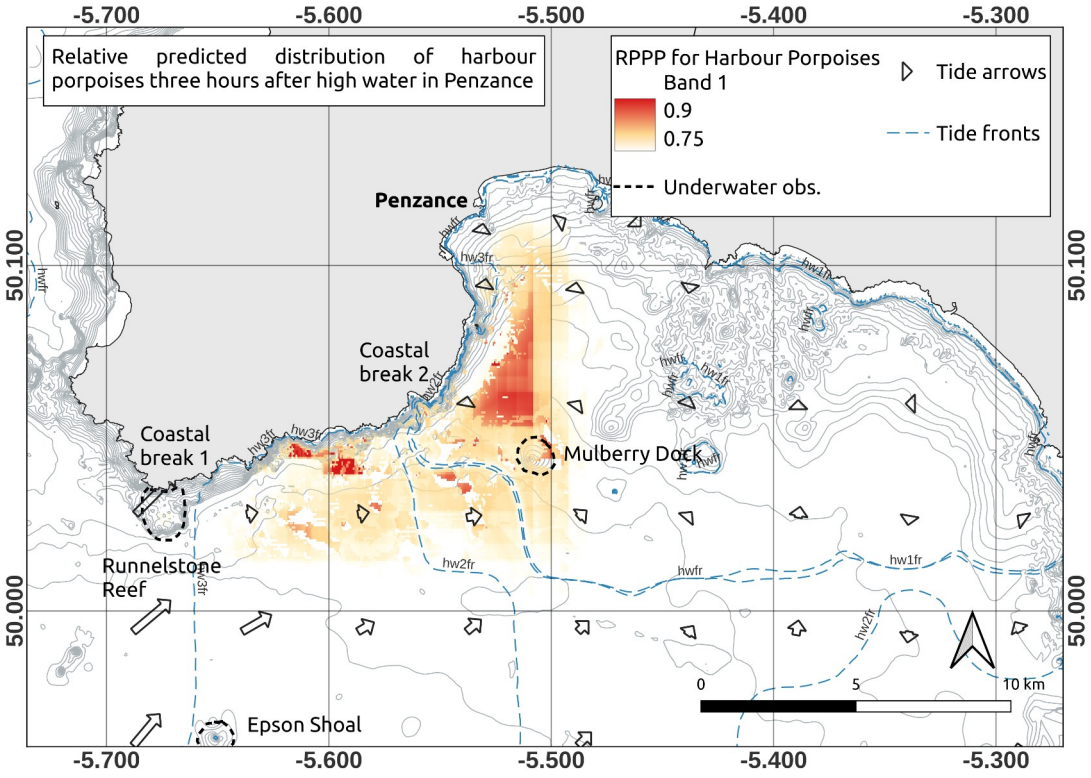

Figure 13: Relative predicted probability of presence three hours after the time of high water in Penzance, Mount's Bay, Cornwall. Only areas with RPPP greater than 0.75 are coloured. The arrows depict the direction and strength of the tidal flow. The dashed boundaries identify key reef and wreck areas. Depth contours are also shown in order to demonstrate the complexity of bathymetry across the area. The blue dashed lines represent the tide fronts used in the modelling.

Three hours after high water in Penzance (Figure 13), the tidal stream east of the Runnelstone Reef has slowed down, but is still flowing in an easterly direction. The largest area of elevated RPPP is located between Penzance and the Mulberry Dock to the east of coastal break 2. During this hour of the tide cycle, the tidal flow is both in the same direction and much weaker compared to the previous two hours. Therefore, it is unlikely to disperse the particulates that were focused during the previous hours of the tide cycle (Thorpe 2005). The raised RPPP to the east of the Mulberry Dock could be evidence of an internal wave (as shown in Figure 4) triggered by the changing tidal flow. The small areas of raised RPPP to the west of the Mulberry dock could represent areas where the tidal change has presented increased foraging opportunities. The ones close to the coast are located next to the tide front, which is established three hours after high water. The areas to the south of coastal break 2 and

to the west of these are located close to the tidal fronts formed at one hour and two hours after high water.

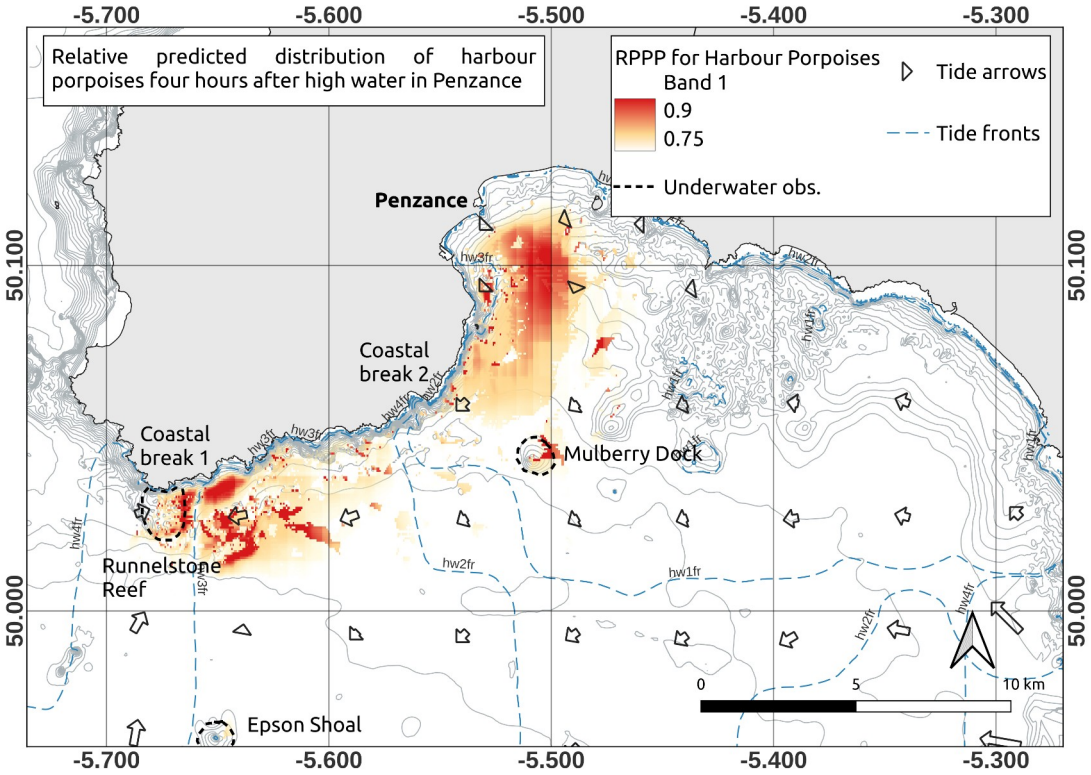

Figure 14: Relative predicted probability of presence four hours after high water in Mount's Bay, Cornwall. Only areas with RPPP greater than 0.75 are coloured. The arrows depict the direction and strength of the tidal flow. The dashed boundaries identify key reef and wreck areas. Depth contours are also shown in order to demonstrate the complexity of bathymetry across the area. The blue dashed lines represent the tide fronts used in the modelling.

Four hours after high water in Penzance, the tide is transitioning to a westerly flow. There are areas of raised RPPP around the Runnelstone Reef and in the area to the east of it (Figure 14). The tide is flowing towards the reef structure so there will be advection along the eastern edge of the reef and over the reef structure (Figure 4). The advection could be the reason for the elevated RPPP in this area. There are also areas with raised RPPP around the Mulberry Dock, which could be due to advection and/or the triggering of an internal wave (Figure 4). Along the east facing coast north of the Mulberry Dock there is a larger area with elevated RPPP. The weak flowing tide in this area is unlikely to have dispersed the product of the previous three hours of the tide cycle and the west south west direction may well be promoting advection a long the coast (Figure 4). This could explain the raised RPPP in this area.

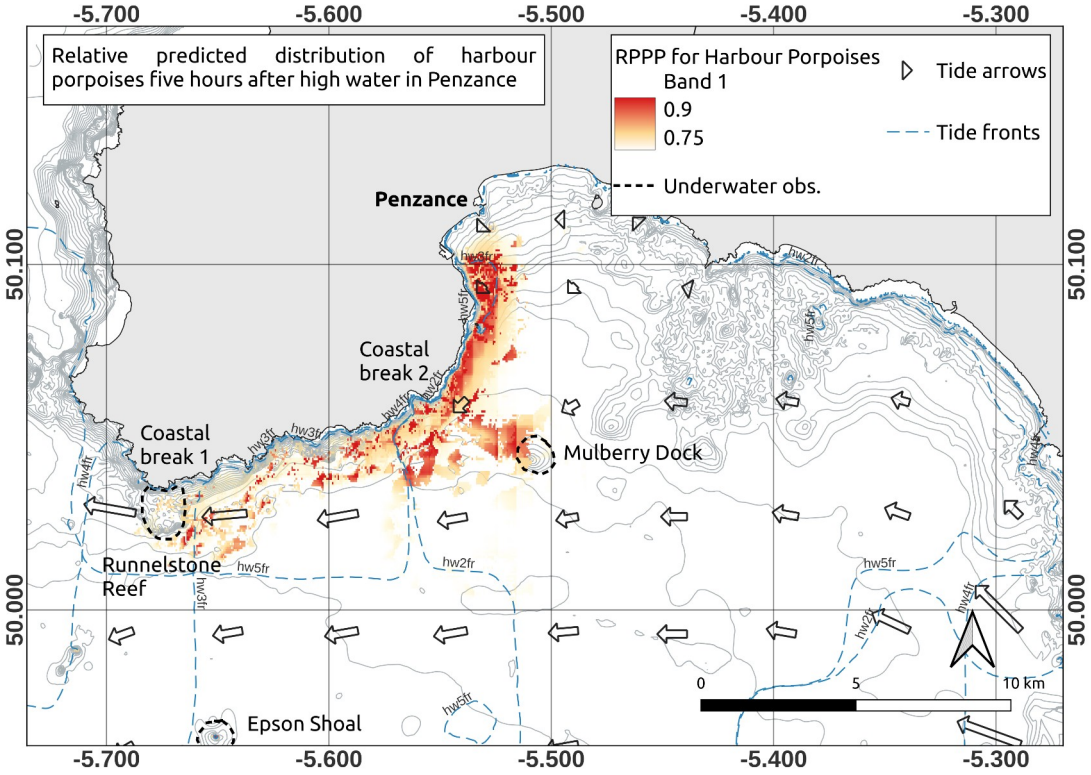

Figure 15: Relative predicted probability of presence five hours after the time of high water at Penzance, in Mount's Bay, Cornwall. Only areas with RPPP greater than 0.75 are coloured. The arrows depict the direction and strength of the tidal flow. The dashed boundaries identify key reef and wreck areas. Depth contours are also shown in order to demonstrate the complexity of bathymetry across the area. The blue dashed lines represent the tide fronts used in the modelling.

Five hours after high water in Penzance, the direction of tidal flow is now in a westerly direction, and the area of raised RPPP between Penzance and the Mulberry Dock is now concentrated along the coast (Figure 15). It is possible that the particulates concentrated during the previous hours of the tide cycle are now being advected and trapped along the coast, which may explain this shift. There is also an area between the Mulberry Dock and coastal break 2. This area is located downstream from the Mulberry Dock and is possibly the result of tidal wake focusing particulates (Figure 4). To the west of this area, there is another patch of raised RPPP which is likely to be a product of tidal wake generated at coastal brake 2. Between coastal brake 2 and the Runnelstone reef, there are numerous patches of raised RPPP. The inner string of them appears to track the shelf above the 40 m contour, while the outer string is between the 40 m and 50 m contours. The steepest slopes in Mount's Bay are found between 20 m and 40 m depth along the coastal shelf. There are also patches to the east of the Runnelstone reef at similar depths, with a particular focus around 40 m depth south east of the reef. These are likely to be the products of wake from coastal break 2 flowing west on the tide, wake turbulence generated along the coastal shelf, and advection (Figure 4) around the Runnelstone reef.

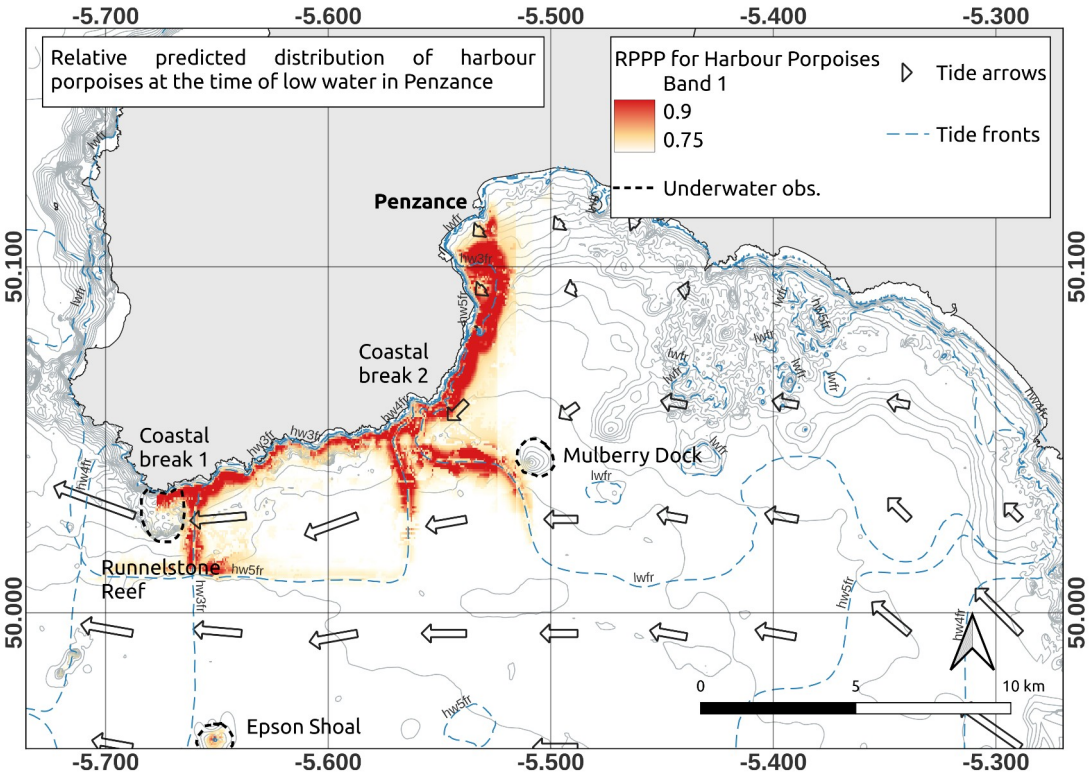

Figure 16: Relative predicted probability of presence at the time of low water in Penzance Mount's Bay, Cornwall. Only areas with RPPP greater than 0.75 are coloured. The arrows depict the direction and strength of the tidal flow. The dashed boundaries identify key reef and wreck areas. Depth contours are also shown in order to demonstrate the complexity of bathymetry across the area. The blue dashed lines represent the tide fronts used in the modelling.

At the time of low water in Penzance, there is a strong westerly tidal flow. The areas with raised RPPP are located in similar areas to the previous hour of the tide cycle but are more consistently focused. They are along the east facing coast between Penzance and the Mulberry Dock and along the south facing coast between the Mulberry Dock and the Runnelstone Reef (Figure 16). There are also areas with high RPPP to the west of the Mulberry Dock. They are along the tide fronts formed five hours after high water and at low water. These are in the wake zone for coastal break 2 (Figure 4) and also at the boundary between the faster flowing and slower flowing tide. There is a further area of raised RPPP on the east side of the Runnelstone Reef, where the westerly flowing tide meets the east facing slope of the Runnelstone Reef. This could be the result of advection, improving foraging opportunities (Figure 4).

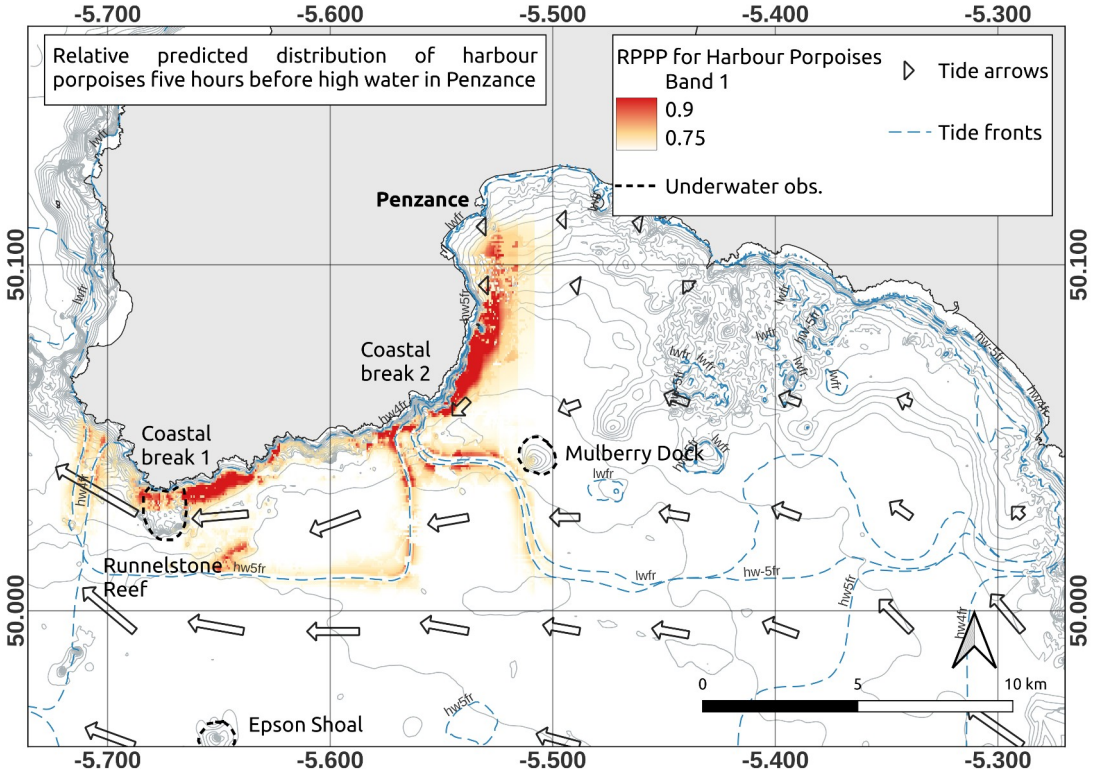

Figure 17: Relative predicted probability of presence five hours before the time of high water at Penzance, Mount's Bay, Cornwall. Only areas with RPPP greater than 0.75 are coloured. The arrows depict the direction and strength of the tidal flow. The dashed boundaries identify key reef and wreck areas. Depth contours are also shown in order to demonstrate the complexity of bathymetry across the area. The blue dashed lines represent the tide fronts used in the modelling.

Five hours before high water in Penzance, the tidal flow is in a westerly direction and similar to the previous hour of the tide cycle (Figure 17). There are areas with raised RPPP along the east facing coast between Penzance and the Mulberry Dock and along the south facing coast around coastal break 2. Additionally, there are areas with raised RPPP along the low water tide front and the tide front formed five hours after high water, just west of the Mulberry Dock. These areas of elevated RPPP are in similar locations to the previous hour of the tide cycle and the drivers are likely to be the same. There is an area with elevated RPPP close to the coast east of the Runnelstone reef and over the reef. The tide flowing in to this area will be causing advection (Figure 4). Furthermore, there is an area south east of the reef along the 50 m contour. This is also an area where advection may be occurring or turbulence due to the wake effect caused by the sudden depth change (Figure 4).

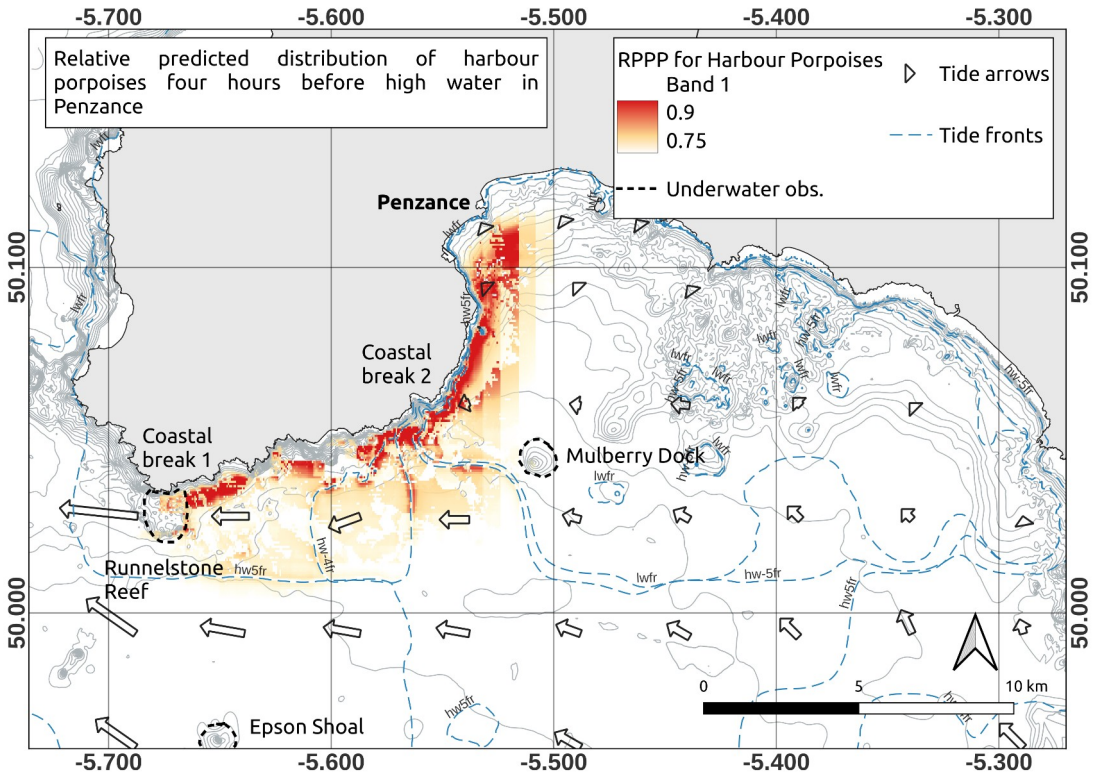

Figure 18: Relative predicted probability of presence four hours before the time of high water in Penzance, Mount's Bay, Cornwall. Only areas with RPPP greater than 0.75 are coloured. The arrows depict the direction and strength of the tidal flow. The dashed boundaries identify key reef and wreck areas. Depth contours are also shown in order to demonstrate the complexity of bathymetry across the area. The blue dashed lines represent the tide fronts used in the modelling.

Four hours before high water at Penzance, the tide is still flowing in a westerly direction but has weakened slightly (Figure 18). The areas with raised RPPP are in similar locations to the previous three hours of the tide cycle. The areas along the east coast between Penzance and the Mulberry Dock and along the south facing coast near Coastal Break 2, while still located in a similar place, have expanded away from the coast. The areas along the tide fronts formed five hours after high water, at low water and five hours before high water have contracted. . The areas along the coast between Coastal Break 2 and the Runnelstone Reef are now broken but still likely to be the product of the wake effect of the tide flowing past Coastal Break 2 and along the coastal shelf (Figure 4). Additionally, there is also an elevated area of RPPP on the east side of the reef close to the coast. This is in an area where advection would be occurring (Figure 4).

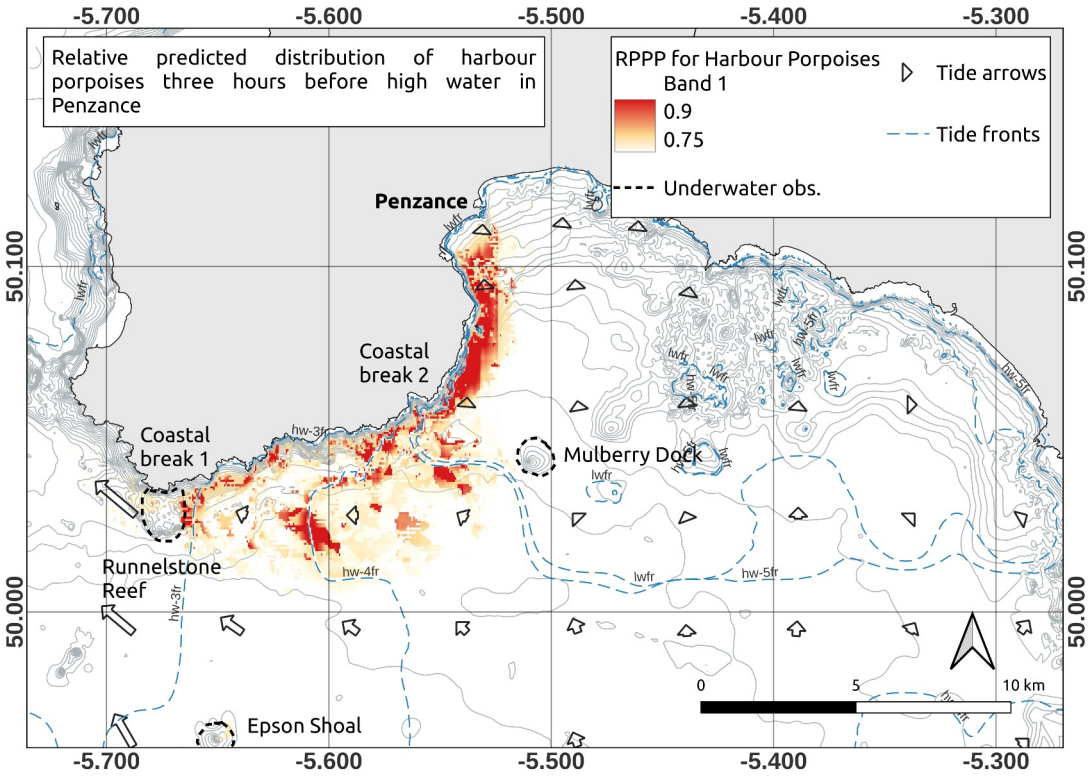

Figure 19: Relative predicted probability of presence three hours before the time of high water at Penzance, Mount's Bay, Cornwall. Only areas with RPPP greater than 0.75 are coloured. The arrows depict the direction and strength of the tidal flow. The dashed boundaries identify key reef and wreck areas. Depth contours are also shown in order to demonstrate the complexity of bathymetry across the area. The blue dashed lines represent the tide fronts used in the modelling.

Three hours before high water at Penzance, the tide flow has slowed and begun to transition. West of the Mulberry Dock, it still flows to the west. To the north and east of the Mulberry Dock the direction of flow is northerly (Figure 19). The area of raised RPPP along the east facing coast north of the Mulberry Dock and the south facing coast around Coastal Break 2 is still present. The likely reason for this is the product of the previous hours of the tide cycle. The slow moving tide at this stage of the cycle is causing it to dissipate slowly. There are also raised areas of RPPP along the tide fronts formed at five hours before high water and low water to the west of the Mulberry Dock. These areas have moved away from the front compared to the last hour of the cycle. Furthermore, there is another area of elevated RPPP located along the tide front formed four hours before high water, midway between the Mulberry Dock and the Runnelstone Reef. There are further areas of raised RPPP along the eastern edge of the Runnelstone Reef and along the south facing coast to the east of the Reef. These areas are located where advection is likely to be occurring and follow the tide front formed three hours before high water.

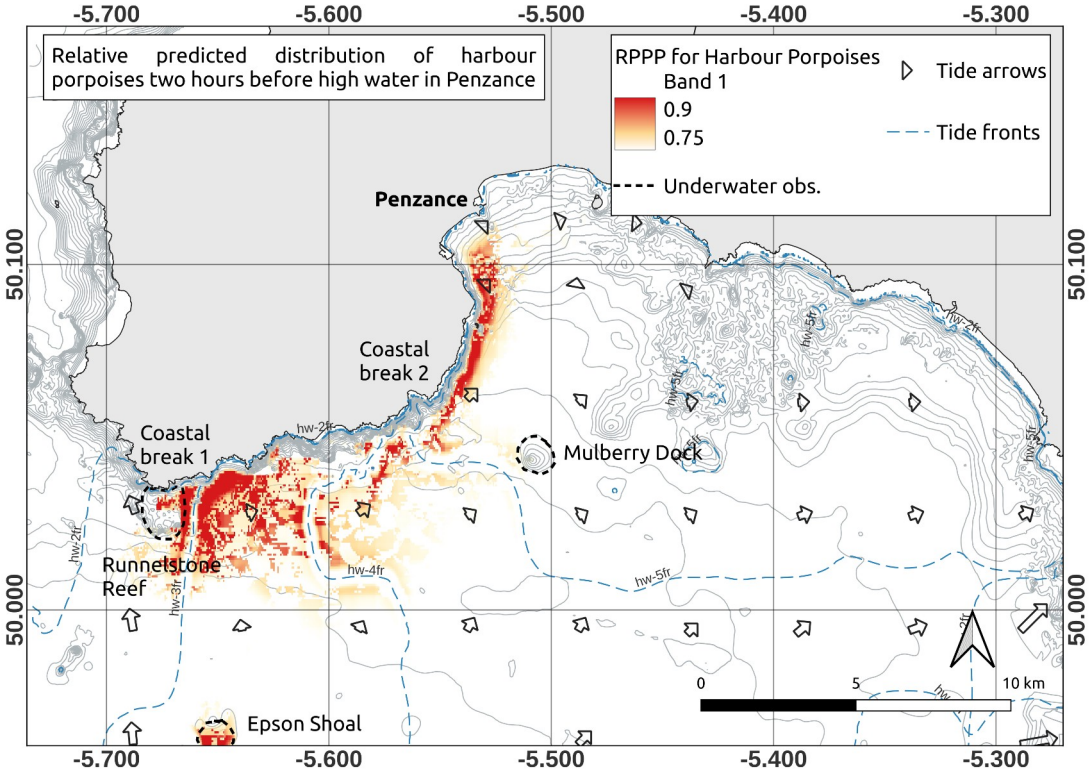

Figure 20: Relative predicted probability of presence two hours before the time of high water high water at Penzance, Mount's Bay, Cornwall. Only areas with RPPP greater than 0.75 are coloured. The arrows depict the direction and strength of the tidal flow. The dashed boundaries identify key reef and wreck areas. Depth contours are also shown in order to demonstrate the complexity of bathymetry across the area. The blue dashed lines represent the tide fronts used in the modelling.

Two hours before high water at Penzance, the tide is in the process of transitioning to an easterly flow. At this stage of the cycle the flow is weak and in a north or north easterly direction (Figure 20). There is a large area with raised RPPP along the east side of the Runnelstone Reef area and further east, which is bisected by tide front formed three hours before high water. These areas stretch east to just past the front formed four hours before high water. South of this area, there are also areas with raised RPPP around the Epson Shoal, which could be the product of advection, wake effect or internal wave formation (Figure 4). There is also raised RPPP along the east facing coast to the north of the Mulberry Dock, similar to the previous stage of the tide cycle, although it is now compressed against the coast. Likewise there is still an area with elevated RPPP to the south west of Tidal Break 2 where it was previously.

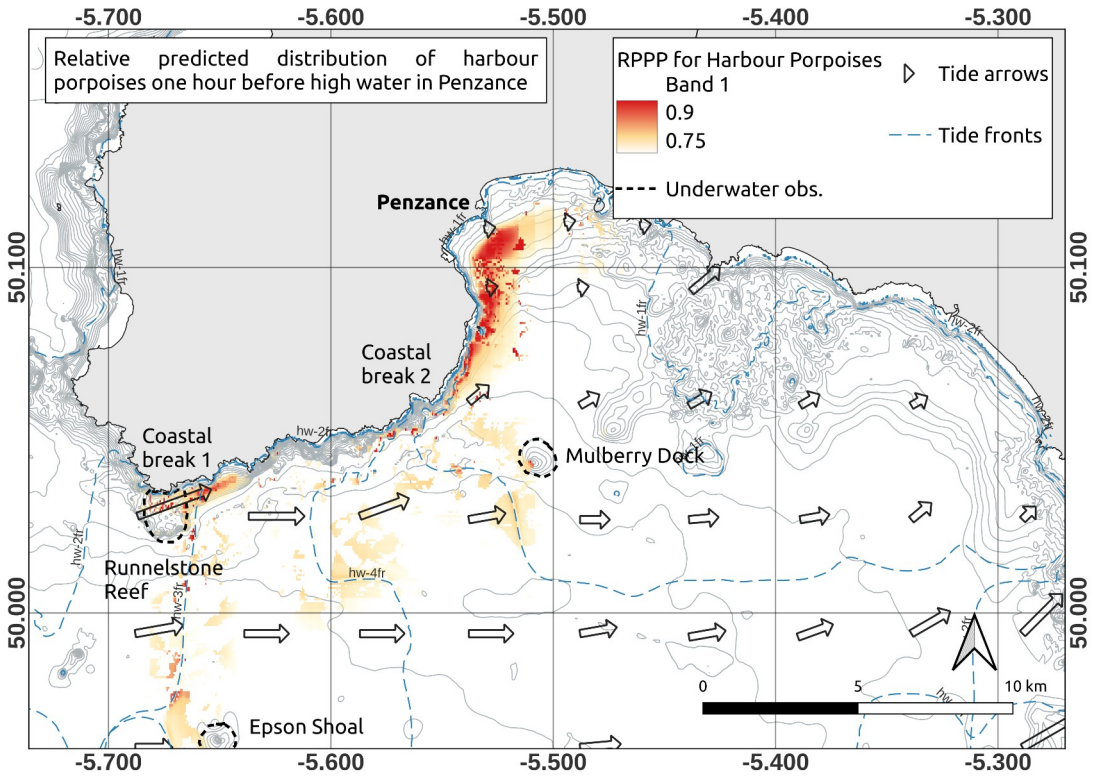

Figure 21: Relative predicted probability of presence one hour before the time of high water at Penzance Mount's Bay, Cornwall. Only areas with RPPP greater than 0.75 are coloured. The arrows depict the direction and strength of the tidal flow. The dashed boundaries identify key reef and wreck areas. Depth contours are also shown in order to demonstrate the complexity of bathymetry across the area. The blue dashed lines represent the tide fronts used in the modelling.

One hour before high water, the tidal stream is easterly (Figure 21). There is an area with raised RPPP focused along the east facing coastline to the north of the Mulberry Dock along the front formed one hour before high water. There is also a tide front in this area two hours before high water. There are a few smaller areas of raised RPPP over the Runnelstone Reef and the east of the reef, along it's south eastern edge. There will be advection caused by the tide flowing over the reef and wake from turbulence and possible tidal jets east of the reef (Figure 4). South of the Runnelstone Reef along the tide front formed three hours before high water, there are small areas with elevated RPPP. The largest of these is to the northwest of the Epson Shoal. There are two small areas of elevated RPPP south west of Coastal Break 2, in an area where advection is likely to be occurring.

4.4 General Additive Models for Locations, Scale and Shape

4.4.1 Data Inspection

The histogram plots in figure 22 show the frequency of effort per value for each of the independent variables and indicate strong effort bias for all variables with the exception of year. It is not possible to investigate how this effort bias relates to the available values of the independent variables, because the values at unvisited locations are not known. It is possible to understand this relationship for month and year because they are categorical variables and there is effort across all categories. Figure 22 also shows sightings frequency by independent variable. A visual inspection suggests that sightings frequency and effort frequency are strongly correlated in most cases. Table 7 shows the correlation coefficients between frequency of effort per independent variable and frequency of sighting occurrences. The correlation coefficient was high for all independent variables with the exception of sea surface temperature and distance to the nearest front. The effort bias was accounted for in the modelling process because the model was a count absence model.

Independent Variable	Correlation coefficient
Month	0.879
Year	0.833
SST	0.284
Chl	0.854
Fdist	0.685
Fside	1
Fden	0.947
Fper	0.945

Table 7: Spearman's rank correlation of effort and sighting event frequency.

Scatter plots were created for all the independent variables initially included in the GAMLSS models (see appendix 3). The data are not normally distributed and there are a high number of zeroes in the count. Chlorophyll appears to be generally left skewed but also bimodal with a smaller peak at higher values. Distance to the nearest front, front persistence and front gradient density are all left skewed. Sea surface temperature, year and month are all right skewed. The scatter plot for front side is bimodal across the three categories. The sightings histograms (Figure 22) show similar distributions to the effort histograms with the exception of year and front distance. The sightings histogram for year is right skewed and the histogram for front distance appears bimodal. It is important to note the temporal (+ or – 3 days) and spatial coarseness (1km^2) of the satellite generated data. It means the satellite variable values do not match up in space and time with the effort or sighting points and this introduces unquantified error.

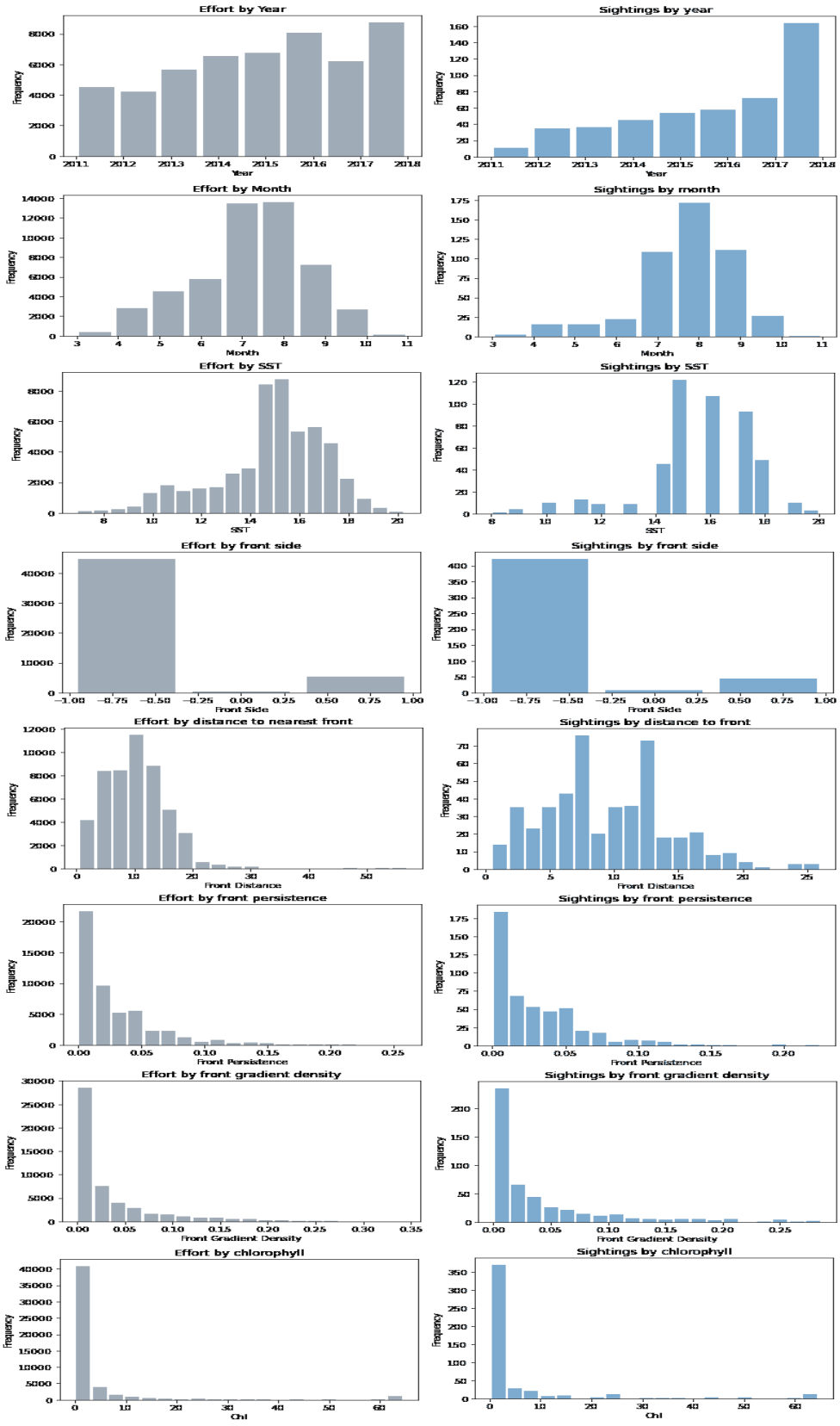

Figure 22: Histograms showing binned effort frequency (grey bars) and sighting event frequency (blue bars) by independent variable values.

4.4.2 Initial Model Selection

Four models were run twice. Once including the independent variable for front gradient density and once including the independent variable for front persistence. Models using NBI, PIG, DEL and ZIP distributions were compared using GD, AIC and SBC to identify the best performing models. The NBI distribution performed the best in both cases. The other three models reverted from the default variance-covariance (VCOV) method for defining standard errors to the QR method.

The VCOV method uses only one iteration to obtain a Hessian matrix. The inverse of the Hessian matrix is used to obtain the standard errors. This is a much more robust way to generate standard errors when compared with QR, which fits the parameters individually to generate standard errors. Standard errors generated in this way should be treated with caution (Stasinopoulos et al. 2008). The use of the QR method, the higher GD, AIC and SBC scores of the other three models identified the NBI model as the best (see table 8).

All data and front persistence				
Distribution	GD	AIC	SBC	
NBI	7192.372	7268.37	7600.647	
PIG	7354.929	7430.931	7763.225	vcov failed
DEL	7186.121	7264.121	7605.15	vcov failed
ZIP	7945.512	8021.51	8353.788	vcov failed
All data and front density				
Distribution	GD	AIC	SBC	
NBI	7195.599	7271.598	7603.876	
PIG	7357.198	7433.204	7765.515	vocv failed
DEL	7189.045	7267.045	7608.071	vcov failed
ZIP	7912.304	7988.303	8320.578	vcov failed

Table 8: Results from the model comparison. The more robust vcov method for identifying standard errors failed on all models a part from NBI.

The NRQR plots (appendix 4) for both models demonstrate the goodness of fit of the models. There is no evidence of heteroscedasticity and the NRQRs show an even spread. The mean of the residuals is close to zero, their variance is close to one, the coefficient of skewness is near to zero and the coefficient of kurtosis is close to three.

4.4.3 Feature Importance

Feature selection was initially conducted using the dropterm() function using Chi squared P values to identify the most informative variables (Stasinopoulos et al. 2008). Both the model with front persistence and the model with front gradient density selected month, year and distance to the nearest front as significant variables. Year and month had highly significant p values and distance to the nearest front was significant at 0.05 in both models. The stepGAIC() function selected the same

features this approach selects the most informative features while maintaining the lowest complexity in the model (Thomas et al. 2018).

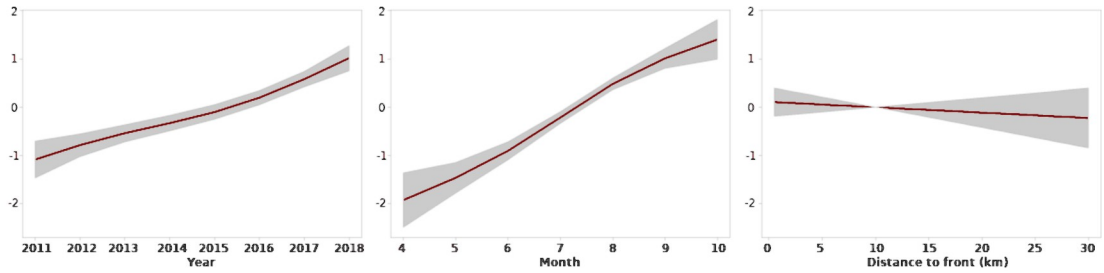

Figure 23: Partial dependence plots from the GAMLSS model from left to right year, month, tide front distance.

This left a single model from the two initial models. The final model included distance to the nearest front, month and year as independent variables. The partial dependence plot for year (Figure 23) shows that the likelihood of encountering harbour porpoises increased yearly between 2011 and 2018. The plot for the variable month (Figure 23) shows that the likelihood of detecting harbour porpoises in Mount's Bay increases between July and November. The plot for distance to the nearest front (Figure 23) shows that when the front is at 10km the likelihood of encountering harbour porpoises increases. At times when the front is closer than 10 km on some occasions the likelihood of encountering porpoises increases. However as the front gets closer the deviation of the likelihood increases. This means that in some instances the likelihood drops below the likelihood of encountering porpoises when the front is at 10km and on other occasions encounters are more likely. The general trend suggests that the more distant the front, the lower the likelihood of an encounter becomes. The uncertainty in the plot demonstrates that other factors are influencing the likelihood of encounters alongside the distance of the front. These results are impacted by the comparatively low resolution of the satellite data and its composite nature. The model is able to pick out the increase of presence across years and the seasonality of harbour porpoise presence. However it is unable to give a clear response to the front distance or intensity.

5 Discussion

Harbour Porpoise encounter rates in this study are very high when compared with encounter rates in other areas. The maximum encounter rate of 39.1 animals per 100 km effort and the average of 16.5 per 100 km effort are higher than records of between 4 and 13 per 100km recorded for the West Coast of Scotland (Booth et al. 2013). However the Booth et al. (2013) study covers a much wider area than this one. The seasonality of sightings in Mount's Bay and the relatively small survey area of 399 km² would suggest that the porpoises recorded must range further than the boundaries of the study area. It appears that the Western side of Mount's Bay (the study area) has a particularly high density of porpoises at certain times of year and that a wider survey area could give a reduced encounter rate. The high encounter rate is certainly notable but it is important to consider that the differing sizes of the survey areas and the differing methodologies for data collection will potentially impact the results (Tessarolo et al. 2014).

The seasonality of sightings in Mount's Bay follow a particular pattern. Encounter rates in March are initially high dropping through April and May before reaching their lowest point in June after this they rise quickly through July and reach a first peak in August followed by a second peak in November. This can be seen in figure 5 and is supported by the GAMLSS partial dependence plot in figure 23. A study carried out on the north side of the Land's End peninsula conducted by Cox et al. (2017) found that harbour porpoise detections peaked in January after which they declined until April. The encounter rate was then low between May and November before rising again (Cox et al. 2017). Their study site is 30 nautical miles from the centre of the Mount's Bay study site and the porpoises recorded in both areas are likely to be part of the same wider population. The early peak of porpoise sightings between March and April in Mount's Bay coincides with the seasonal thermocline moving through the bay. This moves up from the south west and continues to move in a north easterly direction as it progresses past the Lizard Peninsula and in to the Western Channel. At the same time it progresses north into the Celtic Sea (Uncles and Stephens, 2007). The dip in porpoise sightings in Mount's Bay coincides with the thermocline moving further east in to the Western Channel and north into the Celtic Sea (Figure 24). The boundary of the spring thermocline is associated with increased productivity. The boundary between the warm stratified water and the mixed coastal water suspends nutrient rich water at the surface promoting primary productivity, which focuses plankton and nekton (Sastri et al. 2014).

The surface water temperature continues to increase in June and July offshore from Mount's Bay. This creates a vertical temperature boundary between the surface and bottom water creating an increasingly developed thermocline. It also develops a horizontal temperature boundary between the stratified water and the coastal water,

which is constantly mixed by strong tides and wave action. The temperature difference between the surface and bottom water and stratified and coastal water typically peaks in August (Figure 24). The water closer inshore is continually mixed by strong tidal flow maintaining a cooler temperature than that of the offshore water. The boundary between the mixed and the stratified water promotes primary productivity because the mixed water is continually feeding nutrients in to the system. At the same time that this temperature difference is peaking in Mount's Bay the water further up the channel is a more uniform temperature precluding boundary mixing. (Figure 24). This difference coincides with the peak in harbour porpoise sightings per 100 km in Mount's Bay. The location of the thermocline and strengthening of it in late summer in Mount's Bay coincide with the peaks and troughs in the sightings rate for harbour porpoises.

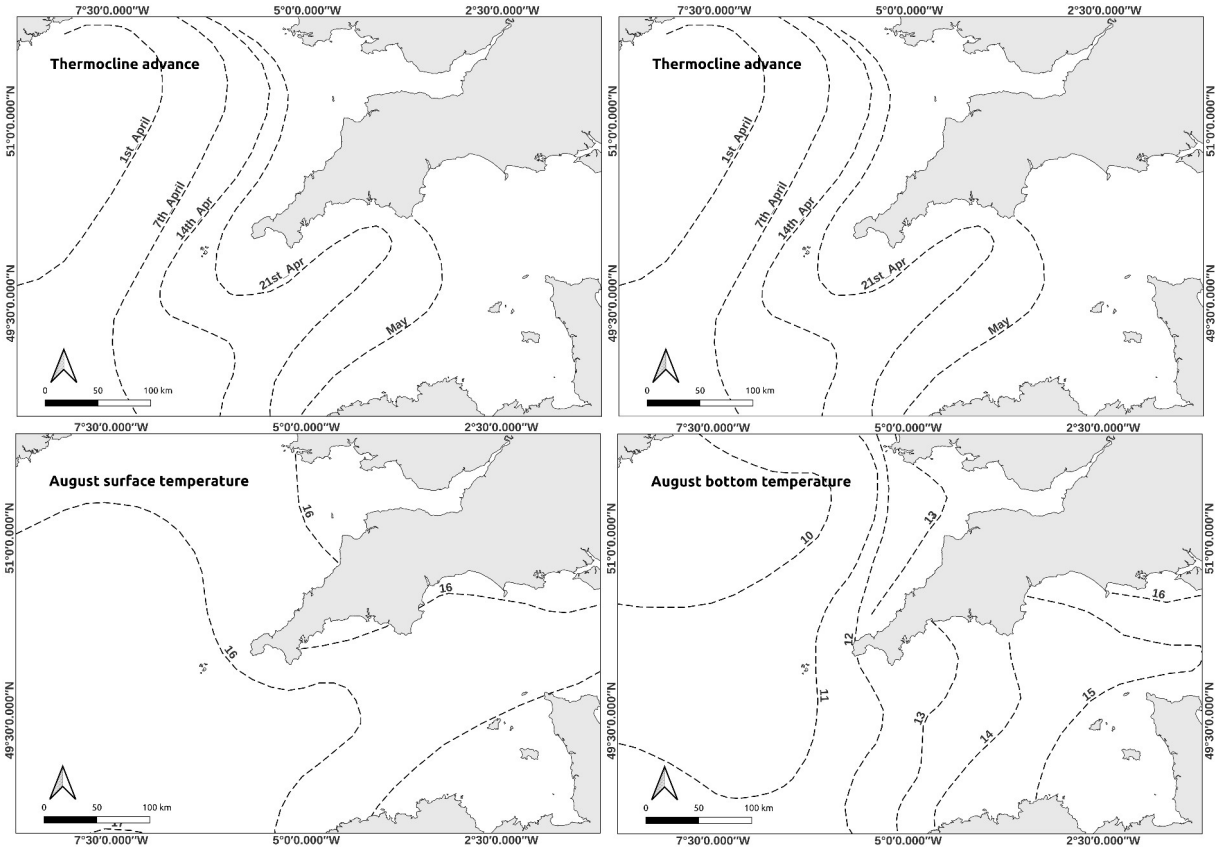

Figure 24: Top left shows the thermocline advance in the Western Approaches, top right shows the thermocline retreat. Bottom left shows the surface temperature in August and bottom right shows the bottom temperature in August. The thermocline and temperature data is digitised from Uncles and Stephens (2007) (Uncles and Stephens, 2007).

The productivity generated by the boundary between mixed and stratified water is amplified by tidal fronts (Suberg 2015; Suberg et al. 2019). The location of these fronts was included in the MaxEnt modelling and proved to be an important factor for predicting the location of harbour porpoises. The other factors that were determined

as being important were longitude, depth and distance from the nearest slope. All of these are factors in the equation for working out the location of tidal fronts and processes. In Mount's Bay the longitude position determines the strength of tidal flow experienced at a location. As a general rule the western part of Mount's Bay experiences stronger tidal flows. Thus the longitudinal position determines were the boundary is between the fastest and slowest moving water. Depth determines how much turbulence is caused by a given tidal flow. Shallower water increases turbulence and deeper water decreases it. Depth also has a relationship with the north south position of the boundary between faster moving tidal flow further offshore and slower moving tidal flow, which is typically closer inshore. The distance from the nearest slope determines how close a position is to a significant depth change. This is another factor which can determine the location of a tidal front (Nimmo Smith et al. 1999; Thorpe 2005).

5.1 Effort Bias

Bias files were included in all of the MaxEnt models in order to account for the spatial sampling bias and for sampling bias across variables (Merow et al. 2013; De Rock et al. 2019). When survey effort is biased it is considered an acceptable approach to weight samples using knowledge of the survey effort (Zhang and Zhu 2018). Johnston et al. (2010) found that sampling bias could be accounted for using weighting to represent effort. Although they found their model predictions were still less accurate in areas of unique habitat type (Johnston et al. 2020). The survey area in this case covers a small geographical range and therefore the environmental characteristics are reasonably comparable across the range. The bias file included in the model represented the survey effort accurately and the response curve/ OMS histogram figure 8 and appendix 5 demonstrate that bias effort was accounted for well in the modelling process. The trends in the OMS largely follow the trends in the response curves. Particularly if it is considered that the response curves are a reflection of predicted relative presence in relation to the influence of all of the variables in the model. The response curves are also smoothed by the model in order to avoid overfitting. However the spatial bias is quite extreme in a number of places and it would be preferable to have greater survey effort at the perimeter of the survey area and in the offshore areas.

The use of inflection curves (appendix 1) in the data preparation stage ensured the removal of effort and sightings under conditions were detection was inconsistent due to excessive sea states, swell heights or boat speed (de Boer 2013; de Boer et al. 2018). 28 119 effort records and 281 sightings records were removed. This ensured that the records included were collected under conditions which allowed for consistent detection. However it also removed more records from areas with already low effort due to their location being exposed to wind and swell.

5.2 MaxEnt

5.2.1 Longitude

Longitude is the most influential variable in all of the models. In the model using all of the data it contributes 62.5% and in all of the other models it contributes between 34% and 51.1%. RPPP values of greater than 0.5 range from -5.77 decimal degrees to -5.44 decimal degrees. Although the importance of longitude demonstrates that the location of significant areas for harbour porpoises change across the tide cycle it does not explain why the locations change or what drives the change because longitude is not a functional variable. If the response curve for the model using all of the data is cropped to display RPPP for the areas with higher effort it can be seen that the distribution of RPPP peaks is bimodal (Figure 25 a and b). This distribution, as would be expected, translates to all of the models. The peaks in the response curves are either centered around -5.67 decimal degrees and/or -5.15 decimal degrees. These line up with the two areas in Mount's Bay where there are consistent tidal boundaries (Figure 25 c) between faster and slower tidal flows. Therefore we can assume longitude is a proxy for other processes in these areas.

The RPPP peak at -5.67 decimal degrees (Figure 25 b) is at the location of a study by Jones et al. (2014). The results and boundaries of this study are represented in Figure 25 b and c 1 (Jones et al. 2014). The study recorded a high sightings rate for harbour porpoises in the area of the Runnelstone Reef. The authors found large aggregations of porpoises coincided with the tidal stream switching direction and the internal waves this triggered (Figure 4). The waves propagated in a SSW direction from the reef structure (Jones et al. 2014). These findings support the model outputs of this study and support the theory that the distribution of the harbour porpoise in Mount's Bay is influenced by tidal process.

Figure 25 c 1 and 2 identify the potential location of other tidal processes considered to have the potential to generate conditions which aggregate small cetaceans. Notably advection, tidal wake, tidal jets and internal waves (Figure 4). Advection is caused when a tidal stream flows towards a slope area at which the depth gets shallower. The mechanical forcing of this process focuses plankton and nekton along the slope (Cox et al. 2018). Tidal wake occurs when a tidal stream flows across a shallower area, around a structure such as an island or passes an abrupt change in coastline direction. The obstruction causes turbulence in the tidal flow down tide from the object which is the tidal wake. Often eddies form along the boundaries of the turbulent flow and these can focus plankton and nekton (Johnston et al. 2005; Benjamins et al. 2015). Tidal jets form in a similar way to tidal wake. In this case the tidal stream passes between two objects such as two islands or rocks. The compression of the tide through the gap causes a tidal jet to form down tide of the obstructions. The jet can focus plankton and

nekton in the top 30 m of the water column. Eddies may also form along the edge of the jet and drift down tide with a focus of plankton and nekton (Benjamins et al. 2015). Internal waves are triggered as the tidal stream passes over and around an object under the water surface under certain circumstances. In some cases a back flow of water behind the object generated by friction as the water flows around the object causes a reverse in the water flow. In other cases the change in tidal stream direction causes the water that was previously down tide of the obstruction to be flowing in the opposite direction to water passing over the obstruction. In both cases at the boundary between the opposing flows friction causes wavelets to form. The wavelets build and then collapse mixing the water. Denser water from deeper in the water column is mixed above less dense water and vice versa. Once the water passes the turbulence the denser water sinks to find equilibrium and the less dense water rises to find equilibrium. The movement of these water parcels catalyses an internal wave, which propagates along the pynocline away from the obstruction. The mechanical forcing between the wave crests focuses plankton and nekton in the wave trough (Thorpe 2005; Thorpe 2007; Jones et al. 2014; Benjamins et al. 2015; Cox et al. 2018). Figure 25 c 1 and 2 identify features with the potential to generate these processes and identify potential areas where plankton and nekton maybe focused due to these processes.

	RPPP > 0.75 overlaps	
Stage of the tide cycle	**Figure 32 c 1**	**Figure 32 c 2**
high water	yes	no
one hour after high water	no	yes
two hours after high water	no	yes
three hours after high water	no	no
four hours after high water	yes	yes
five hours after high water	yes	yes
low water	yes	yes
five hours before high water	yes	yes
four hours before high water	yes	yes
three hours before high water	yes	yes
two hours before high water	yes	yes
one hour before high water	yes	yes

Table 9: Identifies where there is overlap between areas of RPPP greater than 0.75 (Figures 10-21) and the areas in Figure 25 c 1 and 2 identified as having the potential to generate tidal processes that aggregate plankton and nekton

The figures 10 to 21 show how the distribution of areas with higher RPPP change in relation to the geomorphology of the coast and seafloor and it's interactions with tidal flow direction and speed. Table 9 identifies where these areas overlap with the areas in Figure 25 c 1 and 2 identified as having the potential to generate tidal processes that aggregate plankton and nekton. The areas with higher RPPP are consistently located along boundaries between faster and slower moving tide or where the tide stream flows in opposing or perpendicular directions. Typically they are on the side with slower moving tide. They are also around areas with complex bathymetry usually in the deeper water along the edges of steep slopes. The tidal boundaries are

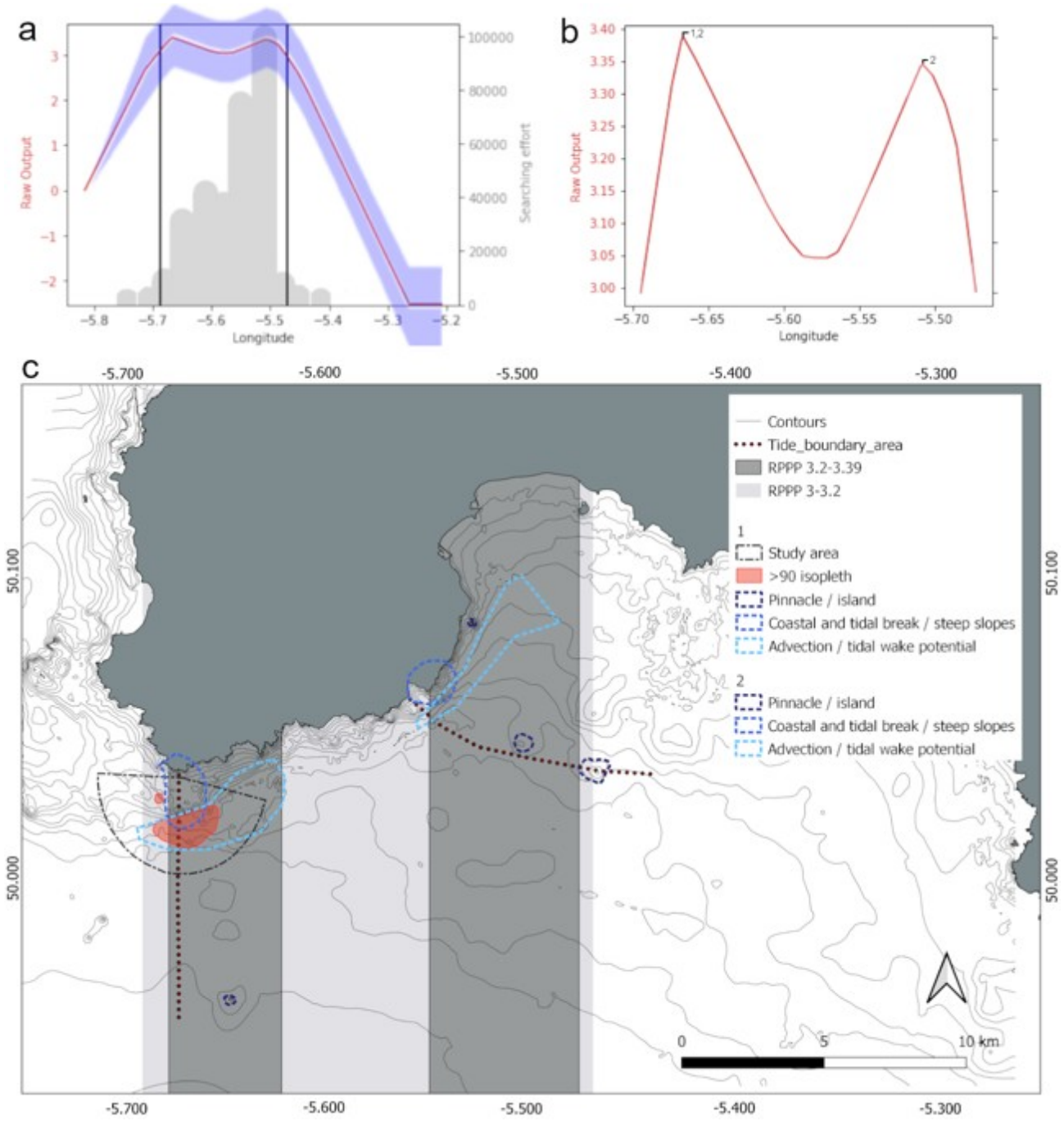

Figure 25: a) The response curve for longitude for all of the data alongside a histogram plot of effort. The shaded area shows variance across 100 models and the vertical black lines show where the data is cropped for b to remove data with low searching effort. b) The cropped response curve after the areas with low searching effort are removed. 1 identifies the location of the study 2014 by Jones et al. and 2 identifies areas where processes described by Cox et al. (2018) and Benjamins et al. (2015) are likely to be present. c is a spatial representation of a and b. The light grey shaded areas have an RPPP of greater than 3 and the dark grey shaded areas have an RPPP greater than 3.2. The dark red spotted lines represent the two major tidal boundaries in the Bay. The black dashed line shows the boundaries of the Jones et al. (2014) study and the red shading shows the areas where greater than 90% of their harbour porpoise records were located. The dark blue dashed lines represent pinnacles or islands and the light blue dashed lines represent areas where tidally driven turbulence or advection would be present (Benjamins et al., 2015; Cox et al., 2018; Jones et al. 2014).

the location of tide fronts for 10 of the 12 hours of the tide cycle. The location of tide fronts is a product of water depth and tide flow speed and these boundaries are locations where there are changes in tidal flow speed and/or depth. Cox et al. (2017) describe these as both tidal mixing fronts and hydrographic fronts. The term tidal front being typically used when they form the boundary between mixed coastal water and seasonally stratified offshore water and the term hydrographic front referring to a shear boundary between turbulent and non turbulent water masses. Both can form at the locations of the tide fronts used in the model for this study and their type depends on the season. Cox et al. (2017) found that fronts could generate elevated persistent productivity across trophic levels (Cox et al. 2017). Furthermore Bjorkstedt et al. (2002) describe the retention of biomass and small nekton caused by strong convergent flows along the edges of such fronts, which is further evidence for increased productivity in frontal areas (Bjorkstedt et al. 2002).

In order to fully understand the relationship between the tidal stream, bathymetry and harbour porpoise relative density in Mount's Bay it would be necessary to study and model the tidal processes within the Bay in more detail.

5.2.2 Depth

Depth is the second or third most influential variable in all of the models. The models show a particularly high RPPP between depths of -60 m and -15 m with the exception of the model one hour before high water (Figure 8 and Appendix 5). The relative likelihood of encountering porpoises is greater than 0.5 at depths between -67 m and -5 m. At one hour before high water the relative likelihood of encountering a harbour porpoise is greater than 0.5 between depths between -23 m and – 15 m.

The raised likelihood covers a large proportion of the survey area for all models except for one hour before high water and all observations sit within the area with greater than 0.5 RPPP (Appendix 5). The area with a raised likelihood of occurrence appears to cover the areas with the most complex bathymetry and the greatest depth change. Figure 26 shows the contours representing depth change. This supports the evidence that porpoise presence is most likely to occur in areas where the tidal processes, which focus plankton and nekton are present.

Tidal processes, boundaries and fronts are typically caused by the tidal flow encountering more complex bathymetry and changing water depths. Shallower water creates more friction and therefore turbulence. This is the reason depth is used in the equation to locate tidal fronts (Thorpe 2007). The models predict a peak likelihood at either -15 and -20 m or -48 and -60 m depending on the stage of the tide cycle. The highest RPPP values found between -15 and -20 m depth are found along steep slope close to the coast and around the edge of the Runnelstone Reef as shown in figures 10

to 21. The deeper area between -48 m and -60 m with the highest RPPP encompasses the area just south and east of the Runnelstone Reef area. Figures 10, 14, 15, 16, 19, 20 and 21 show high RPPPs greater than 0.9 in this area. This region is centered around -5.675 decimal degrees longitude and the RPPP peak in the longitude plot in Figure 25b. The boundary between peak bathymetric complexity and less complexity is centered around -50 m, which supports the idea that peak porpoise presence is focused around areas with the potential to generate tidal wake, jets and internal waves (Figure 4). Within the area of raised likelihood (Figure 26) the relative chance of encountering a harbour porpoise is predicted to be between three and five times higher than the areas with predicted presence (RPPP greater than 0.5). At the peaks the RPPP is between five and eight times higher depending on the stage of the tide cycle. The relationship between complex topography and strong tidal flow generating prosperous foraging opportunities for piscivorous predators such as the harbour porpoise has been discussed already and this idea is widely supported by the literature (Zamon 2003; De Boer et al. 2014; Jones et al. 2014; Benjamins et al. 2015; Nuuttila et al. 2017; Cox et al. 2018).

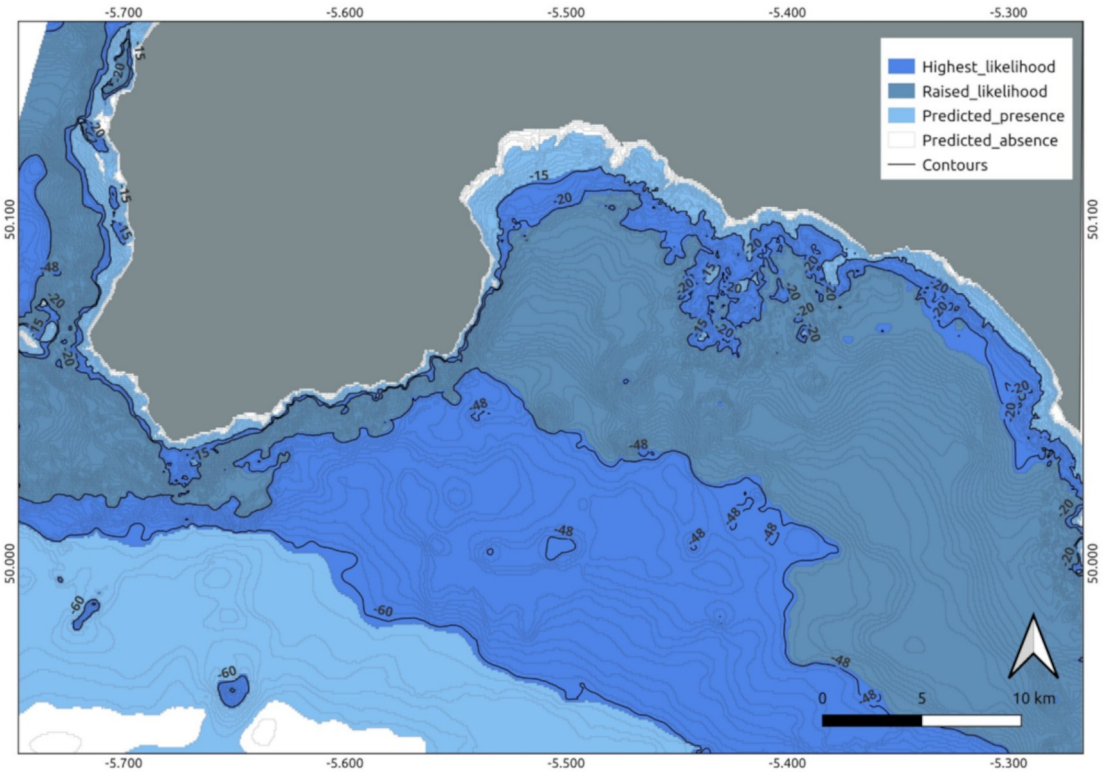

Figure 26: Relative likelihood of harbour porpoise occurrence against water depth. Depth contours are marked in black and key contours are labeled.

5.2.3 Substrate

Substrate was consistently found to be the second or third most influential background variable with the exception of the model for one hour before high water. In this model it was the fourth most influential. Figure 7 shows all harbour porpoise observations in relation to substrate type. Two things are obvious from the figure. The first is that there is an uneven coverage of substrate type within the survey area with sand and muddy sand covering the majority of the area. The second is that the majority of the observations are over sand and muddy sand. There were observations over coarse sediment and rock and diamicton as well however these were few in number. Table 10 shows the area covered by each different type, the number of observations over each substrate type and the observations per km² of each substrate type. There is 16.5 times more sand and muddy sand habitat available than coarse sediment and 70 times more observations over sand and muddy sand than coarse sediment. This is reflected in the higher observations per km² value for sand and muddy sand. Therefore there are more observations per square kilometre of sand and muddy sand. It appears from the model outputs and from the observations shown in figure 7 and table 10 that sand and muddy sand is a habitat favoured by harbour porpoises and the high proportional availability of this habitat in Mount's Bay supports the comparatively high observations of this species in the Bay. These findings are also supported by literature evidence. Williamson et al. (2017) found that harbour porpoises favoured sandy and muddy substrates (Williamson et al. 2017). Booth et al. (2013) found that the percentage of mud in the substrate was an important feature for predicting harbour porpoise presence in some of their models (Booth et al. 2013).

Substrate	Area in km²	Observations	Observations per km²
Sand and muddy sand	537908	1190	0.0022
Coarse sediment	32648	17	0.0005
Rock and diamicton	102834	3	0.0000
Mixed sediment	89338	0	0.0000

Table 10: This shows the area covered by each different type, the number of observations over each substrate type and the observations per km² of each substrate type.

5.2.4 Distance from the Nearest Significant Slope

Distance from the nearest significant slope ranks between third and fifth in the models. One hour before high water it is the third most influential variable, from five hours before to one hour after high water it is the fifth most influential variable and at all other stages of the tide cycle it is the fourth most important variable. The response curves (Figure 8 and Appendix 5) show the model predictions for harbour porpoise presence in relation to the distance from the slope compared with the OMS trend. Abrupt changes in depth cause changes in tidal flow and cause turbulence in the water

column (Bjorkstedt et al. 2002; Thorpe 2007; Jones et al. 2014; Benjamins et al. 2017; Cox et al. 2018). This turbulence generates tidal wake, tidal jets, eddies, internal waves and tidal fronts (Figure 4). These processes focus plankton and nekton (Zamon 2003; De Boer et al. 2014; Jones et al. 2014; Benjamins et al. 2015; Nuuttila et al. 2017; Cox et al. 2018). The steepness of the slope and depth of the water in relation to the tidal flow speed are critical in determining the exact location of these features. Due to variations in tidal flow speed and direction the locations of these features in relation to the slopes causing them changes throughout the tide cycle. Figure 27 shows the significant slopes used in the model and graduated distances from them. Values of RPPP greater than 0.5 represent a higher likelihood a porpoise is present. At high water and three hours after high water the RPPP values do not exceed 0.5 this suggests that in these models the distance to the nearest significant slope does not have an influence on the location of harbour porpoises in Mount's Bay. In all other models values greater than 0.5 start between 100 m and 750 m from the slope and extend to between 1000 m and 8000 m from the slope.

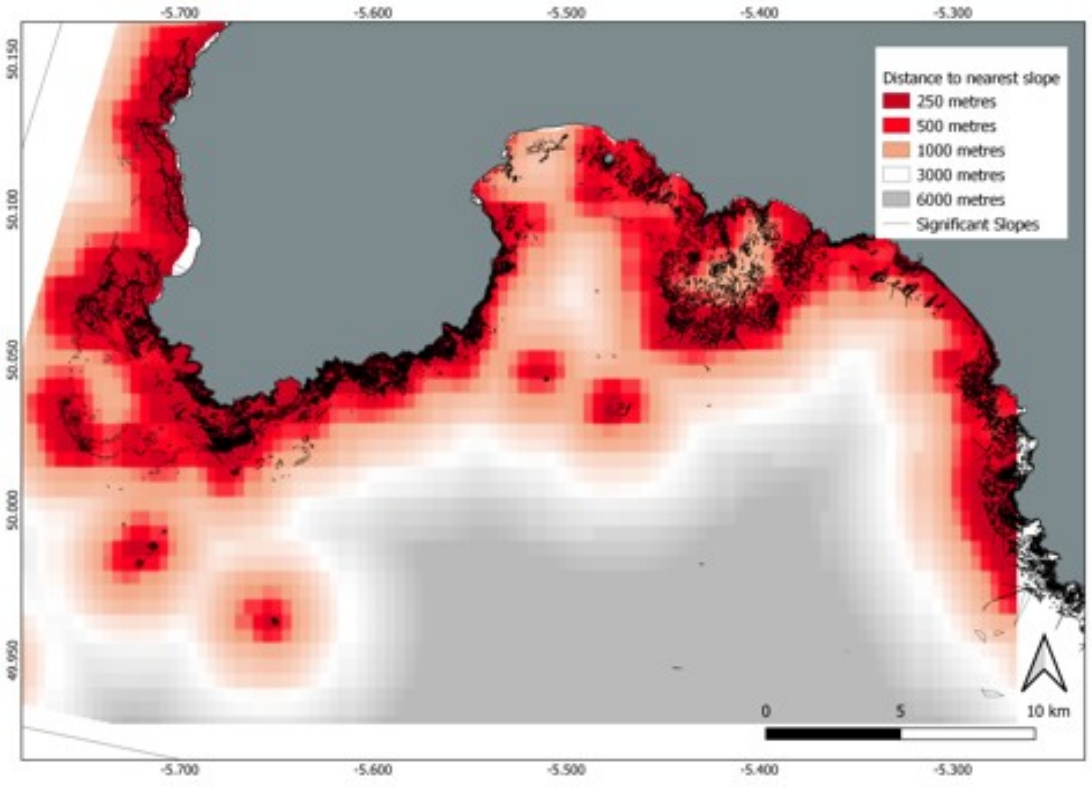

Figure 27: A visual representation of distance from the nearest significant slope.

Peaks in RPPP are typically between 750 m and 2000 m from the slope. As previously discussed the way complex bathymetry and slopes influence tidal processes is not linear. This influence of the variable slope on the model predictions is difficult to interpret exactly. The turbulent processes generated as a tidal stream crosses a shallower area can extend kilometres from their catalyst (Wolanski et al. 1988;

Johnston et al. 2005; Benjamins et al. 2015; Cox et al. 2018). The consistent peak values at distances between 750 m and 2000 m from the slope (five hours before high water is the one exception with a peak at 4000 m) fits well with the scale of turbulent wakes, tidal jets, internal waves and tide fronts that would be generated by the bathymetric features and tidal streams of the strength of those found in Mount's Bay (Thorpe 2007). Table 5 shows a Spearman's rank correlation for available values against survey values of 0.995, which indicates that the survey coverage was not biased and available habitat in relation to slopes was evenly surveyed. The evidence suggests that harbour porpoises favour habitat around the edges of steeper slopes and this is likely to be due to the influence slopes have on tidal processes.

5.2.5 Aspect

Slope aspect was the fifth or sixth most influential variable in all of the models with the exception of the model for one hour after high water in this model it was the fourth most important. Table 11 shows that slopes with an aspect between S – WSW and WSW – WNW represent 60% of the available habitat within the survey area. However the models did not predict a higher likelihood of observing porpoises over them. There is not a clear pattern showing which slopes have a high likelihood of porpoise detections. Although despite representing only 13% of available habitat slopes facing WNW – N are predicted as having the highest likelihood of occurrence in five of the 13 models however these slopes are also predicted as having the lowest likelihood of occurrence in five of the models. Slopes facing between WSW – N are predicted to have the highest likelihood of occurrence in eight of the models and the lowest in six of the models. For the majority of the survey area the slope gradients are less than five percent so it is unlikely the slopes are influencing oceanographic process. It is more likely that the steeper slopes are having more influence on oceanographic processes and the distribution of prey species. The influence of a slope is often spatially removed from the slope and depends on the direction the tidal stream is flowing in relation to the aspect of the slope (Thorpe 2007). The aspect data represents the aspect of the slope at the location of the observation and therefore it is highly possible that the information it is giving is not useful in defining harbour porpoise habitat. However including it in the models did improve AUC scores.

Aspect	% Coverage
N – ENE	9
ENE – ESE	7
ESE – S	12
S – WSW	32
WSW – WNW	28
WNW – N	13

Table 11: This show the percentage of survey area covered by each of the slope aspect categories

5.2.6 Distance from the Nearest Tide Front

Distance from the nearest tide front is consistently ranked as the fifth or sixth most important variable across the models. The RPPP values are greater than 0.5 between 50 m and a maximum of 13 000 m from the front but typically between 50 m and 8000 m. RPPP peaks close to the front in most cases and typically less than 2000 m from the front with the exception of high water where it peaks 10 000 m from the front.

The positions of the tidal fronts used in the model are an estimation. They are also the mean positions calculated using the mean tidal flow speed. This means the exact locations could vary somewhat from the prediction used in the models. The tide front calculation does not include buoyancy frequency, which could also have a small effect on the location of a front depending on the strength of the pynocline (in this case thermocline) (Nimmo Smith et al. 1999). Wind stress, which is dependent on wind speed and direction could also have an impact. Accounting for these factors it can be assumed that the tide front could sit up to a kilometre or more either side of its modelled location (Nimmo Smith et al. 1999; Thorpe 2005; Benjamins et al. 2015; Cox et al. 2018). Boils generated at tidal fronts cannot focus passively moved particulates because the particulates would be focused and dissipated as the boil is focused and dissipated (Benjamins et al. 2015). However if the particulates are not passively moved then the boils could focus them. Zooplankton has the ability to vertically migrate (Gabriel and Thomas 2018) therefore it is possible that billows formed at tidal fronts could generate mechanism that disrupt the vertical movements of zooplankton and focus them at the surface.

Focused patches of zooplankton would have the potential to aggregate the nekton that porpoises would prey on. In some instances these fronts would be described as hydraulic fronts rather than tidal fronts despite them being generated by tidal flow. This is in order to distinguish them from tide fronts associated with the seasonal thermocline. At times when the seasonal thermocline advances northwards it is likely that the hydraulic fronts used in the models mark the boundary between the stratified and mixed water and are therefore also the product of both mechanisms. Whilst the thermocline is present from late April (Figure 24) it intensifies through the summer and peaks in late summer. The peak in thermocline intensity coincides with the peak in harbour porpoise presence in Mount’s Bay (Figure 5). Tidal fronts associated with the thermocline are areas of elevated and persistent productivity (Benjamins et al. 2015; Cox et al. 2018; Suberg et al. 2019).

It would be sensible to assume that there is seasonality to the importance of some of the hydraulic fronts and that this is linked to the presence of the seasonal thermocline. A number of the fronts are associated with the steep slopes around reefs and

headlands. The complex bathymetry in these areas can generate tidal jets, vorticity and internal waves (Jones et al. 2014; Cox et al. 2018). These conditions create high productivity and increased foraging opportunities either by focusing food stuffs and aggregating nekton or disrupting the shoaling behaviour of fish or both (Nimmo et al. 1999; Bjorkstedt et al. 2002; Johnston et al. 2005; Benjamins et al. 2015, 2017; Cox et al. 2018). The temporal influence of the tidal conditions can be difficult to predict and productive conditions typically lag behind the formation of a frontal feature and can also stay as a legacy after the frontal feature has gone. In order to account for this the tidal fronts for the four previous hours of the tidal cycle were included in the tidal front layer for each of the models (Nimmo Smith et al. 1999).

The legacy of fronts depends on how defined they were when present and the tidal stream speed in the following hours of the tide cycle. It is likely that some will only generate conditions focusing plankton and nekton for a short time while others might do so for a few hours. The seasonality of the importance of some sections of the fronts and the complexity of the mechanisms involved in their formation and persistence might explain why the tidal front layer is less influential in the models. Despite this uncertainty the model predicts raised RPPPs in areas close to the fronts in most cases and certainly within the range that the oceanographic processes associated with the fronts will reach.

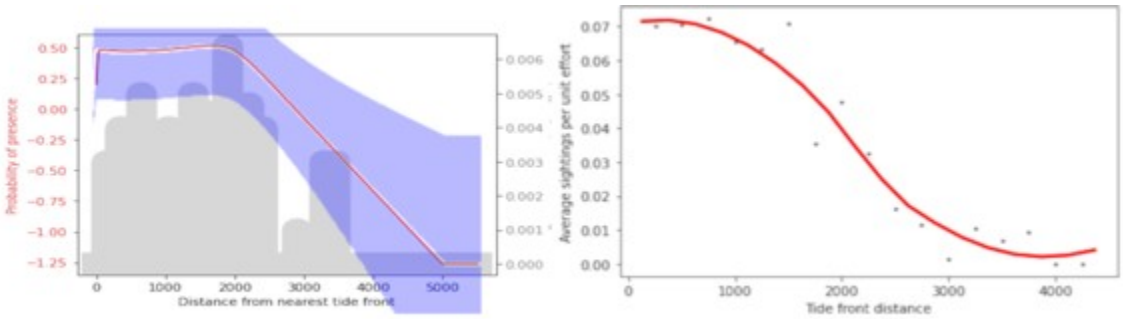

Figure 28: The response curve for all of the data for the variable distance from the nearest tide front is represented with the sightings per unit effort is shown on the left. The shaded area represents variation across 100 models. The plot on the right shows average sightings per unit effort calculated for 250 metre intervals from the nearest tide front against the distance from the nearest tide front in km with a loess line $\alpha = 0.9$ polynomial degrees = 2

Figure 28 shows the response curve on the left next to a plot showing average sightings per unit effort with a loess line plotted on the right. The sightings per effort have a stronger response to distance from the nearest tide front than the response curve. The plot on the right of Figure 28 shows that sightings per effort peak 500 m from the front and are highest within 1000 m of the front, which is within the area that the fronts and their associated mechanisms are likely to influence plankton and nekton distribution.

5.3 GAMLSS Models

The GAMLSS models show an increase in harbour porpoises in Mount's Bay during the study period. It is unclear why this increase has occurred, but there has been a simultaneous increase in other piscivores, such as common dolphins *Delphinus delphis*, minke whales *Balaenoptera acutorostrata*, fin whales *Balaenoptera physalus*, and humpback whales *Megaptera novaeangliae*. Atlantic blue fin tuna *Thunnus thynnus* have also made a documented return to Cornish waters (Horton et al. 2021). It is possible that the increase in these species is due to a rise in the preferred prey species, displacement from other areas due to human activity or a decline in food availability in those areas, as seen in the North Sea (Peschko et al. 2016), or simply due to a population increase in the South West of the UK. Monitoring and understanding this change is crucial, as an increase in harbour porpoises in Mount's Bay could have implications for future conservation efforts (Evans and Prior 2012), particularly if this increase is a result of less favourable conditions in other areas.

The seasonal variation in harbour porpoise presence in Mount's Bay demonstrates that the animals in the Bay form part of a wider population. Harbour porpoise ranges are typically between ~120 km² and ~420 km² (Johnston et al. 2005) and occasionally larger (Bjorge and Oien 1996; Nielsen et al. 2018). The variation in porpoise occurrence correlates with the movement of the spring thermocline and the later development of stronger stratification in Mount's Bay. Harbour porpoises are high foraging animals it is likely that this fluctuation is driven by prey availability (Wisniewska et al. 2016). The availability and density of preferred prey in the area is linked to changes in primary productivity, which are linked to the thermocline and later to stratification and tidal process (Suberg et al. 2019).

The proximity of the thermal front to sightings locations influences the likelihood of animal presence in an area. The closer the front the more likely an animal will be present. The interaction of seasonal thermal fronts with localised tidal fronts enhances the intensity and therefore the productivity at these local fronts (Cox et al. 2017). However there was uncertainty in the models' predictions of the increased likelihood of porpoise occurrences closer to fronts. The composite nature of satellite data, combined with its coarse spatial resolution, introduces uncertainty into the modeling process, which is not accounted for. The spatial and temporal inconsistency in data records and front locations are the source of this uncertainty. The resolution of satellite data is of 1000 m² versus 50 m² for the sightings data. Therefore, caution should be exercised when interpreting the GAMLSS data.

6 Conclusion

High sightings rates per unit of searching effort identify Mount's Bay, Cornwall as an important site for harbour porpoises. The seasonal fluctuations in sighting values suggests the study area does not encompass the entire range for the animals recorded. However the exceptionally high sightings levels per unit effort demonstrate that Mount's Bay is vital part of their wider range. The yearly increase in sighting rates over the time of the study suggest it is becoming an increasingly important area for harbour porpoises.

Harbour porpoise distribution was found to change across the hours of the tide cycle. The distribution of areas with higher RPPP change concurrently with changes in tidal current direction, speeds and identified tidal boundaries. Therefore harbour porpoise distribution appears to be influenced by tidal processes. Although the exact nature of this relationship cannot be conclusively determined. However spatial correlation between the areas of raised RPPP and areas with the conditions necessary to generate advection, internal waves, tidal jets and vorticity is apparent. This relationship suggests that these processes are an important factor influencing harbour porpoise distribution in Mount's Bay, Cornwall.

The high resolution distribution maps generated by the discriminative MaxEnt models offer a valuable tool for identifying overlaps between anthropogenic activities and crucial harbour porpoise habitat. The accuracy of these models demonstrates that the maps effectively represent harbour porpoise distribution across different stages of the tide cycle, allowing for identification of important habitat areas. Implementing controls on gill net fishing in the identified high density areas would reduce the risk of bycatch.

Bibliography

Aguilera, P. A., A. Fernández, F. Reche, and R. Rumí. 2010. Hybrid Bayesian network classifiers: Application to species distribution models. *Environmental Modelling and Software* 25. Elsevier Ltd: 1630–1639. doi:10.1016/j.envsoft.2010.04.016.

Alves, F., R. Ferreira, M. Fernandes, Z. Halicka, L. Dias, and A. Dinis. 2018. Analysis of occurrence patterns and biological factors of cetaceans based on long-term and fine-scale data from platforms of opportunity: Madeira Island as a case study. *Marine Ecology* 39: 1–13. doi:10.1111/maec.12499.

Anderson, R. P. 2013. A framework for using niche models to estimate impacts of climate change on species distributions. *Annals of the New York Academy of Sciences* 1297: 8–28. doi:10.1111/nyas.12264.

Baines, M. E., and S. Earl. 1999. *Analysis of sightings for indications of harbour porpoise breeding off the Welsh coast*. Marine Biodiversity Studies: Technical Science Report 379. Countryside Council for Wales. doi:10.13140/RG.2.2.28680.52483

Baines, M. E., and P. G. H. Evans. 2012. Atlas of the marine mammals of Wales. *CCW Marine Monitoring Report* 68: 139.

Barlow, J., and B. L. Taylor. 2005. Estimates of sperm whale abundance in the northeastern temperate pacific from a combined acoustic and visual survey. *Marine Mammal Science* 21: 429–445. doi:10.1111/j.1748-7692.2005.tb01242.x.

Bas, A. A., F. Christiansen, A. A. Öztürk, B. Öztürk, and C. McIntosh. 2017. The effects of marine traffic on the behaviour of Black Sea harbour porpoises (Phocoena phocoena relicta) within the Istanbul Strait, Turkey. *PLoS ONE* 12: 1–20. doi:10.1371/journal.pone.0172970.

Benjamins, S., A. Dale, G. Hastie, J. Waggitt, M.-A. Lea, B. Scott, and B. Wilson. 2015. Confusion Reigns? A Review of Marine Megafauna Interactions with Tidal-Stream Environments: 1–54. doi:10.1201/b18733-2.

Benjamins, S., N. van Geel, G. Hastie, J. Elliott, and B. Wilson. 2017. Harbour porpoise distribution can vary at small spatiotemporal scales in energetic habitats. *Deep-Sea Research Part II: Topical Studies in Oceanography* 141. Elsevier Ltd: 191–202. doi:10.1016/j.dsr2.2016.07.002.

Berggren, P., and F. Arrhenius. 1995. Sightings of Harbour Porpoises (Phocoena phocoena) in Swedish Waters before 1990. *Biology of the Phocoenids* 1: 100–107.

Bertrand, A., F. Gerlotto, S. Bertrand, M. Gutiérrez, L. Alza, A. Chipollini, E. Díaz, P. Espinoza, et al. 2008. Schooling behaviour and environmental forcing in relation to anchoveta distribution: An analysis across multiple spatial scales. *Progress in Oceanography* 79. Elsevier Ltd: 264–277. doi:10.1016/j.pocean.2008.10.018.

Bjorge, A., and N. Oien. 1996. Distribution and abundance of harbour porpoise, Phocoena phocoena, in Norwegian waters. *Biology of the Phocoenids* 16: 89–98.

Bjorkstedt, E. P., L. K. Rosenfeld, B. A. Grantham, Y. Shkedy, and J. Roughgarden. 2002. Distributions of larval rockfishes Sebastes spp. across nearshore fronts in a coastal upwelling region. *Marine Ecology Progress Series* 242: 215–228.

de Boer, M. N. 2013. Elusive Marine Mammals Explored. Wageningen.

de Boer, M. N., D. Jones, H. Jones, and R. Knee. 2018. Spatial and Temporal Baseline Information on Marine Megafauna-Data Facilitated by a Wildlife Tour Operator. *Open Journal of Marine Science* 08: 76–113. doi:10.4236/ojms.2018.81005.

de Boer, M. N., M. P. Simmonds, P. J. H. Reijnders, and G. Aarts. 2014. The influence of topographic and dynamic cyclic variables on the distribution of small cetaceans in a shallow coastal system. *PLoS ONE* 9. doi:10.1371/journal.pone.0086331.

Booth, C. G., C. Embling, J. Gordon, S. V. Calderan, and P. S. Hammond. 2013. Habitat preferences and distribution of the harbour porpoise Phocoena phocoena west of Scotland. *Marine Ecology Progress Series* 478: 273–285. doi:10.3354/meps10239.

Bosch, S., L. Tyberghein, K. Deneudt, F. Hernandez, and O. De Clerck. 2018. In search of relevant predictors for marine species distribution modelling using the MarineSPEED benchmark dataset. *Diversity and Distributions* 24: 144–157. doi:10.1111/ddi.12668.

Boyce, M. S., P. R. Vernier, S. E. Nielsen, and F. K. A. Schmiegelow. 2002. Evaluating resource selection functions. *Ecological Modelling* 157: 281–300.

Breckling, B., F. Jopp, and H. Reuter. 2011. *Historical background of ecological modelling and its importance for modern ecology*. *Modelling Complex Ecological Dynamics: An Introduction into Ecological Modelling for Students, Teachers & Scientists*. doi:10.1007/978-3-642-05029-9-3.

Brereton, T., D. Jones, K. Leeves, K. Lewis, R. Davies, and T. Russel. 2018. Population structure, mobility and conservation of common bottlenose dolphin off south-west England from photo-identification studies. *Journal of the Marine*

Biological Association of the United Kingdom 98: 1055–1063. doi:10.1017/S0025315417000121.

Brownlee, J. 2020. *Machine Learning Mastery with Python: Understand your data, create accurate models and work projects end to end*. 1.19. Machine Learning Mastery.

Buckland, S. T., D. R. Anderson, K. P. Burnham, J. L. Laake, D. L. Borchers, and L. Thomas. 2004. Advanced Distance Sampling: 416.

Cantor, M., and H. Whitehead. 2013. The interplay between social networks and culture: Theoretically and among Whales and Dolphins. *Philosophical Transactions of the Royal Society B: Biological Sciences* 368. doi:10.1098/rstb.2012.0340.

Cayula, J.F., Cornillon, P. 1995. Multi-image edge detection for SST images. *Journal of Atmospheric and Oceanic Technology* 12 (4), 821–829.

Clay, T. A., J. C. Mangel, J. Alfaro-Shigueto, D. J. Hodgson, and B. J. Godley. 2018. Distribution and habitat use of a cryptic small cetacean, the Burmeister's porpoise, monitored from a small-scale fishery platform. *Frontiers in Marine Science* 5. doi:10.3389/fmars.2018.00220.

Correia, A. M., M. Gandra, M. Liberal, R. Valente, Á. Gil, M. Rosso, G. J. Pierce, and I. Sousa-Pinto. 2019. A dataset of cetacean occurrences in the Eastern North Atlantic. *Scientific data* 6: 177. doi:10.1038/s41597-019-0187-2.

Cox, S. L., M. J. Witt, C. B. Embling, B. J. Godley, P. J. Hosegood, P. I. Miller, S. C. Votier, and S. N. Ingram. 2017. Temporal patterns in habitat use by small cetaceans at an oceanographically dynamic marine renewable energy test site in the Celtic Sea. *Deep-Sea Research Part II: Topical Studies in Oceanography* 141. Elsevier: 178–190. doi:10.1016/j.dsr2.2016.07.001.

Cox, S. L., C. B. Embling, P. J. Hosegood, S. C. Votier, and S. N. Ingram. 2018. Oceanographic drivers of marine mammal and seabird habitat-use across shelf-seas: A guide to key features and recommendations for future research and conservation management. *Estuarine, Coastal and Shelf Science*. Academic Press. doi:10.1016/j.ecss.2018.06.022.

Coyle, K. O., G. L. Hunt, M. B. Decker, and T. J. Weingartner. 1992. Murre foraging, epibenthic sound scattering and tidal advection over a shoal near St George Island, Bering Sea. *Marine Ecology Progress Series* 83: 1–14. doi:10.3354/meps083001.

Desportes, G., J. H. Kristensen, D. Benham, S. Wilson, T. Jepsen, B. Korsgaard, U. Siebert, J. Driver, et al. 2003. Multiple insights into the reproductive function of

harbour porpoises (*Phocoena phocoena*): An ongoing study. *NAMMCO Scientific Publications* 5: 91. doi:10.7557/3.2741.

Dolman, S., S. Baulch, P. G. H. Evans, F. Read, and F. Ritter. 2016. Towards an EU Action Plan on Cetacean Bycatch. *Marine Policy* 72. Elsevier Ltd: 67–75. doi:10.1016/j.marpol.2016.06.020.

Durban, J., D. Ellifrit, M. Dahlheim, J. Waite, C. Matkin, L. Barrett-Lennard, G. Ellis, R. Pitman, et al. 2010. Photographic mark-recapture analysis of clustered mammal-eating killer whales around the Aleutian Islands and Gulf of Alaska. *Marine Biology* 157: 1591–1604. doi:10.1007/s00227-010-1432-6.

Dyndo, M., D. M. Wišniewska, L. Rojano-Doñate, and P. T. Madsen. 2015. Harbour porpoises react to low levels of high frequency vessel noise. *Scientific Reports* 5. Nature Publishing Group: 1–9. doi:10.1038/srep11083.

Elith, J., C. H. Graham, R. P. Anderson, M. Dudík, A. Guisan, R. J. Hijmans, F. Huettmann, J. R. Leathwick, et al. 2006. Novel Methods Improve Prediction of Species ' Distributions from Occurrence Data Published by : Wiley on behalf of Nordic Society Oikos Stable URL : https://www.jstor.org/stable/3683475 REFERENCES Linked references are available on JSTOR for this article .

Elith, J., S. J. Phillips, T. Hastie, M. Dudík, Y. E. Chee, and C. J. Yates. 2011. A statistical explanation of MaxEnt for ecologists. *Diversity and Distributions* 17: 43–57. doi:10.1111/j.1472-4642.2010.00725.x.

Embling, C. B., J. Illian, E. Armstrong, J. van der Kooij, J. Sharples, K. C. J. Camphuysen, and B. E. Scott. 2012. Investigating fine-scale spatio-temporal predator-prey patterns in dynamic marine ecosystems: A functional data analysis approach. *Journal of Applied Ecology* 49: 481–492. doi:10.1111/j.1365-2664.2012.02114.x.

Embling, C. B., J. Sharples, E. Armstrong, M. R. Palmer, and B. E. Scott. 2013. Fish behaviour in response to tidal variability and internal waves over a shelf sea bank. *Progress in Oceanography* 117. Elsevier Ltd: 106–117. doi:10.1016/j.pocean.2013.06.013.

Evans, P. G. H. 2008. Selection criteria for marine protected areas for cetaceans. *Proceedings of the ECS/ASCOBANS/ACCOBAMS workshop*: 1–106.

Evans, P. G. H., and P. S. Hammond. 2004. Monitoring cetaceans in European waters. *Mammal Review* 34: 131–156. doi:10.1046/j.0305-1838.2003.00027.x.

Evans, P. G. H., and J. S. Prior. 2012. Protecting the harbour porpoise in UK seas: 105.

Fernandez, M., C. Yesson, A. Gannier, P. I. Miller, and J. M. N. Azevedo. 2018. A matter of timing: How temporal scale selection influences cetacean ecological niche modelling. *Marine Ecology Progress Series* 595. Inter-Research: 217–231. doi:10.3354/meps12551.

Forney, K. A. 2002. Surveys. In *Encyclopedia of Marine Mammals*, ed. W. F. Perrin, B. Wuersig, and J. G. M. Thewissen, 1203–1205. London: Academic Press.

Gabriel, W., and B. Thomas. 2018. Vertical Migration of Zooplankton as an Evolutionarily Stable Strategy Author (s): Wilfried Gabriel and Bernhard Thomas Source : The American Naturalist , Vol . 132 , No . 2 (Aug ., 1988), pp . 199-216 Published by : The University of Chicago Press fo 132: 199–216.

Gaskin, D. E., S. Yamamoto, and A. Kawamura. 1993. Harbour porpoise, Phocoena phocoena (L), in the coastal waters of northern Japan. *Fish Bulletin* 91: 440–454.

Geman, S., E. Bienenstock, and R. Doursat. 1992. Neural Networks and the Bias/Variance Dilemma. *Neural Computation*. doi:10.1162/neco.1992.4.1.1.

Gilles, A., S. Viquerat, E. A. Becker, K. A. Forney, S. C. V. Geelhoed, J. Haelters, J. Nabe-Nielsen, M. Scheidat, et al. 2016. Seasonal habitat-based density models for a marine top predator, the harbor porpoise, in a dynamic environment. *Ecosphere* 7: 1–22. doi:10.1002/ecs2.1367.

Giné, G. A. F., and D. Faria. 2018. Combining species distribution modeling and field surveys to reappraise the geographic distribution and conservation status of the threatened thin-spined porcupine (Chaetomys subspinosus). *PLoS ONE* 13: 1–22. doi:10.1371/journal.pone.0207914.

Golding, N., and B. V. Purse. 2016. Fast and flexible Bayesian species distribution modelling using Gaussian processes. *Methods in Ecology and Evolution* 7: 598–608. doi:10.1111/2041-210X.12523.

Gómez-Gutiérrez, J., and C. J. Robinson. 2006. Tidal current transport of epibenthic swarms of the euphausiid Nyctiphanes simplex in a shallow, subtropical bay on Baja California peninsula, México. *Marine Ecology Progress Series* 320: 215–231. doi:10.3354/meps320215.

Goodwin, L., and C. Speedie. 2008. Relative abundance, density and distribution of the harbour porpoise (Phocoena phocoena) along the west coast of the UK. *Journal of the Marine Biological Association of the United Kingdom* 88. Lund University Libraries: 1221–1228. doi:10.1017/S0025315408001173.

Guillera-Arroita, G., J. J. Lahoz-Monfort, and J. Elith. 2014. Maxent is not a presence-absence method: A comment on Thibaud et al. *Methods in Ecology and Evolution* 5: 1192–1197. doi:10.1111/2041-210X.12252.

Halvorsen, R. 2013. *A strict maximum likelihood explanation of MaxEnt, and some implications for distribution modelling*. *Sommerfeltia*. Vol. 36. doi:10.2478/v10208-011-0016-2.

Hammond, P. S. 2009. Mark-recapture. *Encyclopedia of Marine Mammals*: 705–709. doi:10.1016/B978-0-12-373553-9.00163-2.

Hammond, P. S., C. Lacey, A. Gilles, S. Viquerat, P. Börjesson, H. Herr, K. Macleod, V. Ridoux, et al. 2021. Estimates of cetacean abundance in European Atlantic waters in summer 2016 from the SCANS-III aerial and shipboard surveys. *Sea Mammal Research Unite, University of St Andrews, UK* 7: 1–42.

Hauser, D. D. W., G. R. Vanblaricom, E. E. Holmes, and R. W. Osborne. 2006. Evaluating the use of whalewatch data in determining killer whale (Orcinus orca) distribution patterns. *Journal of Cetacean Research and Management* 8: 273–281.

Heinänen, S., and H. Skov. 2015. The identification of discrete and persistent areas of relatively high harbour porpoise density in the wider UK marine area, JNCC Report No. 544, JNCC, Peterborough. *JNCC Report No. 544*: 108.

Hoekendijk, J. P. A., J. Spitz, A. J. Read, M. F. Leopold, and M. C. Fontaine. 2018. Resilience of harbor porpoises to anthropogenic disturbance: Must they really feed continuously? *Marine Mammal Science* 34: 258–264. doi:10.1111/mms.12446.

Horton, T. W., B. A. Block, R. Davies, L. A. Hawkes, D. Jones, H. Jones, K. Leeves, N. Maoiléidigh, et al. 2021. Evidence of increased occurrence of Atlantic bluefin tuna in territorial waters of the United Kingdom and Ireland. *ICES Journal of Marine Science* 78: 1672–1683. doi:10.1093/icesjms/fsab039.

Hoyt, E. 2005. *Marine Protected Areas for Whales, Dolphins and Porpoises*. London: Earthscan.

IJsseldijk, L. L., K. C. J. Camphuysen, J. J. Nauw, and G. Aarts. 2015. Going with the flow: Tidal influence on the occurrence of the harbour porpoise (Phocoena phocoena) in the Marsdiep area, The Netherlands. *Journal of Sea Research* 103. Elsevier B.V.: 129–137. doi:10.1016/j.seares.2015.07.010.

International Whaling Commission. 1995. *Biology of the Phocoenids*. Edited by A. Bjorge and G. P. Donovan. First. Cambridge: Cambridge University Press.

JNCC. 2017. *Inshore and Offshore Special Area of Conservation : Bristol Channel Approaches / Dynesfeydd Môr Hafren SAC Selection Assessment Document January 2017 Further information*.

Johnston, D. W., A. J. Westgate, and A. J. Read. 2005. Effects of fine-scale oceanographic features on the distribution and movements of harbour porpoises Phocoena phocoena in the Bay of Fundy. *Marine Ecology Progress Series* 295: 279–293. doi:10.3354/meps295279.

Jones, A. R., P. Hosegood, R. B. Wynn, M. N. De Boer, S. Butler-Cowdry, and C. B. Embling. 2014. Fine-scale hydrodynamics influence the spatio-temporal distribution of harbour porpoises at a coastal hotspot. *Progress in Oceanography* 128. Elsevier Ltd: 30–48. doi:10.1016/j.pocean.2014.08.002.

Keener, W., M. A. Webber, I. D. Szczepaniak, T. M. Markowitz, and D. N. Orbach. 2018. The sex life of harbor porpoises (Phocoena phocoena): Lateralized and aerial behavior. *Aquatic Mammals* 44: 620–632. doi:10.1578/AM.44.6.2018.620.

King, S. L., R. S. Schick, C. Donovan, C. G. Booth, M. Burgman, L. Thomas, and J. Harwood. 2015. An interim framework for assessing the population consequences of disturbance. *Methods in Ecology and Evolution* 6: 1150–1158. doi:10.1111/2041-210X.12411.

Kiszka, J., K. Macleod, O. Van Canneyt, D. Walker, and V. Ridoux. 2007. Distribution, encounter rates, and habitat characteristics of toothed cetaceans in the Bay of Biscay and adjacent waters from platform-of-opportunity Data. *ICES Journal of Marine Science* 64: 1033–1043. doi:10.1093/icesjms/fsm067.

Knee, R. 2018. Harbour porpoise.

Koopman, H. N., D. A. Pabst, W. A. McLellan, R. M. Dillaman, and J. Read. 2002. Topptraphical distribution of the blubber of harbour porpoises (Phocoena phocoena). *Phisiological biochemical zoology* 75: 498–512.

Kyhn, L. A., J. Tougaard, K. Beedholm, F. H. Jensen, E. Ashe, R. Williams, and P. T. Madsen. 2013. Clicking in a Killer Whale Habitat: Narrow-Band, High-Frequency Biosonar Clicks of Harbour Porpoise (Phocoena phocoena) and Dall's Porpoise (Phocoenoides dalli). *PLoS ONE* 8. doi:10.1371/journal.pone.0063763.

Lambert, C., E. Pettex, G. Dorémus, S. Laran, E. Stéphan, O. Van Canneyt, and V. Ridoux. 2017. How does ocean seasonality drive habitat preferences of highly mobile top predators? Part II: The eastern North-Atlantic. *Deep-Sea Research Part II: Topical Studies in Oceanography* 141. Elsevier: 133–154. doi:10.1016/j.dsr2.2016.06.011.

Leopold, M. 2015. Eat and be eaten: Porpoise diet studies. Wageningen University. doi:10.4324/9780203169353_chapter_11.

Lockyer, C. 2003a. A review of methods for defining population structure in the harbour porpoise (*Phocoena phocoena*). *NAMMCO Scientific Publications* 5: 41.

doi:10.7557/3.2739.

Lockyer, C. 2003b. Harbour porpoises (*Phocoena phocoena*) in the North Atlantic: Biological parameters. *NAMMCO Scientific Publications* 5: 71. doi:10.7557/3.2740.

MacLoed, C. D. 2013. Creating a Species Distribution Model (SDM). In *An introduction to using GIS in Marine Biology: Supplementary workbook three. Integrating GIS and species distributuon modelling.*, 1st ed., 59–83. Glasgow: Pictish Beast Publications.

Marmion, M., M. Parviainen, M. Luoto, R. K. Heikkinen, and W. Thuiller. 2009. Evaluation of consensus methods in predictive species distribution modelling. *Diversity and Distributions* 15: 59–69. doi:10.1111/j.1472-4642.2008.00491.x.

McMahon, L. A., J. L. Rachlow, L. A. Shipley, J. S. Forbey, and T. R. Johnson. 2017. Habitat selection differs across hierarchical behaviors: Selection of patches and intensity of patch use: Selection. *Ecosphere* 8. doi:10.1002/ecs2.1993.

Merckx, B., M. Steyaert, A. Vanreusel, M. Vincx, and J. Vanaverbeke. 2011. Null models reveal preferential sampling, spatial autocorrelation and overfitting in habitat suitability modelling. *Ecological Modelling* 222. Elsevier B.V.: 588–597. doi:10.1016/j.ecolmodel.2010.11.016.

Merow, C., and J. A. Silander. 2014. A comparison of Maxlike and Maxent for modelling species distributions. *Methods in Ecology and Evolution* 5: 215–225. doi:10.1111/2041-210X.12152.

Merow, C., J. M. Allen, M. Aiello-Lammens, and J. A. Silander. 2013. A practical guide to MaxEnt for modeling species' distributions: What it does, and why inputs and settings matter - Supplementary material. *Global Ecology and Biogeography* 25.

Merow, C., J. M. Allen, M. Aiello-Lammens, and J. A. Silander. 2016. Improving niche and range estimates with Maxent and point process models by integrating spatially explicit information. *Global Ecology and Biogeography* 25: 1022–1036. doi:10.1111/geb.12453.

Miller P. 2009. Composite front maps for improved visibility of dynamic sea-surface features on cloudy SeaWiFS and AVHRR data. *Journal of Marine systems* 78: 327-336

Mikkelsen, L., F. F. Rigét, L. A. Kyhn, S. Sveegaard, R. Dietz, J. Tougaard, J. A. K. Carlström, I. Carlén, et al. 2016. Comparing Distribution of Harbour Porpoises (Phocoena phocoena) Derived from Satellite Telemetry and Passive Acoustic Monitoring. *PloS one* 11: e0158788. doi:10.1371/journal.pone.0158788.

Morales, N. S., I. C. Fernández, and V. Baca-González. 2017. MaxEnt's parameter configuration and small samples: Are we paying attention to recommendations? A systematic review. *PeerJ* 2017: 1–16. doi:10.7717/peerj.3093.

Murphy, S., J. L. Barber, J. A. Learmonth, F. L. Read, R. Deaville, M. W. Perkins, A. Brownlow, N. Davison, et al. 2015. Reproductive failure in UK harbour porpoises phocoena phocoena: Legacy of pollutant exposure? *PLoS ONE* 10: 1–32. doi:10.1371/journal.pone.0131085.

Neave, D. J., and B. S. Wright. 1968. Seasonal migrations in the harbour porpoise and other cetatceans in the Bay of Fundy. *Mammalogy* 49: 259–264.

Nielsen, N. H., J. Teilmann, S. Sveegaard, R. G. Hansen, M. H. S. Sinding, R. Dietz, and M. P. Heide-Jørgensen. 2018. Oceanic movements, site fidelity and deep diving in harbour porpoises from Greenland show limited similarities to animals from the North Sea. *Marine Ecology Progress Series* 597: 259–272. doi:10.3354/meps12588.

Nimmo Smith, W. A. M., S. A. Thorpe, and A. Graham. 1999. Surface effects of bottom-generated turbulence in a shallow tidal sea. *Nature* 400: 251–254. doi:10.1038/22295.

Nuuttila, H. K., W. Courtene-Jones, S. Baulch, M. Simon, and P. G. H. Evans. 2017. Don't forget the porpoise: acoustic monitoring reveals fine scale temporal variation between bottlenose dolphin and harbour porpoise in Cardigan Bay SAC. *Marine Biology* 164. Springer Verlag. doi:10.1007/s00227-017-3081-5.

Oakley, J. A., R. E. Jenkins, T. Thomas, A. T. Williams, and M. R. Phillips. 2016. Assessing harbour porpoise populations in south-west Wales, data issues and implications for conservation and management. *Ocean and Coastal Management* 119. Elsevier Ltd: 45–57. doi:10.1016/j.ocecoaman.2015.09.011.

Oakley, J. A., A. T. Williams, and T. Thomas. 2017. Reactions of harbour porpoise (Phocoena phocoena) to vessel traffic in the coastal waters of South West Wales, UK. *Ocean and Coastal Management* 138. Elsevier Ltd: 158–169. doi:10.1016/j.ocecoaman.2017.01.003.

Peschko, V., K. Ronnenberg, U. Siebert, and A. Gilles. 2016. Trends of harbour porpoise (Phocoena phocoena) density in the southern North Sea. *Ecological Indicators* 60: 174–183. doi:10.1016/j.ecolind.2015.06.030.

Phillips, S. J. 2017. A Brief Tutorial on Maxent.

Phillips, S. J., and M. Dudík. 2008. Modeling of species distributions with Maxent: New extensions and a comprehensive evaluation. *Ecography* 31: 161–175. doi:10.1111/j.0906-7590.2008.5203.x.

Pierce, G. J., M. B. Santos, and S. Cerviño. 2007. Assessing sources of variation underlying estimates of cetacean diet composition: A simulation study on analysis of harbour porpoise diet in Scottish (UK) waters. *Journal of the Marine Biological Association of the United Kingdom* 87: 213–221. doi:10.1017/S0025315407055348.

Quantum GIS. 2021.

R Core Team. 2017. R: A Language and Environment for Statistical Computing. Vienna, Austria.

Reiss, H., H. Cunze, K. König, K. Neumann, and I. Kröncke. 2011. Species distribution modelling of marine benthos: A North Sea case study. *Marine Ecology Progress Series* 442: 71–86. doi:10.3354/meps09391.

Robbins, J., L. Babey, and C. Embling. 2019. Citizen science in the marine environment: A case-study estimating common dolphin densities in the north-east Atlantic. *PeerJ Preprints*. doi:10.7287/peerj.preprints.27569.

Roberts, L., S. Collier, S. Law, and A. Gaion. 2019. The impact of marine vessels on the presence and behaviour of harbour porpoise (Phocoena phocoena) in the waters off Berry Head, Brixham (South West England). *Ocean and Coastal Management* 179. Elsevier: 104860. doi:10.1016/j.ocecoaman.2019.104860.

de Rock, P., S. H. Elwen, J. P. Roux, R. H. Leeney, B. S. James, V. Visser, M. J. Martin, and T. Gridley. 2019. Predicting large-scale habitat suitability for cetaceans off Namibia using MinxEnt. *Marine Ecology Progress Series* 619: 149–167. doi:10.3354/meps12934.

Rojano-Donãte, L., B. I. McDonald, D. M. Wisniewska, M. Johnson, J. Teilmann, M. Wahlberg, J. Højer-Kristensen, and P. T. Madsen. 2018. High field metabolic rates of wild harbour porpoises. *Journal of Experimental Biology* 221. doi:10.1242/jeb.185827.

Romero, V., R. Rumí, and A. Salmerón. 2006. Learning hybrid Bayesian networks using mixtures of truncated exponentials. *International Journal of Approximate Reasoning* 42: 54–68. doi:10.1016/j.ijar.2005.10.004.

Sastri, A. R., J. Gauthier, P. Juneau, and B. E. Beisner. 2014. Biomass and productivity responses of zooplankton communities to experimental thermocline deepening. *Limnology and Oceanography* 59: 1–16. doi:10.4319/lo.2014.59.1.0001.

Schick, R. S. 2002. Spatial Correlation Between Bluefin Tuna and Sea Surface Temperature Fronts. In *Marine Geography GIS for Oceans and Seas*, ed. J. Breman, 1st ed., 61–66. Redlands: Esri Press.

Sergeant, D. E., and H. D. Fisher. 1957. The Smaller Cetacea of eastern Canadian Waters. *Fish Research* 14: 83–115.

Simon, M., H. Nuuttila, M. M. Reyes-Zamudio, F. Ugarte, U. Verfub, and P. G. H. Evans. 2010. Passive acoustic monitoring of bottlenose dolphin and harbour porpoise, in Cardigan Bay, Wales, with implications for habitat use and partitioning. *Journal of the Marine Biological Association of the United Kingdom* 90: 1539–1545. doi:10.1017/S0025315409991226.

Speakman, T. R., S. M. Lane, L. H. Schwacke, P. A. Fair, and E. S. Zolman. 2010. Mark-recapture estimates of seasonal abundance and survivorship for bottlenose dolphins (Tursiops truncatus) near Charleston, South Carolina, USA. *Journal of Cetacean Research and Management* 11: 153–162.

Stasinopoulos, M., R. A. Rigby, and C. Akantziliotou. 2008. Instructions on how to use the GAMLSS package in R: 206.

Stern, S. J., W. Keener, I. D. Szczepaniak, and M. A. Webber. 2017. Return of Harbor porpoises (Phocoena phocoena) to San Francisco Bay. *Aquatic Mammals* 43: 691–702. doi:10.1578/AM.43.6.2017.691.

Suberg, L. A. 2015. Investigations of the variability of tidal mixing fronts and their importance for shelf-sea ecosystems across multiple trophic levels 3: 106–107.

Suberg, L. A., P. I. Miller, and R. B. Wynn. 2019. On the use of satellite-derived frontal metrics in time series analyses of shelf-sea fronts, a study of the Celtic Sea. *Deep-Sea Research Part I: Oceanographic Research Papers* 149. Elsevier Ltd: 103033. doi:10.1016/j.dsr.2019.04.011.

Tessarolo, G., T. F. Rangel, M. B. Araújo, and J. Hortal. 2014. Uncertainty associated with survey design in species distribution models. *Diversity and Distributions* 20: 1258–1269. doi:10.1111/ddi.12236.

Thibaud, E., B. Petitpierre, O. Broennimann, A. C. Davison, and A. Guisan. 2014. Measuring the relative effect of factors affecting species distribution model predictions. *Methods in Ecology and Evolution* 5: 947–955. doi:10.1111/2041-210X.12203.

Thompson, P. M., K. L. Brookes, and L. S. Cordes. 2015. Patterns of Occurrence in Coastal Dolphins. *ICES Journal of Marine Science* 72: 651–660.

Thorpe, S. A. 2005. Mixing by tidal process. In *The Turbulent Ocean*, 1st ed., 282–322. Cambridge: Cambridge University Press.

Thorpe, S. 2007. Turbulence in oceanic boundary layers. In *An Introduction to Ocean Turbulence*, 1st ed., pp. 77-115. Cambridge: Cambridge University Press.

Uncles, R. J., and J. A. Stephens. 2007. SEA 8 Technical Report - Hydrography. *UK Department of Trade and Industry's offshore energy Strategic Environmental Assessment programme*: 1–105.

Venables W. N., and Ripley B. D. 2002. *Modern Applied Statistics with S*. Fourth. New York: Springer.

Verfuß, U. K., L. A. Miller, P. K. D. Pilz, and H. Schnitzler. 2009. Echolocation by two foraging harbour porpoises (Phocoena phocoena): 823–834. doi:10.1242/jeb.022137.

Viddi, F. A., R. Hucke-Gaete, J. P. Torres-Florez, and S. Ribeiro. 2010. Spatial and seasonal variability in cetacean distribution in the fjords of northern Patagonia, Chile. *ICES Journal of Marine Science* 67: 959–970. doi:10.1093/icesjms/fsp288.

Virgili, A., M. Authier, P. Monestiez, and V. Ridoux. 2018. How many sightings to model rare marine species distributions. *PLoS ONE* 13: 1–21. doi:10.1371/journal.pone.0193231.

Waggitt, J. J., H. K. Dunn, P. G. H. Evans, J. G. Hiddink, L. J. Holmes, E. Keen, B. D. Murcott, M. Piano, et al. 2018. Regional-scale patterns in harbour porpoise occupancy of tidal stream environments. *ICES Journal of Marine Science* 75: 701–710. doi:10.1093/icesjms/fsx164.

Waggitt, J. J., P. G. H. Evans, J. Andrade, A. N. Banks, O. Boisseau, M. Bolton, G. Bradbury, T. Brereton, et al. 2019. Distribution maps of cetacean and seabird populations in the North-East Atlantic. *Journal of Applied Ecology*. doi:10.1111/1365-2664.13525.

Williams, R., E. Ashe, K. Gaut, R. Gryba, J. E. Moore, E. Rexstad, D. Sandilands, J. Steventon, et al. 2017. Animal counting toolkit: A practical guide to small-boat surveys for estimating abundance of coastal marine mammals. *Endangered Species Research* 34. Inter-Research: 149–165. doi:10.3354/esr00845.

Williamson, L. D., K. L. Brookes, B. E. Scott, I. M. Graham, and P. M. Thompson. 2017. Diurnal variation in harbour porpoise detection-potential implications for management. *Marine Ecology Progress Series* 570: 223–232. doi:10.3354/meps12118.

Wisniewska, D. M. M., M. Johnson, J. Teilmann, L. Rojano-Doñate, J. Shearer, S. Sveegaard, L. A. A. Miller, U. Siebert, et al. 2016. Ultra-High Foraging Rates of Harbor Porpoises Make Them Vulnerable to Anthropogenic Disturbance. *Current Biology* 26: 1441–1446. doi:10.1016/j.cub.2016.03.069.

Witman, J. D., J. J. Leichter, S. J. Genovese, and D. A. Brooks. 1993. Pulsed phytoplankton supply to the rocky subtidal zone: Influence of internal waves. *Proceedings of the National Academy of Sciences of the United States of America* 90: 1686–1690. doi:10.1073/pnas.90.5.1686.

Wolanski, E., E. Drew, K. M. Abel, and J. O'Brien. 1988. Tidal jets, nutrient upwelling and their influence on the productivity of the alga Halimeda in the Ribbon Reefs, Great Barrier Reef. *Estuarine, Coastal and Shelf Science* 26: 169–201. doi:10.1016/0272-7714(88)90049-2.

Yasui, W. Y., and D. E. Gaskin. 1986. Energy budget of a small cetacean, the harbour porpoise, phocoena phocoena (L.). *Ophelia* 25: 183–197. doi:10.1080/00785326.1986.10429749.

Zamon, J. E. 2003. Mixed species aggregations feeding upon herring and sandlance schools in a nearshore archipelago depend on flooding tidal currents. *Marine Ecology Progress Series* 261: 243–255. doi:10.3354/meps261243.

Zhang, G., and A. X. Zhu. 2018. The representativeness and spatial bias of volunteered geographic information: a review. *Annals of GIS* 24. Taylor & Francis: 151–162. doi:10.1080/19475683.2018.1501607.

Zimmer, W. M. X. 2011. *Passive Acoustic Monitoring of Ceataceans*. Cambridge.

Zurr, A. F., E. N. Ieno, N. Walker, A. A. Saveliev, and G. M. Smith. 2009. *Mixed effects models and extensions in ecology with RStatistics for Biology and Health*. Edited by M. Gail, K. Krickeberg, J. Samet, A. Tsiatsis, and W. Wong. New York: Springer.

Appendix 1

Detection curves

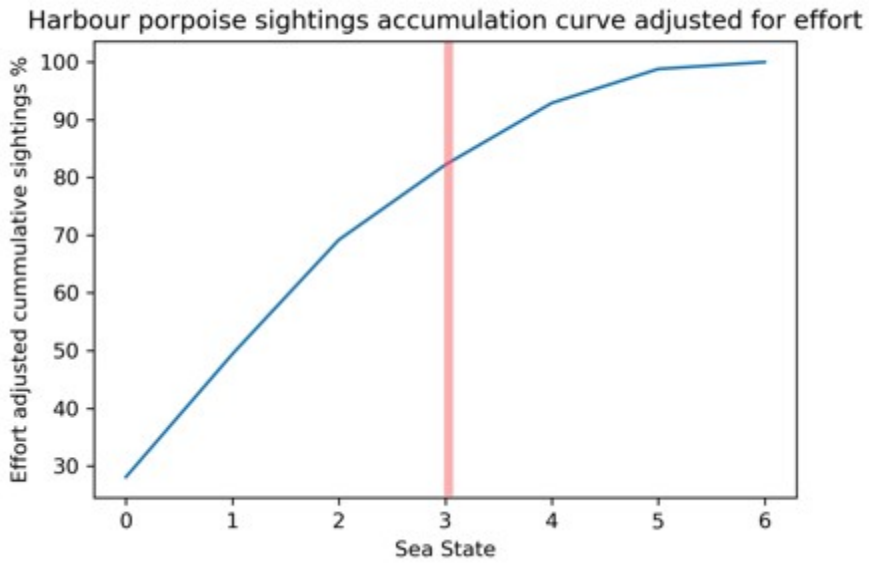

Effort adjusted cumulative sightings by sea state. Data recorded in sea state three and below were included. This is demarcated by the red line.

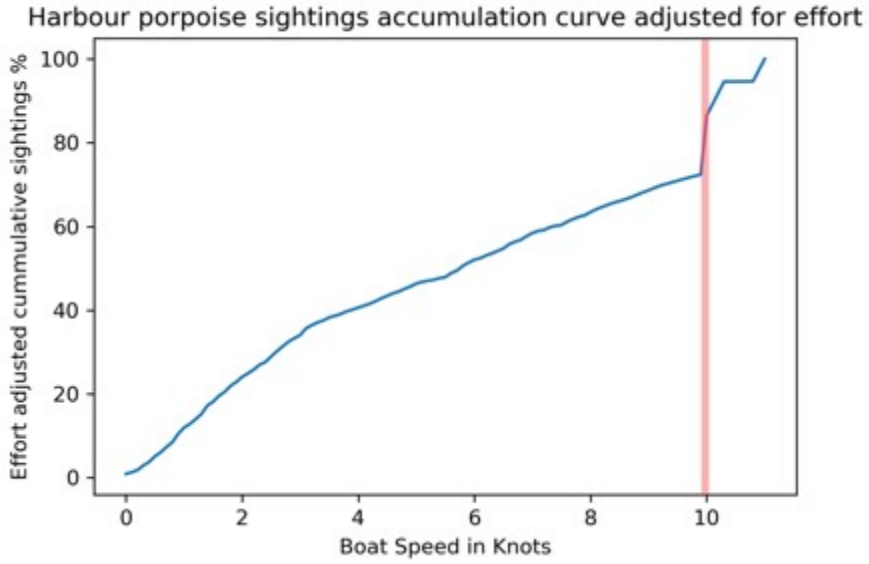

Effort adjusted cumulative sightings by boat speed. Data recorded at boat speeds of 10 knots and below were included. This is demarcated by the red line.

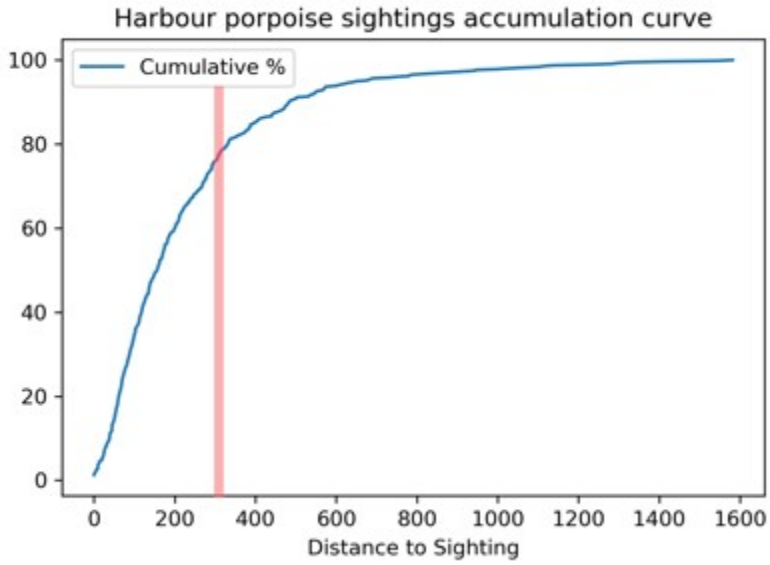

Effort adjusted cumulative sightings by distance to sighting. Porpoises were consistently sighted at a distance of <=300 m. This is demarcated by the red line.

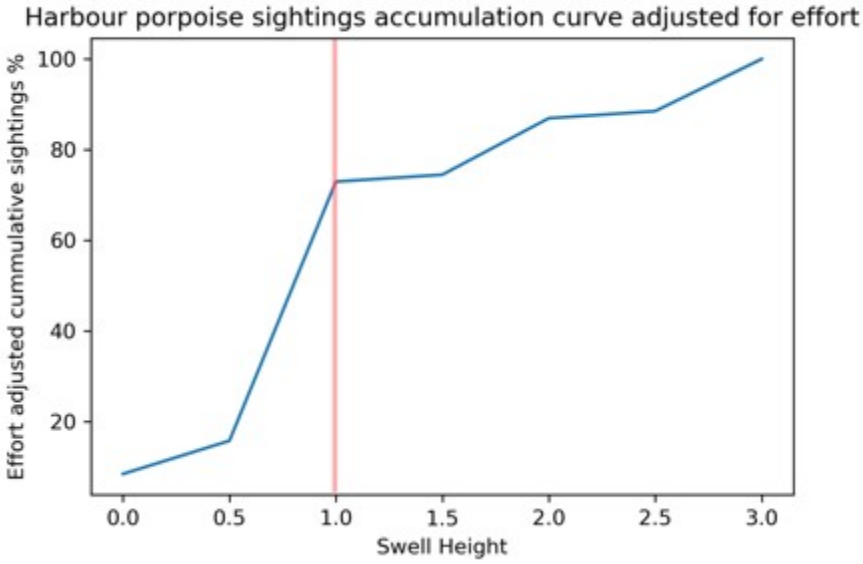

Effort adjusted cumulative sightings by swell height. Porpoises were consistently sighted up to a swell height of one metre. This is demarcated by the red line.

Appendix 2

Correlation Matrix for all Variables

	MONTH	YEAR	Y	X	SWELL	SSTATE	SP_KNT	Aspect	Depth	Slope%	SST	Time to	Substrate	Chl	fr_dist	fr_side	FrGrdDen	FrPerDen	tide_dir	tide_spd	distance	aspect	TiDrAsp	weight_eff
MONTH	1.000	-0.023	-0.108	0.052	0.012	-0.034	-0.011	0.037	-0.123	-0.049	0.607	0.011	-0.036	0.044	-0.124	0.100	0.042	0.065	-0.003	-0.036	0.189	-0.005	-0.003	-0.057
YEAR	-0.023	1.000	0.001	0.063	0.017	-0.033	-0.422	0.021	-0.014	-0.027	-0.046	0.011	-0.055	-0.043	-0.002	0.046	0.057	-0.092	-0.036	-0.041	0.128	0.013	-0.005	0.012
Y	-0.108	0.001	1.000	0.644	-0.172	-0.039	0.000	-0.100	0.874	0.046	-0.199	0.056	0.066	0.142	0.481	-0.009	-0.492	-0.493	-0.149	-0.521	-0.438	0.074	0.042	0.436
X	0.052	0.063	0.644	1.000	-0.179	-0.079	-0.061	0.053	0.477	-0.111	-0.039	0.136	-0.039	0.103	0.435	0.000	-0.312	-0.339	-0.185	-0.699	0.190	0.070	0.008	0.121
SWELL	0.012	0.017	-0.172	-0.179	1.000	0.468	-0.011	-0.020	-0.158	0.011	-0.055	0.027	-0.019	-0.048	-0.043	-0.027	-0.003	0.072	0.036	0.099	0.005	-0.012	-0.006	-0.002
SSTATE	-0.034	-0.033	-0.039	-0.079	0.468	1.000	0.031	-0.016	-0.030	0.010	-0.082	0.006	-0.018	-0.024	0.065	0.020	-0.066	-0.009	0.022	0.034	-0.035	-0.007	-0.005	0.041
SP_KNT	-0.011	-0.422	0.000	-0.061	-0.011	0.031	1.000	-0.003	0.002	0.007	0.008	-0.014	0.029	-0.008	0.061	-0.026	-0.044	0.012	0.031	0.050	-0.072	-0.032	-0.022	0.105
aspect	0.037	0.021	-0.100	0.053	-0.020	-0.016	-0.003	1.000	-0.100	-0.057	0.050	0.012	0.026	-0.001	-0.030	0.019	0.077	0.064	0.004	-0.004	0.184	0.055	-0.021	-0.145
Depth	-0.123	-0.014	0.874	0.477	-0.158	-0.030	0.002	-0.100	1.000	0.195	-0.192	0.043	0.193	0.127	0.399	-0.007	-0.350	-0.379	-0.106	-0.366	-0.402	0.061	0.052	0.436
Slope%	-0.049	-0.027	0.046	-0.111	0.011	0.010	0.007	-0.057	0.195	1.000	-0.040	-0.025	0.064	-0.002	-0.015	-0.002	-0.019	-0.021	0.010	0.098	-0.198	0.003	0.013	0.079
SST	0.607	-0.046	-0.199	-0.039	-0.055	-0.082	0.008	0.050	-0.192	-0.040	1.000	-0.023	-0.012	0.048	-0.209	-0.109	0.247	0.179	-0.022	0.054	0.195	-0.030	-0.013	-0.083
Time to HW	0.011	0.011	0.056	0.136	0.027	0.006	-0.014	0.012	0.043	-0.025	-0.023	1.000	0.004	0.015	0.072	0.037	-0.037	-0.040	-0.310	-0.167	0.070	0.001	-0.014	-0.012
NUMBER	0.038	0.027	-0.002	0.010	-0.007	-0.028	-0.025	0.000	-0.004	-0.006	0.024	-0.001	-0.005	0.008	-0.003	-0.002	0.010	0.002	-0.011	-0.009	0.013	0.002	-0.002	-0.006
Substrate	-0.036	-0.055	0.066	-0.039	-0.019	-0.018	0.029	0.026	0.193	0.064	-0.012	0.004	1.000	0.011	-0.005	-0.007	0.030	0.006	0.013	0.143	-0.104	-0.024	0.019	-0.086
Chl	0.044	-0.043	0.142	0.103	-0.048	-0.024	-0.008	-0.001	0.127	-0.002	0.048	0.015	0.011	1.000	0.020	-0.015	-0.079	-0.068	-0.010	-0.082	-0.043	0.016	0.002	0.017
fr_dist	-0.124	-0.002	0.481	0.435	-0.043	0.065	0.061	-0.030	0.399	-0.015	-0.209	0.072	-0.005	0.020	1.000	-0.106	-0.386	-0.432	-0.105	-0.343	-0.127	0.021	0.016	0.188
fr_side	0.100	0.046	-0.009	0.000	-0.027	0.020	-0.026	0.019	-0.007	-0.002	-0.109	0.037	-0.007	-0.015	-0.106	1.000	-0.103	-0.112	0.006	-0.011	0.036	0.008	-0.020	-0.012
FrGrdDen_E	0.042	0.057	-0.492	-0.312	-0.003	-0.066	-0.044	0.077	-0.350	-0.019	0.247	-0.037	0.030	-0.079	-0.386	-0.103	1.000	0.652	0.049	0.228	0.313	-0.050	0.013	-0.204
FrPerDen_E	0.065	-0.092	-0.493	-0.339	0.072	-0.009	0.012	0.064	-0.379	-0.021	0.179	-0.040	0.006	-0.068	-0.432	-0.112	0.652	1.000	0.096	0.262	0.249	-0.057	0.011	-0.202
tide_dir	-0.003	-0.036	-0.149	-0.185	0.036	0.022	0.031	0.004	-0.106	0.010	-0.022	-0.310	0.013	-0.010	-0.105	0.006	0.049	0.096	1.000	0.001	-0.012	-0.033	0.029	-0.008
tide_spd	-0.036	-0.041	-0.521	-0.699	0.099	0.034	0.050	-0.004	-0.366	0.098	0.054	-0.167	0.143	-0.082	-0.343	-0.011	0.228	0.262	0.001	1.000	-0.070	-0.023	0.007	-0.211
distance	0.189	0.128	-0.438	0.190	0.005	-0.035	-0.072	0.184	-0.402	-0.198	0.195	0.070	-0.104	-0.043	-0.127	0.036	0.313	0.249	-0.012	-0.070	1.000	-0.064	-0.030	-0.316
aspect	-0.005	0.013	0.074	0.070	-0.012	-0.007	-0.032	0.055	0.061	0.003	-0.030	0.001	-0.024	0.016	0.021	0.008	-0.050	-0.057	-0.033	-0.023	-0.064	1.000	0.056	-0.063
TiDrAsp	-0.003	-0.005	0.042	0.008	-0.006	-0.005	-0.022	-0.021	0.052	0.013	-0.013	-0.014	0.019	0.002	0.016	-0.020	0.013	0.011	0.029	0.007	-0.030	0.056	1.000	0.009
weight_eff	-0.057	0.012	0.436	0.121	-0.002	0.041	0.105	-0.145	0.436	0.079	-0.083	-0.012	-0.086	0.017	0.188	-0.012	-0.204	-0.202	-0.008	-0.211	-0.316	-0.063	0.009	1.000

Correlation for all Variables

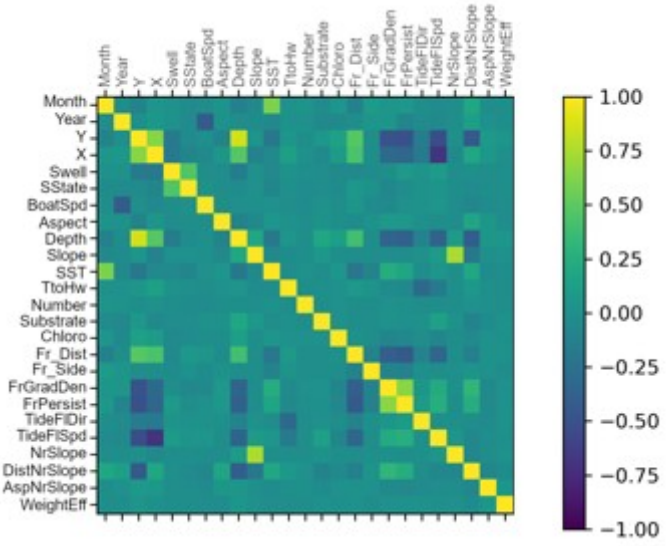

Correlation matrix for all variables

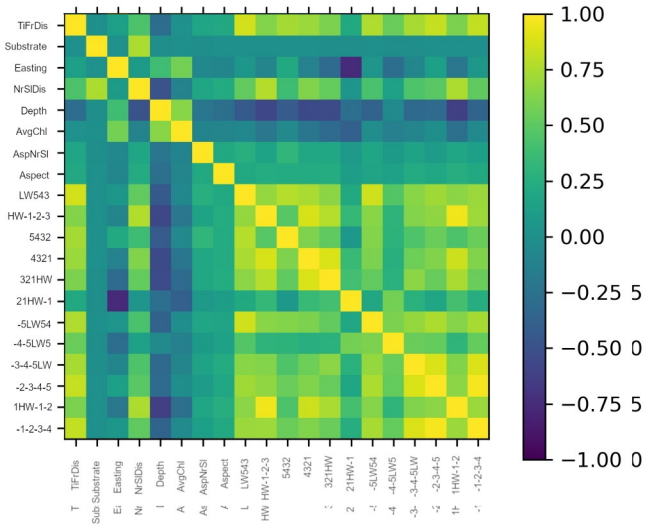

Correlation results for MaxEnt background features

	TiFrDis	substrate	easting	distNrSl	depth	AVRGchl	aspect_nr_	aspect	lw543	hw-1-2-3	5432	4321	321hw	21hw-1	-5lw54	-4-5lw5	-3-4-5lw	-2-3-4-5	1hw-1-2	-1-2-3-4
TiFrDis	1.00	0.04	0.16	0.53	-0.30	0.00	0.06	0.23	0.89	0.72	0.78	0.82	0.80	0.46	0.78	0.61	0.78	0.78	0.69	0.80
substrate	0.04	1.00	-0.11	-0.07	0.01	-0.10	0.10	0.09	0.04	0.00	0.04	0.04	0.18	0.09	0.01	0.08	0.17	0.02	-0.01	0.03
easting	0.16	-0.11	1.00	0.28	0.38	0.63	-0.10	-0.08	0.09	0.03	0.19	0.01	-0.12	-0.52	0.17	-0.08	0.12	0.29	-0.07	0.19
distNrSl	0.53	-0.07	0.28	1.00	-0.43	-0.06	0.05	0.20	0.57	0.65	0.55	0.62	0.54	0.10	0.54	0.17	0.54	0.59	0.64	0.57
depth	-0.30	0.01	0.38	-0.43	1.00	0.64	-0.17	-0.25	-0.45	-0.54	-0.48	-0.54	-0.54	-0.31	-0.37	-0.07	-0.33	-0.30	-0.58	-0.35
AVRGchl	0.00	-0.10	0.63	-0.06	0.64	1.00	-0.12	-0.12	-0.05	-0.12	-0.08	-0.20	-0.26	-0.31	0.07	-0.07	-0.06	0.01	-0.19	-0.03
aspect_nr_	0.06	0.10	-0.10	0.05	-0.17	-0.12	1.00	0.22	0.15	0.02	0.20	0.11	0.13	0.03	0.04	-0.02	-0.03	-0.09	0.03	-0.04
aspect	0.23	0.09	-0.08	0.20	-0.25	-0.12	0.22	1.00	0.25	0.26	0.25	0.26	0.29	0.21	0.18	0.18	0.25	0.19	0.26	0.24
lw543	0.89	0.04	0.09	0.57	-0.45	-0.05	0.15	0.25	1.00	0.77	0.87	0.86	0.85	0.45	0.86	0.51	0.68	0.65	0.73	0.68
hw-1-2-3	0.72	0.00	0.03	0.65	-0.54	-0.12	0.02	0.26	0.77	1.00	0.58	0.79	0.80	0.55	0.82	0.48	0.81	0.79	0.95	0.85
5432	0.78	0.04	0.19	0.55	-0.48	-0.08	0.20	0.25	0.87	0.58	1.00	0.82	0.76	0.26	0.69	0.32	0.49	0.50	0.54	0.53
4321	0.82	0.04	0.01	0.62	-0.54	-0.20	0.11	0.26	0.86	0.79	0.82	1.00	0.95	0.46	0.70	0.32	0.62	0.62	0.77	0.64
321hw	0.80	0.18	-0.12	0.54	-0.54	-0.26	0.13	0.29	0.85	0.80	0.76	0.95	1.00	0.60	0.69	0.44	0.68	0.60	0.77	0.64
21hw-1	0.46	0.09	-0.52	0.10	-0.31	-0.31	0.03	0.21	0.45	0.55	0.26	0.46	0.60	1.00	0.49	0.73	0.50	0.35	0.64	0.46
-5lw54	0.78	0.01	0.17	0.54	-0.37	0.07	0.04	0.18	0.86	0.82	0.69	0.70	0.69	0.49	1.00	0.63	0.75	0.74	0.82	0.76
-4-5lw5	0.61	0.08	-0.08	0.17	-0.07	-0.07	-0.02	0.18	0.51	0.48	0.32	0.32	0.44	0.73	0.63	1.00	0.68	0.57	0.51	0.63
-3-4-5lw	0.78	0.17	0.12	0.54	-0.33	-0.06	-0.03	0.25	0.68	0.81	0.49	0.62	0.68	0.50	0.75	0.68	1.00	0.93	0.77	0.95
-2-3-4-5	0.78	0.02	0.29	0.59	-0.30	0.01	-0.09	0.19	0.65	0.79	0.50	0.62	0.60	0.35	0.74	0.57	0.93	1.00	0.74	0.96
1hw-1-2	0.69	-0.01	-0.07	0.64	-0.58	-0.19	0.03	0.26	0.73	0.95	0.54	0.77	0.77	0.64	0.82	0.51	0.77	0.74	1.00	0.81
-1-2-3-4	0.80	0.03	0.19	0.57	-0.35	-0.03	-0.04	0.24	0.68	0.85	0.53	0.64	0.64	0.46	0.76	0.63	0.95	0.96	0.81	1.00

Correlation coefficients for GAMLSS independent variables

Appendix 3

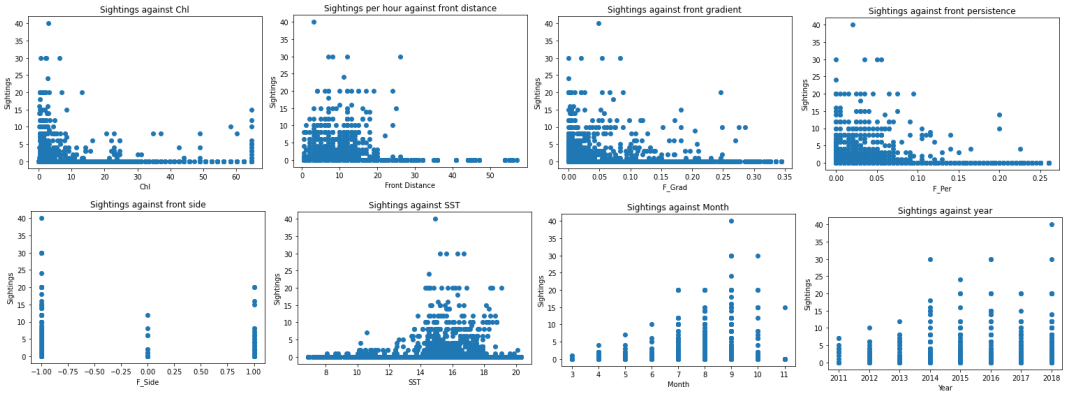

Scattergraphs showing the distribution of data across the independent variables used in the GAMLSS model

Scattergraphs showing the distribution of data across the independent variables used in the GAMLSS model

Appendix 4

Alldat fper NBI

****

Summary of the Randomised Quantile Residuals

mean = 0.00368444

variance = 1.008043

coef. of skewness = -0.009199229

coef. of kurtosis = 2.97877

Filliben correlation coefficient = 0.9999847

****

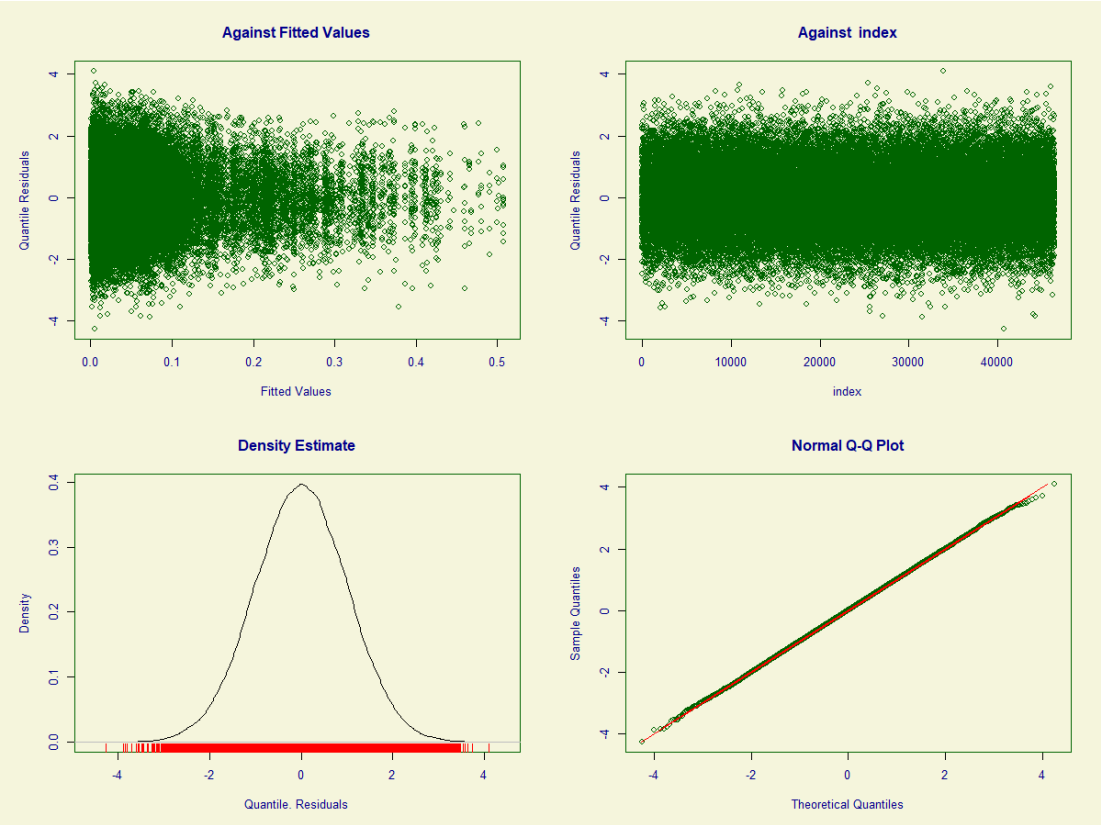

Feature selection

```
> dropterm(allNB, test="Chisq")
Single term deletions for
mu

Model:
num ~ cs(sst, df = 5) + cs(fr_dist, df = 5) + cs(chl, df = 5) +
    cs(frper, df = 5) + cs(mnth, df = 5) + cs(yr, df = 5)
                   Df    AIC    LRT   Pr(Chi)
<none>                   7268.4
cs(sst, df = 5)     5.9991 7261.5  5.091   0.53214
cs(fr_dist, df = 5) 6.0010 7269.0 12.595   0.04997 *
cs(chl, df = 5)     6.0007 7260.7  4.347   0.62995
cs(frper, df = 5)   5.9988 7262.9  6.488   0.37067
cs(mnth, df = 5)    5.9991 7328.4 72.075 1.532e-13 ***
cs(yr, df = 5)      5.9995 7338.2 81.814 1.506e-15 ***
---
Signif. codes:  0 ‘***’ 0.001 ‘**’ 0.01 ‘*’ 0.05 ‘.’ 0.1 ‘ ’ 1

> allNBstep<-stepGAIC.VR(allNB)
```

```
Distribution parameter:  mu
Start:  AIC= 7268.37
 num ~ cs(sst, df = 5) + cs(fr_dist, df = 5) + cs(chl, df = 5) +
    cs(frper, df = 5) + cs(mnth, df = 5) + cs(yr, df = 5)

                      Df    AIC
- cs(chl, df = 5)     6.0007 7260.7
- cs(sst, df = 5)     5.9991 7261.5
- cs(frper, df = 5)   5.9988 7262.9
<none>                      7268.4
- cs(fr_dist, df = 5) 6.0010 7269.0
- cs(mnth, df = 5)    5.9991 7328.4
- cs(yr, df = 5)      5.9995 7338.2

Step:  AIC= 7260.72
 num ~ cs(sst, df = 5) + cs(fr_dist, df = 5) + cs(frper, df = 5) +
    cs(mnth, df = 5) + cs(yr, df = 5)

                      Df    AIC
- cs(sst, df = 5)     5.9991 7254.3
- cs(frper, df = 5)   5.9988 7254.7
<none>                      7260.7
- cs(fr_dist, df = 5) 6.0010 7261.6
- cs(mnth, df = 5)    5.9991 7321.4
- cs(yr, df = 5)      5.9995 7328.3

Step:  AIC= 7254.26
 num ~ cs(fr_dist, df = 5) + cs(frper, df = 5) + cs(mnth, df = 5) +
    cs(yr, df = 5)

                      Df    AIC
- cs(frper, df = 5)   5.9988 7248.5
<none>                      7254.3
- cs(fr_dist, df = 5) 6.0010 7256.1
- cs(yr, df = 5)      5.9995 7330.7
- cs(mnth, df = 5)    6.0001 7362.1

Step:  AIC= 7248.55
 num ~ cs(fr_dist, df = 5) + cs(mnth, df = 5) + cs(yr, df = 5)

                      Df    AIC
<none>                      7248.5
```

- cs(fr_dist, df = 5) 6.0010 7250.6
- cs(yr, df = 5) 5.9995 7326.3
- cs(mnth, df = 5) 6.0001 7353.9

All Data NBI fden

****

Summary of the Randomised Quantile Residuals
mean = 0.0004442008
variance = 1.001852
coef. of skewness = -0.004708093
coef. of kurtosis = 3.014481
Filliben correlation coefficient = 0.9999844

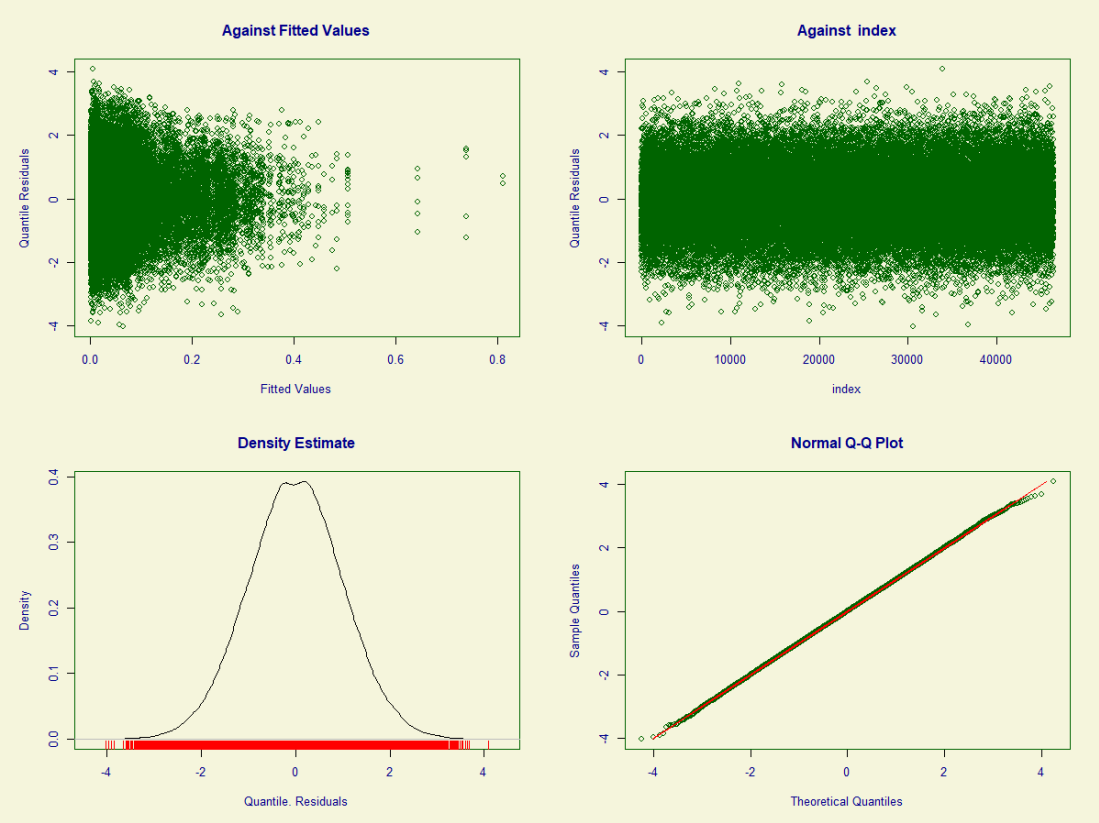

Feature selection

Model:
num ~ cs(sst, df = 5) + cs(fr_dist, df = 5) + cs(chl, df = 5) +
  cs(frden, df = 5) + cs(mnth, df = 5) + cs(yr, df = 5)
Df AIC LRT Pr(Chi)
<none> 7271.6

```
cs(sst, df = 5)     5.9991 7264.4  4.794   0.57039
cs(fr_dist, df = 5) 6.0009 7272.1 12.481   0.05208 .
cs(chl, df = 5)     6.0007 7263.6  3.979   0.67955
cs(frden, df = 5)   5.9990 7262.9  3.261   0.77534
cs(mnth, df = 5)    5.9990 7329.6 70.011 4.062e-13 ***
cs(yr, df = 5)      5.9995 7338.5 78.883 6.072e-15 ***
---
Signif. codes:  0 ‘***’ 0.001 ‘**’ 0.01 ‘*’ 0.05 ‘.’ 0.1 ‘ ’ 1


> allNBstep1<-stepGAIC.VR(allNB1)
Distribution parameter:  mu
Start:  AIC= 7271.6
 num ~ cs(sst, df = 5) + cs(fr_dist, df = 5) + cs(chl, df = 5) +
    cs(frden, df = 5) + cs(mnth, df = 5) + cs(yr, df = 5)

                      Df    AIC
- cs(frden, df = 5)   5.9990 7262.9
- cs(chl, df = 5)     6.0007 7263.6
- cs(sst, df = 5)     5.9991 7264.4
<none>                     7271.6
- cs(fr_dist, df = 5) 6.0009 7272.1
- cs(mnth, df = 5)    5.9990 7329.6
- cs(yr, df = 5)      5.9995 7338.5

Step:  AIC= 7262.86
 num ~ cs(sst, df = 5) + cs(fr_dist, df = 5) + cs(chl, df = 5) +
    cs(mnth, df = 5) + cs(yr, df = 5)

                      Df    AIC
- cs(chl, df = 5)     6.0007 7254.7
- cs(sst, df = 5)     5.9991 7256.1
<none>                     7262.9
- cs(fr_dist, df = 5) 6.0009 7263.6
- cs(mnth, df = 5)    5.9990 7320.1
- cs(yr, df = 5)      5.9995 7331.3

Step:  AIC= 7254.69
 num ~ cs(sst, df = 5) + cs(fr_dist, df = 5) + cs(mnth, df = 5) +
    cs(yr, df = 5)

                      Df    AIC
```

- cs(sst, df = 5) 5.9991 7248.5
<none> 7254.7
- cs(fr_dist, df = 5) 6.0009 7255.6
- cs(mnth, df = 5) 5.9990 7312.8
- cs(yr, df = 5) 5.9995 7321.8

Step: AIC= 7248.55
 num ~ cs(fr_dist, df = 5) + cs(mnth, df = 5) + cs(yr, df = 5)

Df AIC
<none> 7248.5
- cs(fr_dist, df = 5) 6.0010 7250.6
- cs(yr, df = 5) 5.9995 7326.3
- cs(mnth, df = 5) 6.0001 7353.9

Appendix 5

The plots comparing response curves (red line in appendix 5.1 to 5.12 with observations per minute effort (OMS) (grey histograms in appendix 5.1 to 5.12) are shown below. The plots demonstrate the influence of OMS on the model response and indicate how well the models fit observations of porpoises. The performance of the variables at different hours of the tide cycle are also summarised in table 6 section 4.2.2 of the main text.

5.1 At the time of High Water in Penzance

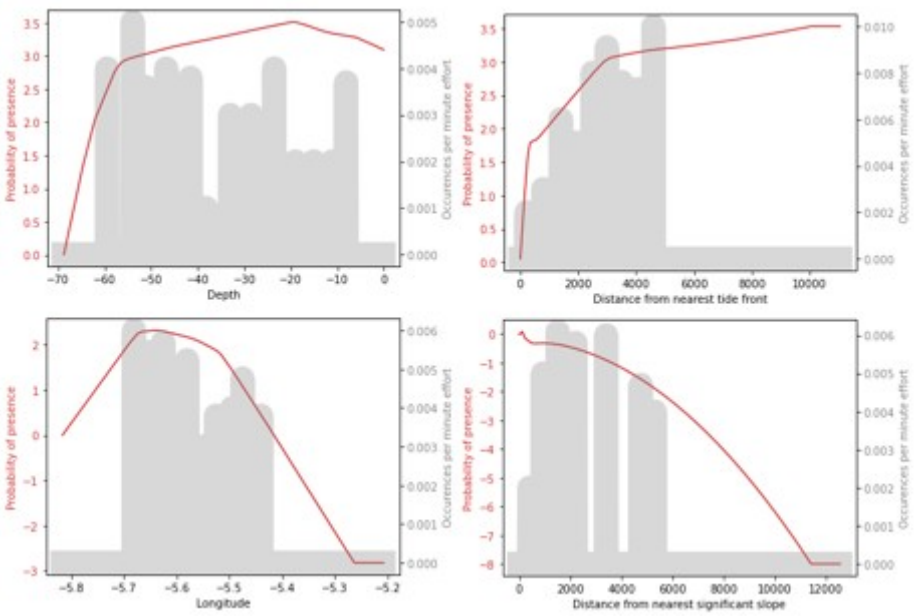

5.2 One hour after High Water in Penzance

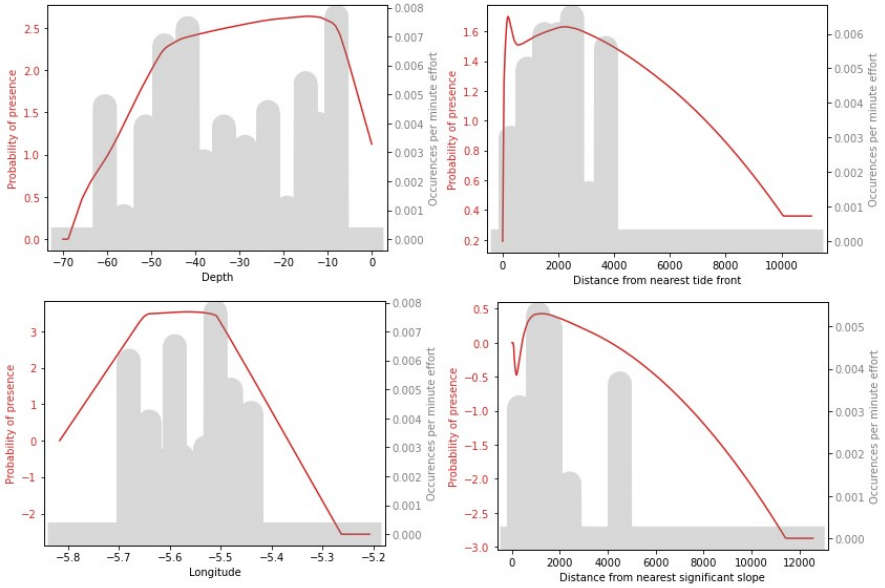

5.3 Two hours after High Water in Penzance

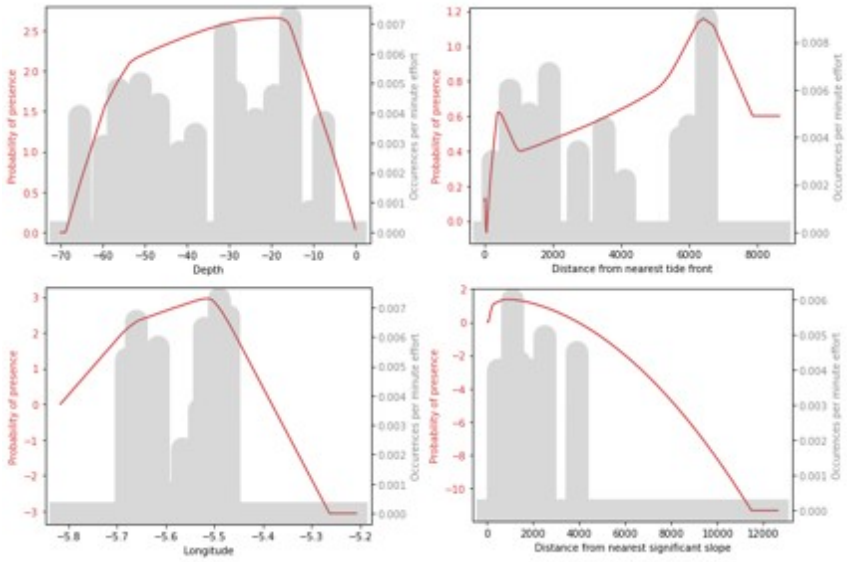

5.4 Three hours after High Water in Penzance

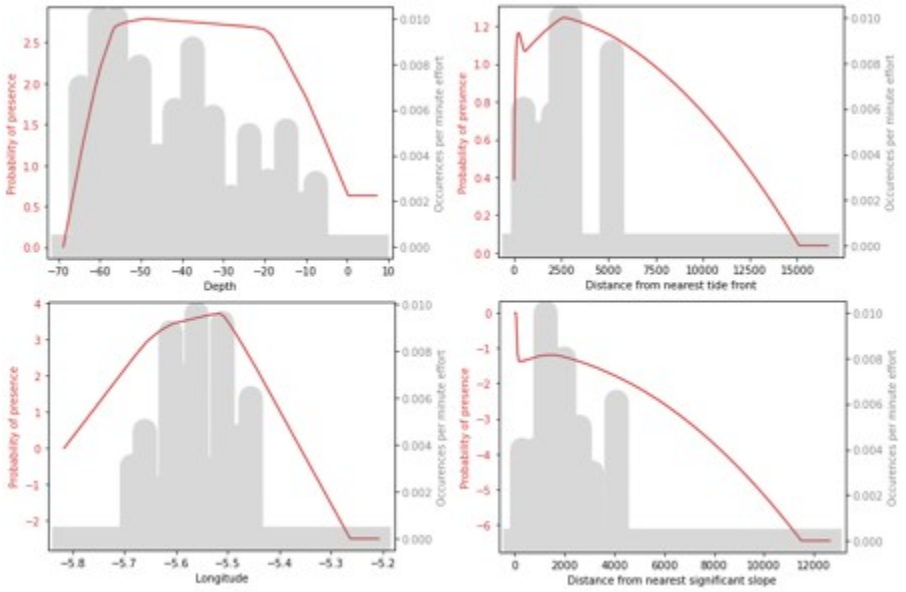

5.5 Four hours after High Water in Penzance

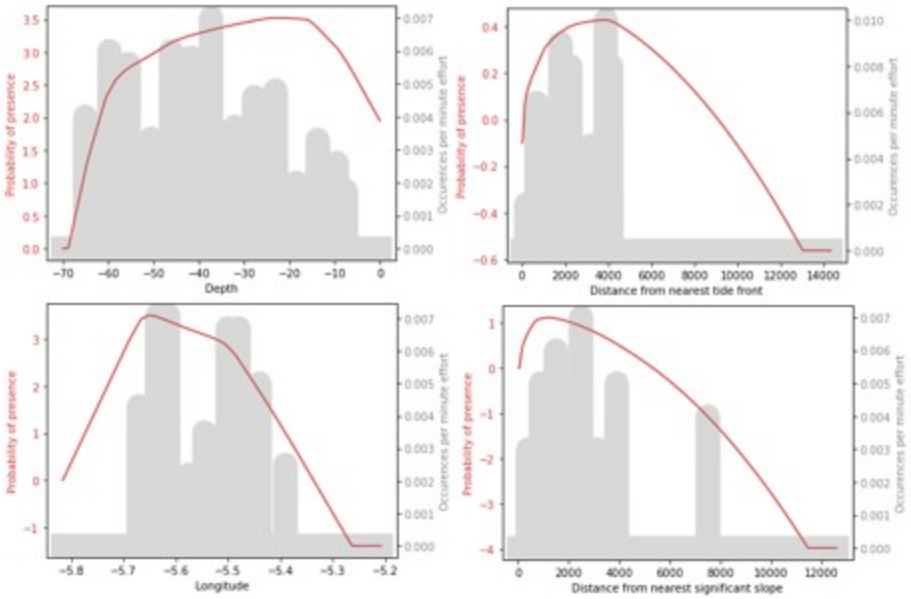

5.6 Five hours after High Water in Penzance

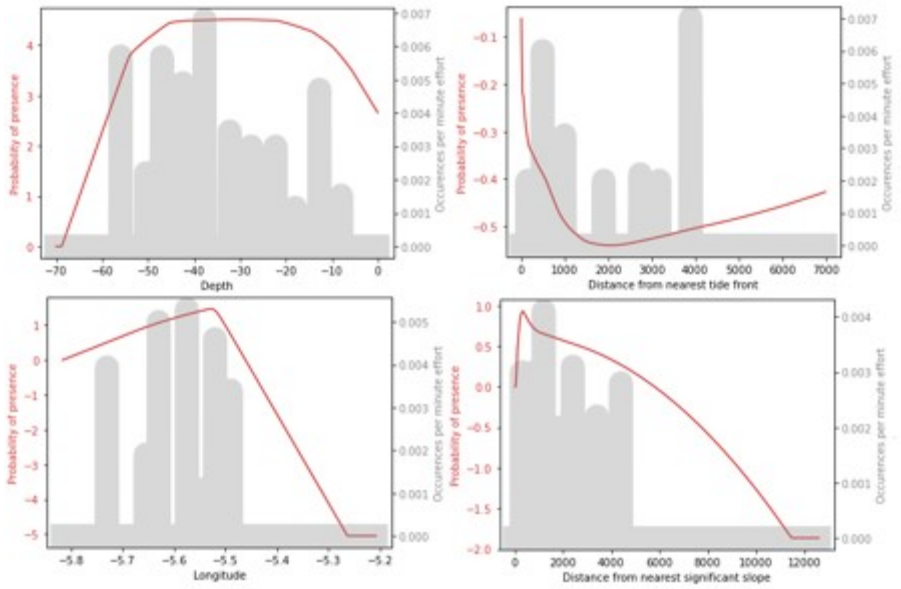

5.7 At Low Water in Penzance

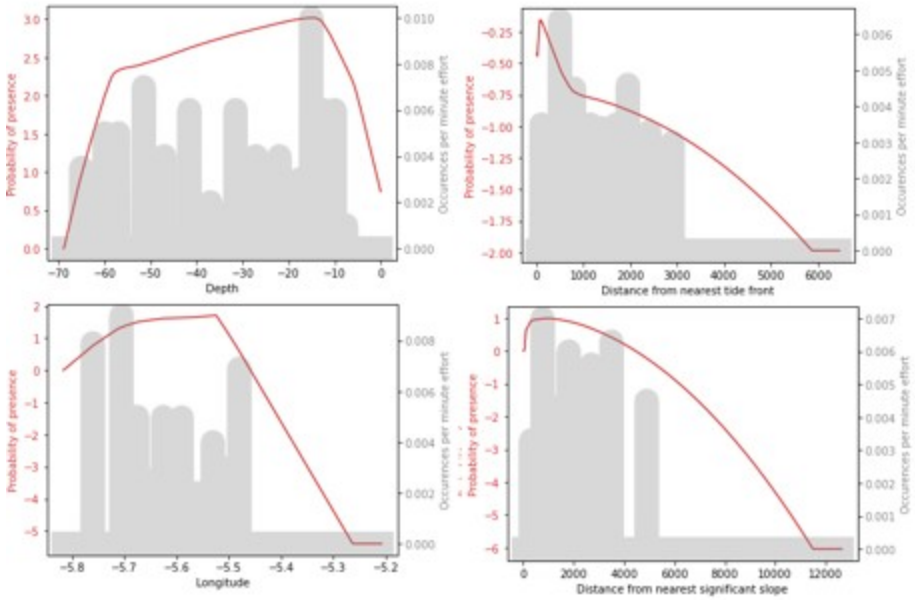

5.8 Five hours before High Water in Penzance

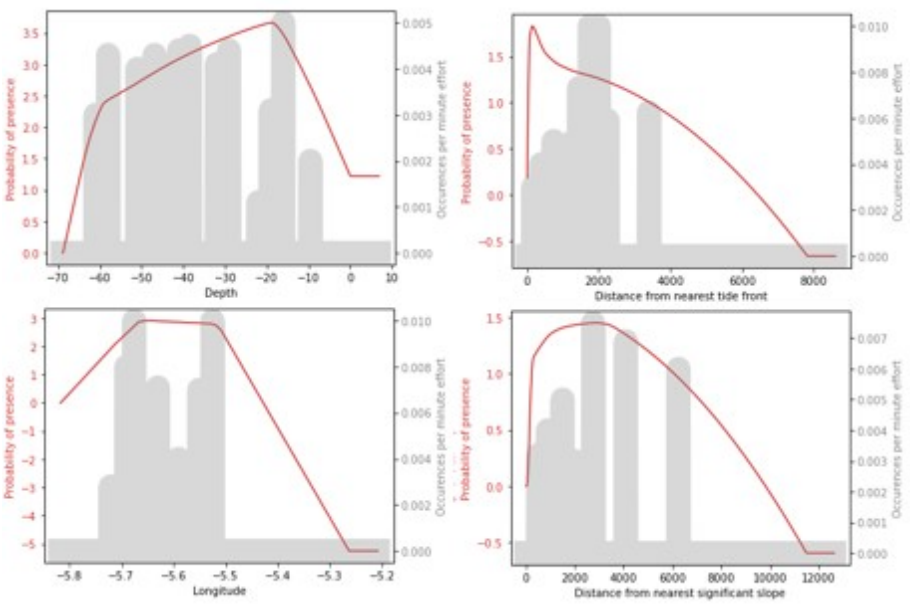

5.9 Four hours before High Water in Penzance

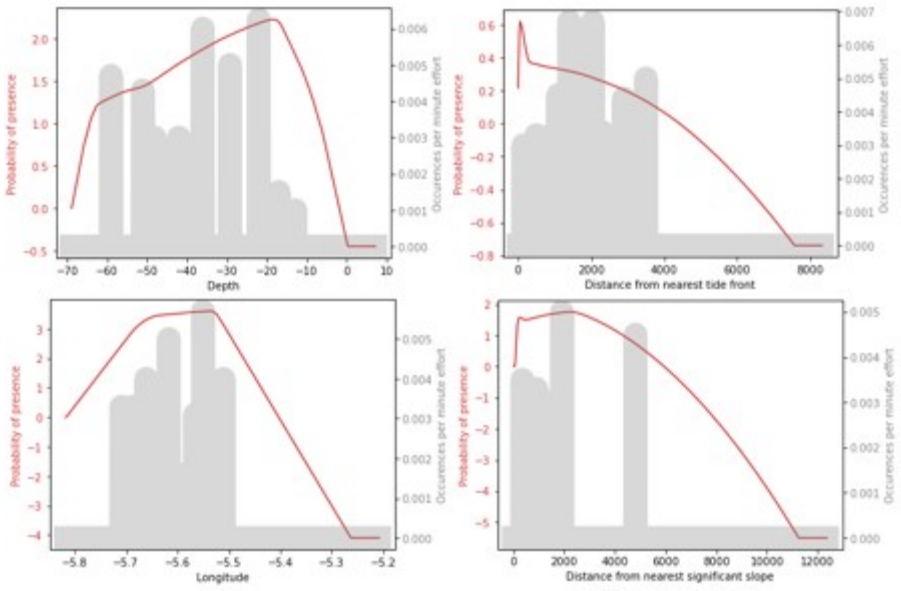

5.10 Three hours before High Water in Penzance

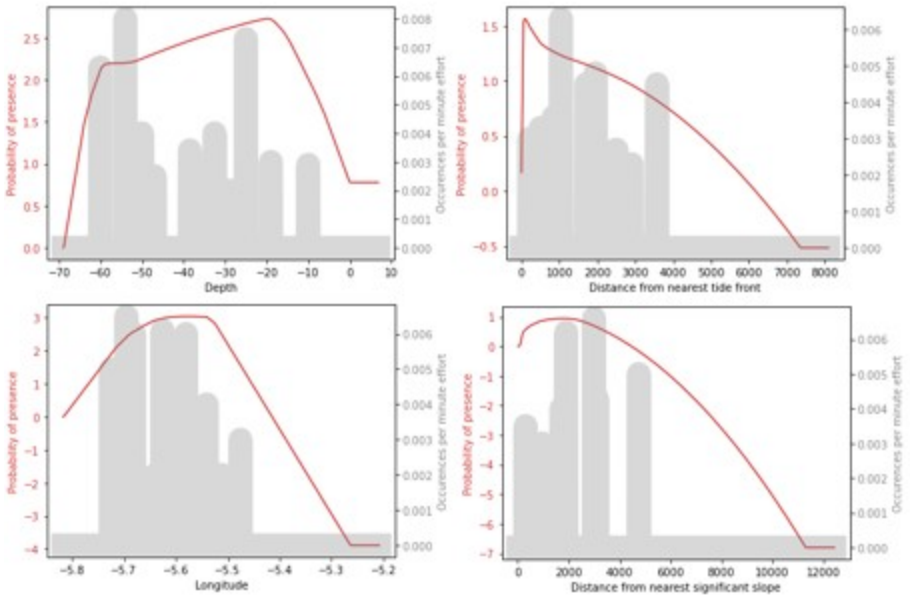

5.11 Two hours before High Water in Penzance

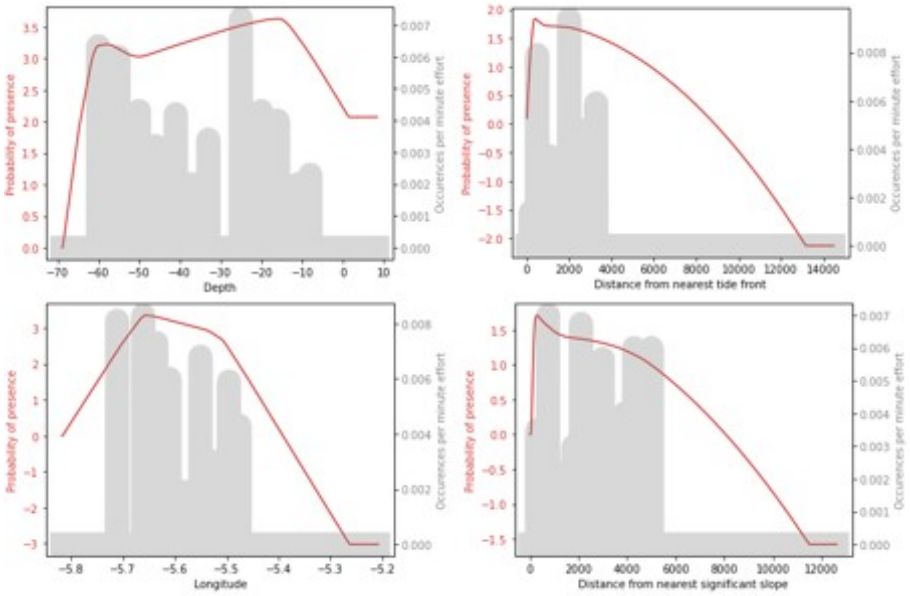

5.12 One hour before High Water in Penzance

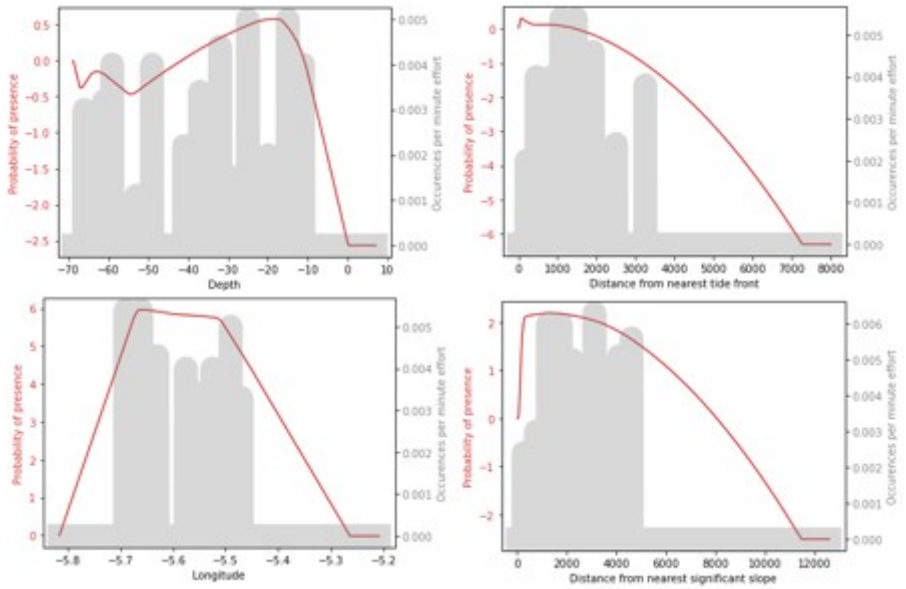

Series from Lund University

Department of Physical Geography and Ecosystem Science

Master Thesis in Geographical Information Science

1. *Anthony Lawther:* The application of GIS-based binary logistic regression for slope failure susceptibility mapping in the Western Grampian Mountains, Scotland (2008).
2. *Rickard Hansen:* Daily mobility in Grenoble Metropolitan Region, France. Applied GIS methods in time geographical research (2008).
3. *Emil Bayramov:* Environmental monitoring of bio-restoration activities using GIS and Remote Sensing (2009).
4. *Rafael Villarreal Pacheco:* Applications of Geographic Information Systems as an analytical and visualization tool for mass real estate valuation: a case study of Fontibon District, Bogota, Columbia (2009).
5. *Siri Oestreich Waage:* a case study of route solving for oversized transport: The use of GIS functionalities in transport of transformers, as part of maintaining a reliable power infrastructure (2010).
6. *Edgar Pimiento:* Shallow landslide susceptibility – Modelling and validation (2010).
7. *Martina Schäfer:* Near real-time mapping of floodwater mosquito breeding sites using aerial photographs (2010).
8. *August Pieter van Waarden-Nagel:* Land use evaluation to assess the outcome of the programme of rehabilitation measures for the river Rhine in the Netherlands (2010).
9. *Samira Muhammad:* Development and implementation of air quality data mart for Ontario, Canada: A case study of air quality in Ontario using OLAP tool. (2010).
10. *Fredros Oketch Okumu*: Using remotely sensed data to explore spatial and temporal relationships between photosynthetic productivity of vegetation and malaria transmission intensities in selected parts of Africa (2011).
11. *Svajunas Plunge:* Advanced decision support methods for solving diffuse water pollution problems (2011).
12. *Jonathan Higgins:* Monitoring urban growth in greater Lagos: A case study using GIS to monitor the urban growth of Lagos 1990 - 2008 and produce future growth prospects for the city (2011).
13. *Mårten Karlberg:* Mobile Map Client API: Design and Implementation for Android (2011).
14. *Jeanette McBride:* Mapping Chicago area urban tree canopy using color infrared imagery (2011).
15. *Andrew Farina:* Exploring the relationship between land surface temperature and vegetation abundance for urban heat island mitigation in Seville, Spain (2011).
16. *David Kanyari*: Nairobi City Journey Planner: An online and a Mobile Application (2011).
17. *Laura V. Drews:* Multi-criteria GIS analysis for siting of small wind power plants - A case study from Berlin (2012).
18. *Qaisar Nadeem:* Best living neighborhood in the city - A GIS based multi criteria evaluation of ArRiyadh City (2012).

19. *Ahmed Mohamed El Saeid Mustafa:* Development of a photo voltaic building rooftop integration analysis tool for GIS for Dokki District, Cairo, Egypt (2012).
20. *Daniel Patrick Taylor*: Eastern Oyster Aquaculture: Estuarine Remediation via Site Suitability and Spatially Explicit Carrying Capacity Modeling in Virginia's Chesapeake Bay (2013).
21. *Angeleta Oveta Wilson:* A Participatory GIS approach to *unearthing* Manchester's Cultural Heritage '*gold mine'* (2013).
22. *Ola Svensson:* Visibility and Tholos Tombs in the Messenian Landscape: A Comparative Case Study of the Pylian Hinterlands and the Soulima Valley (2013).
23. *Monika Ogden:* Land use impact on water quality in two river systems in South Africa (2013).
24. *Stefan Rova:* A GIS based approach assessing phosphorus load impact on Lake Flaten in Salem, Sweden (2013).
25. *Yann Buhot:* Analysis of the history of landscape changes over a period of 200 years. How can we predict past landscape pattern scenario and the impact on habitat diversity? (2013).
26. *Christina Fotiou:* Evaluating habitat suitability and spectral heterogeneity models to predict weed species presence (2014).
27. *Inese Linuza:* Accuracy Assessment in Glacier Change Analysis (2014).
28. *Agnieszka Griffin:* Domestic energy consumption and social living standards: a GIS analysis within the Greater London Authority area (2014).
29. *Brynja Guðmundsdóttir:* Detection of potential arable land with remote sensing and GIS - A Case Study for Kjósarhreppur (2014).
30. *Oleksandr Nekrasov:* Processing of MODIS Vegetation Indices for analysis of agricultural droughts in the southern Ukraine between the years 2000-2012 (2014).
31. *Sarah Tressel:* Recommendations for a polar Earth science portal in the context of Arctic Spatial Data Infrastructure (2014).
32. *Caroline Gevaert:* Combining Hyperspectral UAV and Multispectral Formosat-2 Imagery for Precision Agriculture Applications (2014).
33. *Salem Jamal-Uddeen:* Using GeoTools to implement the multi-criteria evaluation analysis - weighted linear combination model (2014).
34. *Samanah Seyedi-Shandiz:* Schematic representation of geographical railway network at the Swedish Transport Administration (2014).
35. *Kazi Masel Ullah:* Urban Land-use planning using Geographical Information System and analytical hierarchy process: case study Dhaka City (2014).
36. *Alexia Chang-Wailing Spitteler:* Development of a web application based on MCDA and GIS for the decision support of river and floodplain rehabilitation projects (2014).
37. *Alessandro De Martino:* Geographic accessibility analysis and evaluation of potential changes to the public transportation system in the City of Milan (2014).
38. *Alireza Mollasalehi:* GIS Based Modelling for Fuel Reduction Using Controlled Burn in Australia. Case Study: Logan City, QLD (2015).

39. *Negin A. Sanati:* Chronic Kidney Disease Mortality in Costa Rica; Geographical Distribution, Spatial Analysis and Non-traditional Risk Factors (2015).
40. *Karen McIntyre:* Benthic mapping of the Bluefields Bay fish sanctuary, Jamaica (2015).
41. *Kees van Duijvendijk:* Feasibility of a low-cost weather sensor network for agricultural purposes: A preliminary assessment (2015).
42. *Sebastian Andersson Hylander:* Evaluation of cultural ecosystem services using GIS (2015).
43. *Deborah Bowyer:* Measuring Urban Growth, Urban Form and Accessibility as Indicators of Urban Sprawl in Hamilton, New Zealand (2015).
44. *Stefan Arvidsson:* Relationship between tree species composition and phenology extracted from satellite data in Swedish forests (2015).
45. *Damián Giménez Cruz*: GIS-based optimal localisation of beekeeping in rural Kenya (2016).
46. *Alejandra Narváez Vallejo:* Can the introduction of the topographic indices in LPJ-GUESS improve the spatial representation of environmental variables? (2016).
47. *Anna Lundgren:* Development of a method for mapping the highest coastline in Sweden using breaklines extracted from high resolution digital elevation models (2016).
48. *Oluwatomi Esther Adejoro:* Does location also matter? A spatial analysis of social achievements of young South Australians (2016).
49. *Hristo Dobrev Tomov:* Automated temporal NDVI analysis over the Middle East for the period 1982 - 2010 (2016).
50. *Vincent Muller:* Impact of Security Context on Mobile Clinic Activities A GIS Multi Criteria Evaluation based on an MSF Humanitarian Mission in Cameroon (2016).
51. *Gezahagn Negash Seboka:* Spatial Assessment of NDVI as an Indicator of Desertification in Ethiopia using Remote Sensing and GIS (2016).
52. *Holly Buhler:* Evaluation of Interfacility Medical Transport Journey Times in Southeastern British Columbia. (2016).
53. *Lars Ole Grottenberg*: Assessing the ability to share spatial data between emergency management organisations in the High North (2016).
54. *Sean Grant:* The Right Tree in the Right Place: Using GIS to Maximize the Net Benefits from Urban Forests (2016).
55. *Irshad Jamal:* Multi-Criteria GIS Analysis for School Site Selection in Gorno-Badakhshan Autonomous Oblast, Tajikistan (2016).
56. *Fulgencio Sanmartín:* Wisdom-volkano: A novel tool based on open GIS and time-series visualization to analyse and share volcanic data (2016).
57. *Nezha Acil:* Remote sensing-based monitoring of snow cover dynamics and its influence on vegetation growth in the Middle Atlas Mountains (2016).
58. *Julia Hjalmarsson:* A Weighty Issue: Estimation of Fire Size with Geographically Weighted Logistic Regression (2016).
59. *Mathewos Tamiru Amato:* Using multi-criteria evaluation and GIS for chronic food and nutrition insecurity indicators analysis in Ethiopia (2016).
60. *Karim Alaa El Din Mohamed Soliman El Attar:* Bicycling Suitability in Downtown, Cairo, Egypt (2016).

61. *Gilbert Akol Echelai:* Asset Management: Integrating GIS as a Decision Support Tool in Meter Management in National Water and Sewerage Corporation (2016).
62. *Terje Slinning:* Analytic comparison of multibeam echo soundings (2016).
63. *Gréta Hlín Sveinsdóttir:* GIS-based MCDA for decision support: A framework for wind farm siting in Iceland (2017).
64. *Jonas Sjögren:* Consequences of a flood in Kristianstad, Sweden: A GIS-based analysis of impacts on important societal functions (2017).
65. *Nadine Raska:* 3D geologic subsurface modelling within the Mackenzie Plain, Northwest Territories, Canada (2017).
66. *Panagiotis Symeonidis*: Study of spatial and temporal variation of atmospheric optical parameters and their relation with PM 2.5 concentration over Europe using GIS technologies (2017).
67. *Michaela Bobeck:* A GIS-based Multi-Criteria Decision Analysis of Wind Farm Site Suitability in New South Wales, Australia, from a Sustainable Development Perspective (2017).
68. *Raghdaa Eissa*: Developing a GIS Model for the Assessment of Outdoor Recreational Facilities in New Cities Case Study: Tenth of Ramadan City, Egypt (2017).
69. *Zahra Khais Shahid*: Biofuel plantations and isoprene emissions in Svea and Götaland (2017).
70. *Mirza Amir Liaquat Baig*: Using geographical information systems in epidemiology: Mapping and analyzing occurrence of diarrhea in urban - residential area of Islamabad, Pakistan (2017).
71. *Joakim Jörwall*: Quantitative model of Present and Future well-being in the EU-28: A spatial Multi-Criteria Evaluation of socioeconomic and climatic comfort factors (2017).
72. *Elin Haettner*: Energy Poverty in the Dublin Region: Modelling Geographies of Risk (2017).
73. *Harry Eriksson*: Geochemistry of stream plants and its statistical relations to soil- and bedrock geology, slope directions and till geochemistry. A GIS-analysis of small catchments in northern Sweden (2017).
74. *Daniel Gardevärn:* PPGIS and Public meetings – An evaluation of public participation methods for urban planning (2017).
75. *Kim Friberg:* Sensitivity Analysis and Calibration of Multi Energy Balance Land Surface Model Parameters (2017).
76. *Viktor Svanerud:* Taking the bus to the park? A study of accessibility to green areas in Gothenburg through different modes of transport (2017).
77. *Lisa-Gaye Greene*: Deadly Designs: The Impact of Road Design on Road Crash Patterns along Jamaica's North Coast Highway (2017).
78. *Katarina Jemec Parker*: Spatial and temporal analysis of fecal indicator bacteria concentrations in beach water in San Diego, California (2017).
79. *Angela Kabiru*: An Exploratory Study of Middle Stone Age and Later Stone Age Site Locations in Kenya's Central Rift Valley Using Landscape Analysis: A GIS Approach (2017).
80. *Kristean Björkmann*: Subjective Well-Being and Environment: A GIS-Based Analysis (2018).

81. *Williams Erhunmonmen Ojo*: Measuring spatial accessibility to healthcare for people living with HIV-AIDS in southern Nigeria (2018).
82. *Daniel Assefa*: Developing Data Extraction and Dynamic Data Visualization (Styling) Modules for Web GIS Risk Assessment System (WGRAS). (2018).
83. *Adela Nistora*: Inundation scenarios in a changing climate: assessing potential impacts of sea-level rise on the coast of South-East England (2018).
84. *Marc Seliger*: Thirsty landscapes - Investigating growing irrigation water consumption and potential conservation measures within Utah's largest master-planned community: Daybreak (2018).
85. *Luka Jovičić*: Spatial Data Harmonisation in Regional Context in Accordance with INSPIRE Implementing Rules (2018).
86. *Christina Kourdounouli*: Analysis of Urban Ecosystem Condition Indicators for the Large Urban Zones and City Cores in EU (2018).
87. *Jeremy Azzopardi*: Effect of distance measures and feature representations on distance-based accessibility measures (2018).
88. *Patrick Kabatha*: An open source web GIS tool for analysis and visualization of elephant GPS telemetry data, alongside environmental and anthropogenic variables (2018).
89. *Richard Alphonce Giliba*: Effects of Climate Change on Potential Geographical Distribution of Prunus africana (African cherry) in the Eastern Arc Mountain Forests of Tanzania (2018).
90. *Eiður Kristinn Eiðsson*: Transformation and linking of authoritative multi-scale geodata for the Semantic Web: A case study of Swedish national building data sets (2018).
91. *Niamh Harty*: HOP!: a PGIS and citizen science approach to monitoring the condition of upland paths (2018).
92. *José Estuardo Jara Alvear*: Solar photovoltaic potential to complement hydropower in Ecuador: A GIS-based framework of analysis (2018).
93. *Brendan O'Neill*: Multicriteria Site Suitability for Algal Biofuel Production Facilities (2018).
94. *Roman Spataru*: Spatial-temporal GIS analysis in public health – a case study of polio disease (2018).
95. *Alicja Miodońska*: Assessing evolution of ice caps in Suðurland, Iceland, in years 1986 - 2014, using multispectral satellite imagery (2019).
96. *Dennis Lindell Schettini*: A Spatial Analysis of Homicide Crime's Distribution and Association with Deprivation in Stockholm Between 2010-2017 (2019).
97. *Damiano Vesentini*: The Po Delta Biosphere Reserve: Management challenges and priorities deriving from anthropogenic pressure and sea level rise (2019).
98. *Emilie Arnesten*: Impacts of future sea level rise and high water on roads, railways and environmental objects: a GIS analysis of the potential effects of increasing sea levels and highest projected high water in Scania, Sweden (2019).
99. *Syed Muhammad Amir Raza*: Comparison of geospatial support in RDF stores: Evaluation for ICOS Carbon Portal metadata (2019).
100. *Hemin Tofiq*: Investigating the accuracy of Digital Elevation Models from UAV images in areas with low contrast: A sandy beach as a case study (2019).

101. *Evangelos Vafeiadis*: Exploring the distribution of accessibility by public transport using spatial analysis. A case study for retail concentrations and public hospitals in Athens (2019).
102. *Milan Sekulic*: Multi-Criteria GIS modelling for optimal alignment of roadway by-passes in the Tlokweng Planning Area, Botswana (2019).
103. *Ingrid Piirisaar*: A multi-criteria GIS analysis for siting of utility-scale photovoltaic solar plants in county Kilkenny, Ireland (2019).
104. *Nigel Fox*: Plant phenology and climate change: possible effect on the onset of various wild plant species' first flowering day in the UK (2019).
105. *Gunnar Hesch*: Linking conflict events and cropland development in Afghanistan, 2001 to 2011, using MODIS land cover data and Uppsala Conflict Data Programme (2019).
106. *Elijah Njoku*: Analysis of spatial-temporal pattern of Land Surface Temperature (LST) due to NDVI and elevation in Ilorin, Nigeria (2019).
107. *Katalin Bunyevácz*: Development of a GIS methodology to evaluate informal urban green areas for inclusion in a community governance program (2019).
108. *Paul dos Santos*: Automating synthetic trip data generation for an agent-based simulation of urban mobility (2019).
109. *Robert O' Dwyer*: Land cover changes in Southern Sweden from the mid-Holocene to present day: Insights for ecosystem service assessments (2019).
110. *Daniel Klingmyr*: Global scale patterns and trends in tropospheric NO2 concentrations (2019).
111. *Marwa Farouk Elkabbany*: Sea Level Rise Vulnerability Assessment for Abu Dhabi, United Arab Emirates (2019).
112. *Jip Jan van Zoonen*: Aspects of Error Quantification and Evaluation in Digital Elevation Models for Glacier Surfaces (2020).
113. *Georgios Efthymiou*: The use of bicycles in a mid-sized city – benefits and obstacles identified using a questionnaire and GIS (2020).
114. *Haruna Olayiwola Jimoh*: Assessment of Urban Sprawl in MOWE/IBAFO Axis of Ogun State using GIS Capabilities (2020).
115. *Nikolaos Barmpas Zachariadis*: Development of an iOS, Augmented Reality for disaster management (2020).
116. *Ida Storm*: ICOS Atmospheric Stations: Spatial Characterization of CO2 Footprint Areas and Evaluating the Uncertainties of Modelled CO2 Concentrations (2020).
117. *Alon Zuta*: Evaluation of water stress mapping methods in vineyards using airborne thermal imaging (2020).
118. *Marcus Eriksson*: Evaluating structural landscape development in the municipality Upplands-Bro, using landscape metrics indices (2020).
119. *Ane Rahbek Vierø*: Connectivity for Cyclists? A Network Analysis of Copenhagen's Bike Lanes (2020).
120. *Cecilia Baggini*: Changes in habitat suitability for three declining Anatidae species in saltmarshes on the Mersey estuary, North-West England (2020).
121. *Bakrad Balabanian*: Transportation and Its Effect on Student Performance (2020).

122. *Ali Al Farid*: Knowledge and Data Driven Approaches for Hydrocarbon Microseepage Characterizations: An Application of Satellite Remote Sensing (2020).
123. *Bartlomiej Kolodziejczyk*: Distribution Modelling of Gene Drive-Modified Mosquitoes and Their Effects on Wild Populations (2020).
124. *Alexis Cazorla*: Decreasing organic nitrogen concentrations in European water bodies - links to organic carbon trends and land cover (2020).
125. *Kharid Mwakoba*: Remote sensing analysis of land cover/use conditions of community-based wildlife conservation areas in Tanzania (2021).
126. *Chinatsu Endo*: Remote Sensing Based Pre-Season Yellow Rust Early Warning in Oromia, Ethiopia (2021).
127. *Berit Mohr*: Using remote sensing and land abandonment as a proxy for long-term human out-migration. A Case Study: Al-Hassakeh Governorate, Syria (2021).
128. *Kanchana Nirmali Bandaranayake*: Considering future precipitation in delineation locations for water storage systems - Case study Sri Lanka (2021).
129. *Emma Bylund*: Dynamics of net primary production and food availability in the aftermath of the 2004 and 2007 desert locust outbreaks in Niger and Yemen (2021).
130. *Shawn Pace*: Urban infrastructure inundation risk from permanent sea-level rise scenarios in London (UK), Bangkok (Thailand) and Mumbai (India): A comparative analysis (2021).
131. *Oskar Evert Johansson*: The hydrodynamic impacts of Estuarine Oyster reefs, and the application of drone technology to this study (2021).
132. *Pritam Kumarsingh*: A Case Study to develop and test GIS/SDSS methods to assess the production capacity of a Cocoa Site in Trinidad and Tobago (2021).
133. *Muhammad Imran Khan*: Property Tax Mapping and Assessment using GIS (2021).
134. *Domna Kanari*: Mining geosocial data from Flickr to explore tourism patterns: The case study of Athens (2021).
135. *Mona Tykesson Klubien*: Livestock-MRSA in Danish pig farms (2021).
136. *Ove Njøten*: Comparing radar satellites. Use of Sentinel-1 leads to an increase in oil spill alerts in Norwegian waters (2021).
137. *Panagiotis Patrinos*: Change of heating fuel consumption patterns produced by the economic crisis in Greece (2021).
138. *Lukasz Langowski*: Assessing the suitability of using Sentinel-1A SAR multi-temporal imagery to detect fallow periods between rice crops (2021).
139. *Jonas Tillman*: Perception accuracy and user acceptance of legend designs for opacity data mapping in GIS (2022).
140. *Gabriela Olekszyk*: ALS (Airborne LIDAR) accuracy: Can potential low data quality of ground points be modelled/detected? Case study of 2016 LIDAR capture over Auckland, New Zealand (2022).
141. *Luke Aspland*: Weights of Evidence Predictive Modelling in Archaeology (2022).
142. *Luís Fareleira Gomes*: The influence of climate, population density, tree species and land cover on fire pattern in mainland Portugal (2022).

143. *Andreas Eriksson*: Mapping Fire Salamander (Salamandra salamandra) Habitat Suitability in Baden-Württemberg with Multi-Temporal Sentinel-1 and Sentinel-2 Imagery (2022).
144. *Lisbet Hougaard Baklid*: Geographical expansion rate of a brown bear population in Fennoscandia and the factors explaining the directional variations (2022).
145. *Victoria Persson*: Mussels in deep water with climate change: Spatial distribution of mussel (Mytilus galloprovincialis) growth offshore in the French Mediterranean with respect to climate change scenario RCP 8.5 Long Term and Integrated Multi-Trophic Aquaculture (IMTA) using Dynamic Energy Budget (DEB) modelling (2022).
146. *Benjamin Bernard Fabien Gérard Borgeais*: Implementing a multi-criteria GIS analysis and predictive modelling to locate Upper Palaeolithic decorated caves in the Périgord noir, France (2022).
147. *Bernat Dorado-Guerrero*: Assessing the impact of post-fire restoration interventions using spectral vegetation indices: A case study in El Bruc, Spain (2022).
148. *Ignatius Gabriel Aloysius Maria Perera*: The Influence of Natural Radon Occurrence on the Severity of the COVID-19 Pandemic in Germany: A Spatial Analysis (2022).
149. *Mark Overton*: An Analysis of Spatially-enabled Mobile Decision Support Systems in a Collaborative Decision-Making Environment (2022).
150. *Viggo Lunde*: Analysing methods for visualizing time-series datasets in open-source web mapping (2022).
151. *Johan Viscarra Hansson*: Distribution Analysis of Impatiens glandulifera in Kronoberg County and a Pest Risk Map for Alvesta Municipality (2022).
152. *Vincenzo Poppiti*: GIS and Tourism: Developing strategies for new touristic flows after the Covid-19 pandemic (2022).
153. *Henrik Hagelin*: Wildfire growth modelling in Sweden - A suitability assessment of available data (2023).
154. *Gabriel Romeo Ferriols Pavico*: Where there is road, there is fire (influence): An exploratory study on the influence of roads in the spatial patterns of Swedish wildfires of 2018 (2023).
155. *Colin Robert Potter*: Using a GIS to enable an economic, land use and energy output comparison between small wind powered turbines and large-scale wind farms: the case of Oslo, Norway (2023).
156. *Krystyna Muszel*: Impact of Sea Surface Temperature and Salinity on Phytoplankton blooms phenology in the North Sea (2023).
157. *Tobias Rydlinge*: Urban tree canopy mapping - an open source deep learning approach (2023).
158. *Albert Wellendorf*: Multi-scale Bark Beetle Predictions Using Machine Learning (2023).
159. *Manolis Papadakis*: Use of Satellite Remote Sensing for Detecting Archaeological Features: An Example from Ancient Corinth, Greece (2023).

160. *Konstantinos Sourlamtas*: Developing a Geographical Information System for a water and sewer network, for monitoring, identification and leak repair - Case study: Municipal Water Company of Naoussa, Greece (2023).
161. *Xiaoming Wang*: Identification of restoration hotspots in landscape-scale green infrastructure planning based on model-predicted connectivity forest (2023).
162. *Sarah Sienaert*: Usability of Sentinel-1 C-band VV and VH SAR data for the detection of flooded oil palm (2023).
163. *Katarina Ekeroot*: Uncovering the spatial relationships between Covid-19 vaccine coverage and local politics in Sweden (2023).
164. *Nikolaos Kouskoulis*: Exploring patterns in risk factors for bark beetle attack during outbreaks triggered by drought stress with harvester data on attacked trees: A case study in Southeastern Sweden (2023).
165. *Jonas Almén*: Geographic polarization and clustering of partisan voting: A local-level analysis of Stockholm Municipality (2023).
166. *Sara Sharon Jones*: Tree species impact on Forest Fire Spread Susceptibility in Sweden (2023).
167. *Takura Matswetu*: Towards a Geographic Information Systems and Data-Driven Integration Management. Studying holistic integration through spatial accessibility of services in Tampere, Finland. (2023).
168. *Duncan Jones*: Investigating the influence of the tidal regime on harbour porpoise *Phocoena phocoena* distribution in Mount's Bay, Cornwall. (2023).